batteries

MDPI

Review

All-Solid-State Thin Film Li-Ion Batteries: New Challenges, New Materials, and New Designs

Baolin Wu [1,2], Chunguang Chen [3,4,*], Dmitri L. Danilov [1,5,*], Rüdiger-A. Eichel [1,2] and Peter H. L. Notten [1,5,6,*]

1 Forschungszentrum Jülich (IEK-9), D-52425 Jülich, Germany
2 Department of Chemistry, RWTH Aachen University, D-52074 Aachen, Germany
3 LNM, Institute of Mechanics, Chinese Academy of Sciences, Beijing 100190, China
4 School of Engineering Sciences, University of Chinese Academy of Sciences, Beijing 100049, China
5 Department of Chemistry and Chemical Engineering, Eindhoven University of Technology, P.O. Box 513, 5600 MB Eindhoven, The Netherlands
6 Centre for Clean Energy Technology, University of Technology Sydney, Broadway, Sydney, NSW 2007, Australia
* Correspondence: chenchunguang@imech.ac.cn (C.C.); d.danilov@tue.nl (D.L.D.); p.h.l.notten@tue.nl (P.H.L.N.)

Abstract: All-solid-state batteries (ASSBs) are among the remarkable next-generation energy storage technologies for a broad range of applications, including (implantable) medical devices, portable electronic devices, (hybrid) electric vehicles, and even large-scale grid storage. All-solid-state thin film Li-ion batteries (TFLIBs) with an extended cycle life, broad temperature operation range, and minimal self-discharge rate are superior to bulk-type ASSBs and have attracted considerable attention. Compared with conventional batteries, stacking dense thin films reduces the Li-ion diffusion length, thereby improving the rate capability. It is vital to develop TFLIBs with higher energy density and stability. However, multiple challenges, such as interfacial instability, low volumetric energy density, and high manufacturing cost, still hinder the widespread application of TFLIBs. At present, many approaches, such as materials optimization and novel architecture design, have been explored to enhance the stability and energy density of TFLIBs. An overview of these discoveries and developments in TFLIBs is presented in this review, together with new insights into the intrinsic mechanisms of operation; this is of great value to the batteries research community and facilitates further improvements in batteries in the near future.

Keywords: all-solid-state; Li-ion batteries; thin film; architecture designs; three-dimensional (3D)

check for updates

Citation: Wu, B.; Chen, C.; Danilov, D.L.; Eichel, R.-A.; Notten, P.H.L. All-Solid-State Thin Film Li-Ion Batteries: New Challenges, New Materials, and New Designs. *Batteries* **2023**, *9*, 186. https://doi.org/10.3390/batteries9030186

Academic Editor: Regina Garcia-Mendez

Received: 18 December 2022
Revised: 6 March 2023
Accepted: 17 March 2023
Published: 21 March 2023

1. Introduction

Lithium-ion batteries (LIBs) have become ubiquitous in our modern lives, with various applications, such as portable electronic devices, electric vehicles, and grid storage [1–3]. In conventional LIBs, liquid electrolytes are favored for their high electrochemical stability voltage window, high ionic conductivity, and excellent wettability with other internal composites of batteries [4]. Liquid electrolytes are typically based on a mixture of carbonate-based organic solvents with Li-salts and additives. Liquid electrolytes face significant drawbacks, such as high flammability, limited operating temperature range, and the possibility of irreversible decomposition [5]. In addition, forming Li-dendrites in organic liquid electrolytes will cause internal short circuits, resulting in the complete failure of the whole battery [6,7].

All-solid-state batteries (ASSBs), with non-volatile solid-state electrolytes (SSEs), present a viable alternative to replace traditional liquid-electrolyte LIBs [8], which can improve the energy density [9–12]. ASSBs are categorized into two types: bulk and thin film types. Compared to bulk-type ASSBs, all-solid-state thin film LIBs (TFLIBs) permit higher charge/discharge rates thanks to the improved contact between the thin film electrodes and SSEs [13].

TFLIBs have been used for many low-power microelectronic devices as onboard energy supply [14,15]. Compared with the porous electrodes in bulk-type ASSBs, the thin film electrode materials are very dense. In addition, as the electrolyte and electrode of the TFLIBs are deposited on an atomic/molecular level, various microscopic defects at the solid-solid interfaces can be avoided, which implies fewer interfacial issues. In addition to the inherent benefits of ASSBs, such as high energy density, a wide operating temperature range, and long cycle life, TFLIBs also have the following key features in comparison to bulk-type ASSBs [16]: (1) the electrode/electrolyte interfaces are in good contact, and the electrolyte layer is very thin, which facilitates fast charging and discharging; (2) the electrode material is more compact and can therefore achieve higher energy densities, a lower self-discharge rate (<1% per year), and a longer cycle life; (3) small-sized batteries can be designed to match semiconductor production processes, and can be integrated into electronic chips. Therefore, TFLIBs can be widely used in smart cards, electronic tags, integrated circuits, medical implants, and other fields. It is regarded as an enormously prospective energy source for microelectronics and a fantastic way of powering wearable electronic devices [17].

With the continuous advancements, TFLBs have become a promising power supplier for many devices owing to their compact size, flexibility, and impressive energy density [18–21]. Some of the most promising applications of TFLIBs include [22,23]: (1) Wearable Devices: TFLIBs are the ideal power source for wearable devices such as smartwatches, fitness trackers, and medical sensors due to their small size, flexibility, and lightweight; (2) Internet of Things Devices: TFLIBs can power internet of things devices that require small, low-power batteries, such as smart home sensors, wireless tags, and environmental monitoring devices; (3) Medical Implants: TFLIBs can power medical implants, such as pacemakers and defibrillators, in which a small size and long-term reliability are required; (4) Military and Aerospace Applications: TFLBs are suitable for military and aerospace applications owing to their lightweight construction, small size, and high energy density; (5) Energy Harvesting: TFLBs can be used in energy harvesting applications, where they can store energy generated by solar panels, thermoelectric generators, or other energy sources; (6) Smart Cards: TFLBs can be used in smart cards for secure transactions, such as credit cards, passports, and other identification documents. Understanding the correlation of the performance with the materials composition, solid-state interfaces, and battery architectures will provide insight into enhancing the performance of TFLIBs. However, TFLBs face significant challenges arising from the permanent growth in demands of electrical devices, such as ultra-long life, high capacity, and fast charging rates. However, more issues have to be resolved to reach: (1) High specific electrode storage capacities and ionic conductivities of SSEs; (2) Good interface stability and low interfacial resistance between inorganic SSEs and electrodes; (3) High voltage and good rate performance of TFLIBs.

Although serval reviews have recently been published to report the progress of TFLIBs [18–21], the majority of the reviews have been directed towards the recent progress in SSEs and electrode materials. Few reviews have discussed the advanced architecture design of TFLIBs to increase the energy density and reduce the manufacturing costs. However, these components are crucial for the practical applications of TFLIBs [22,23].

This review outlines the recent advancements and achievements of new constituent materials and architectural designs in TFLIBs. The historical developments and current challenges of TFLIBs are presented first. The following section summarizes the novel constituent materials developed to improve the TFLIBs' performance, including electrode materials, electrolytes, and current collectors. Then, the novel designs of TFLIBs' architectures, developed in recent years to achieve higher energy densities, are described. Finally, future research opportunities in constituent materials and manufacturing technologies are discussed. The prospect of novel architecture designs for high-energy TFLIBs, including advanced planar TFLIBs, three-dimensional (3D) TFLIBs, and other novel structural TFLIBs, are outlined. Such a thorough evaluation will help to guide future developments of TFLIBs with a high specific capacity, high safety, and extended cycle life.

2. History and Challenges

2.1. Brief History of TFLIBs

TFLIBs are deposited by thin film deposition methods, such as physical vapor deposition (PVD), vacuum evaporation, chemical vapor deposition (CVD), or atomic layer deposition (ALD) [24]. TFLIBs are typically manufactured on a solid substrate, such as glass, ceramic, or even polymer. The construction typically comprises a current collector layer, an anode layer, an electrolyte layer, a cathode layer, and another current collector layer. Sator reported the first thin film cell in 1952 [25]; it featured a lead chloride electrolyte deposited by vacuum evaporation. Then, the first Li-ion thin film batteries (AgI||LiI||Li) were reported in 1969 [26]. Over the next 20 years, the primary focus of research was on enhancing the performance of SSEs and electrode materials. As a result, TFLIBs were rapidly developed. In 1994, C/$LiCoO_2$ (LCO) batteries had a potential exceeding 3.6 V and boasted an impressive energy density, ranging between 120 and 150 Wh/kg (2 to 3 times that of ordinary NiCd batteries), which were successfully commercialized, and were considered the highest-performance portable power device [27]. Since then, $LiCoO_2$ has become the most popular and widely used cathode material. Another milestone was SSE films of lithium phosphorus oxynitride (LiPON), prepared by Bates in 1992 [28]. At present, LiPON is widely acknowledged as a conventional solid electrolyte utilized in TFLIBs. Subsequently, a series of microscale TFLIBs have been gradually designed. In 2002, the microscale TFLIBs ($LiCoO_2$||LiPON||Li) were reported to deliver a highly stable volumetric capacity of 40 μAh $cm^{-2}\cdot\mu m^{-1}$, operating at 3.9 V [29]. To further enhance the energy density of TFLIBs, the 3D integrated TFLIBs ($LiCoO_2$||LiPON||Si) were proposed in 2007 [30]. The utilization of a 3D structural design is promising for increasing the footprint capacity and volumetric capacity density. Then, various promising electrode materials and solid electrolytes were gradually explored for TFLIBs to improve their stability and capacity. In 2015, Cras et al. reported the microscale TFLIBs ($Li_{1.2}TiO_{0.5}S_{2.1}$||LiPON||Si), which demonstrated a cycled volumetric capacity of approximately 38 μAh$\cdot cm^{-2}\cdot\mu m^{-1}$ over 740 cycles [31]. In 2017, STMicroelectronics proposed TFLIBs of $LiCoO_2$||LiPON||Li achieving a nominal voltage of 3.9 V and a capacity of 1 mAh [29]. In 2018, Rupp et al. used PLD to deposit the $Li_7La_3Zr_2O_{12}$ (LLZO) film and achieved promising solid electrolyte films for future TFLIBs by changing the deposition temperature to enhance the ionic conductivity [32]. In 2020, TDK Electronics introduced an all-ceramic structured TFLB with a capacity of 100 μAh and a nominal voltage of 1.5 V [18]. In addition to the mentioned developments, several companies, such as Infinite Power Solutions, Cymbet, and EnFilm, have initiated the commercialization of TFLBs for powering microelectronic devices.

2.2. Current Challenges

With the development of new manufacturing processes and the explosive growth in new chemistries, many promising materials have been investigated for TFLIBs (Figure 1). However, few TFLIBs have been commercialized. Mismatches in the voltage range, chemical reactions between various battery components, and high solid-state interface impedances result in the batteries possessing a lower capacity, cycle life, and energy density. In addition, as electronic devices continue to rapidly be developed, there is an increasing demand for batteries with improved performance, such as faster charging rates, larger capacities, higher energy densities, and better cycling performance [33]. This section reviews the main challenges and improvements for the current TFLIBs.

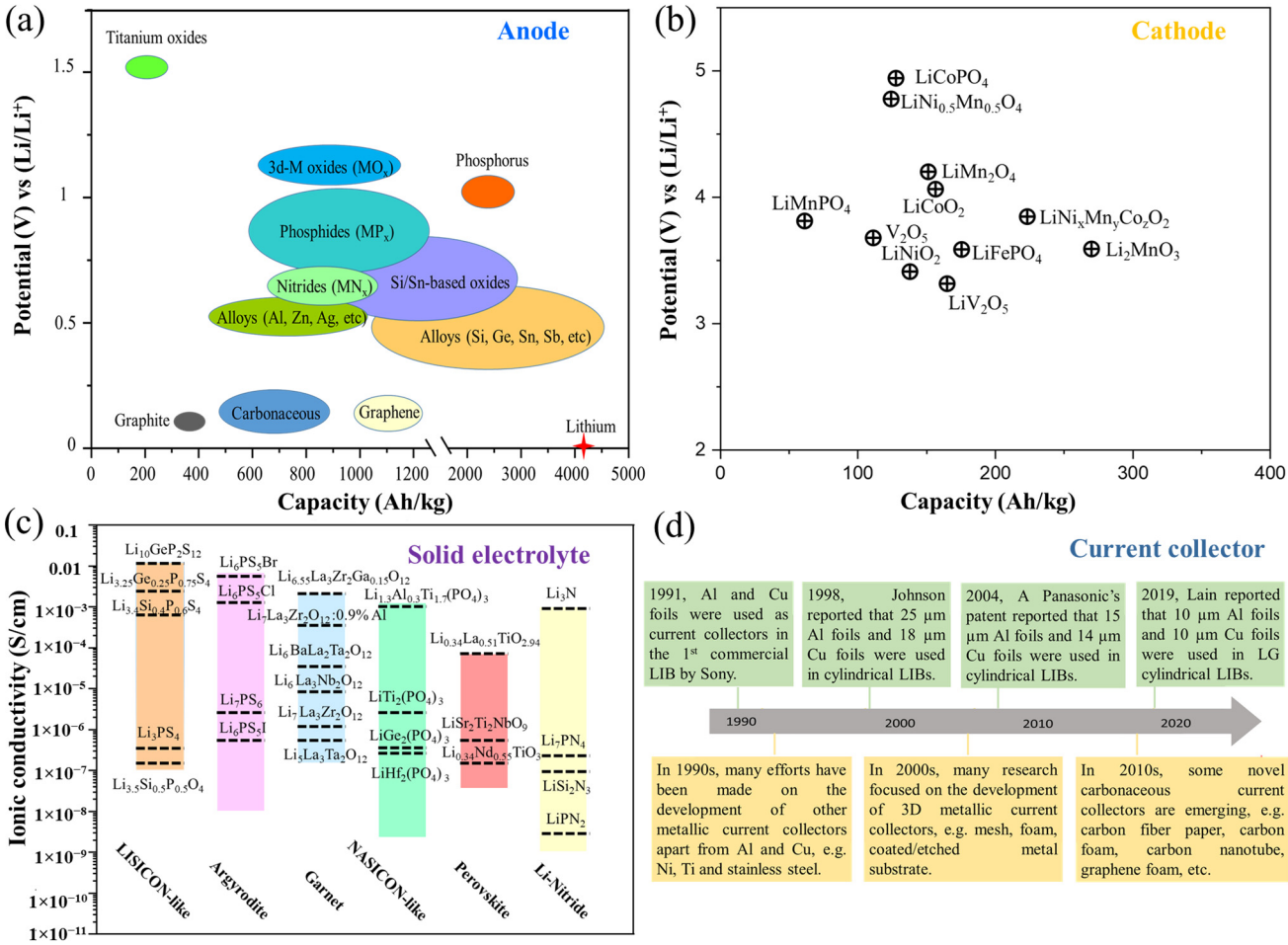

Figure 1. Schematic view of the development of battery materials for TFLIBs: (**a**) Anode materials, (**b**) cathode materials, (**c**) electrolytes, and (**d**) current collectors.

2.2.1. Materials and Deposition Technologies

The properties of the materials utilized significantly impact the performance of batteries. The SSE film plays a critical role in the safety and electrochemical performance of TFLIBs, which is a bottleneck for the development of TFLIBs. A high-performance SSE should show high ionic and low electronic conductivity, induce low electrode corrosion, and have a wide electrochemical operating window, etc. In order to obtain high ionic conductivity, the composition and structure of the electrolytes must be adjustable [20]. More importantly, the electrolyte must be compatible with the electrode materials, forming a stable solid/electrolyte interface. Li_3PO_4 and LIPON are still commonly used solid electrolytes, but their conductivity and stability are insufficient for high-energy batteries. Exploring solid electrolyte films with high ionic conductivity, high compatibility, broad electrochemical stability windows, and cycling stability is imminent [34].

In addition, electrode materials also face significant challenges in improving the batteries' performance. Safety, theoretical capacity, cost, and recyclability must be carefully considered when selecting electrode materials. However, the current electrode materials significantly reduce the electrode materials' sustainability because they contain rare elements and are produced by complex ceramic processing. Furthermore, the actual energy cost of battery manufacturing must include the overall cost of the electrode synthesis and manufacturing equipment [35,36].

Furthermore, negative electrodes should preferably have a low reduction potential. In contrast, positive electrodes should exhibit a high oxidation potential to ensure a high output voltage. Although many novel electrode materials have been synthesized, such as

carbon and $LiCoO_2$, most of them excel in only a few aspects, which cannot really meet all of the requirements for high-performance TFLIBs [37]. For example, carbon and Li-metal are the most widely used anode materials. Carbon combines high stability and conductivity, but its low theoretical capacity limits its application. Li-metal anodes have a high storage capacity, but their poor stability results in low recyclability. Combining these performance requirements is crucial in exploring better electrode materials.

Thin film deposition technologies are also a great challenge for the fabrication of TFLIBs. The quality and the composition homogeneity of the films directly affect the battery's performance. According to the deposition mechanism, the methods to fabricate TFLIBs can be roughly classified into CVD and PVD. PVD involves evaporating the material source in a vacuum to create gaseous atoms, molecules, or ions [38]. The thin film, with specific functions, is deposited on the substrate surface using a low-pressure gas or plasma. The most common PVD methods are vacuum evaporation, sputtering, and ion plating. PVD can deposit metals, alloys, compounds, ceramics, polymer films, and semiconductors. CVD is a method that uses one or more gaseous compounds or simple substances to form thin films on substrate surfaces by chemical reaction. CVD can be used to deposit a variety of inorganic materials, including single-crystal, polycrystalline, or glassy thin films.

CVD is typically carried out using different techniques, such as plasma-enhanced CVD (PECVD), metal-organic CVD (MOCVD), and low-pressure CVD (LPCVD), etc. [20]. However, as the component materials include increasingly constituent elements and complex structures, the battery's design becomes more complex. The mentioned deposition techniques are insufficient to produce such films. In addition, many powder materials with better performance have been explored recently, such as lithium lanthanum titanates (LLT) [39], $Li_7La_3Zr_2O_{12}$ (LLZO) [40], $LiNi_xCo_yMn_zO_2$ [41], etc. However, due to their complex structure and composition, the quality and homogeneity of the corresponding films cannot be easily controlled by the above deposition methods. Therefore, innovation in deposition techniques is needed, along with exploring new active and conductive materials. Fortunately, the recent development of novel deposition technologies, such as ALD, PLD, and 3D printing, will provide more advanced methods for depositing complex thin film battery materials.

2.2.2. Solid-Solid Interfaces

Although the performance of the individual battery components (e.g., electrodes or electrolytes) has been improved considerably, the performance improvement of the whole cell is still lean. Moreover, the power density and lifetime of TFLIBs do not yet meet the practical application requirements. The low performance is mainly attributed to the significant interface resistance that exists between the electrodes and SSEs [42]. This includes the following aspects, depicted in Figure 2: poor contact, formation of an interlayer, and interfacial reactions.

The interface resistance between the electrodes and electrolyte largely depends on the change in the electrode volume during the cycling process [43]. This would lead to poor contact between the electrodes and electrolyte, which can eventually result in crack formation [44] and interfacial delamination [45,46]. Insufficient mechanical contacts can also lead to "dead corner" areas caused by electrode contacts separated by solid electrolytes [47]. The absence of conductive pathways inhibits the electrons and Li^+ ions from transferring to dead corners, thus increasing the interface resistance and capacity attenuation. In addition, a large volume change in the electrode materials may also result in a loss of effective contact between the electrodes and electrolyte during repeated charging and discharging [48].

In TFLIBs, the appearance of interface resistance due to the intermediate layer formation is also a well-known phenomenon. One of the leading causes of interface resistance is the formation of space charge regions. Space charge regions are driven by high potential gradients, leading to Li-depletion near the cathode-SSEs interface in TFLIBs [49]. As a result of the difference in potential at such an interface, Li^+ moves to a higher potential area, leading to Li-depletion and an increase in the interface resistance. In addition, the high

interfacial resistance may also be a result of the interfacial chemical reactions that occur due to the mutual diffusion between the SSEs and electrodes [50]. These interfacial reactions irreversibly change the electrode material into inactive substances during operation. The inactive substances consume the Li^+ but also hinder the Li^+ migration between the electrolyte and electrodes, which significantly reduces the battery cycle life [51]. Reducing the solid interface impedance and improving the stability of the solid interface is the greatest challenge for improving the performance of TFLIBs. Recently, it has been reported that the solid interface can be modified by introducing an intermediate layer to reduce the interfacial resistance; this will be discussed in the next section.

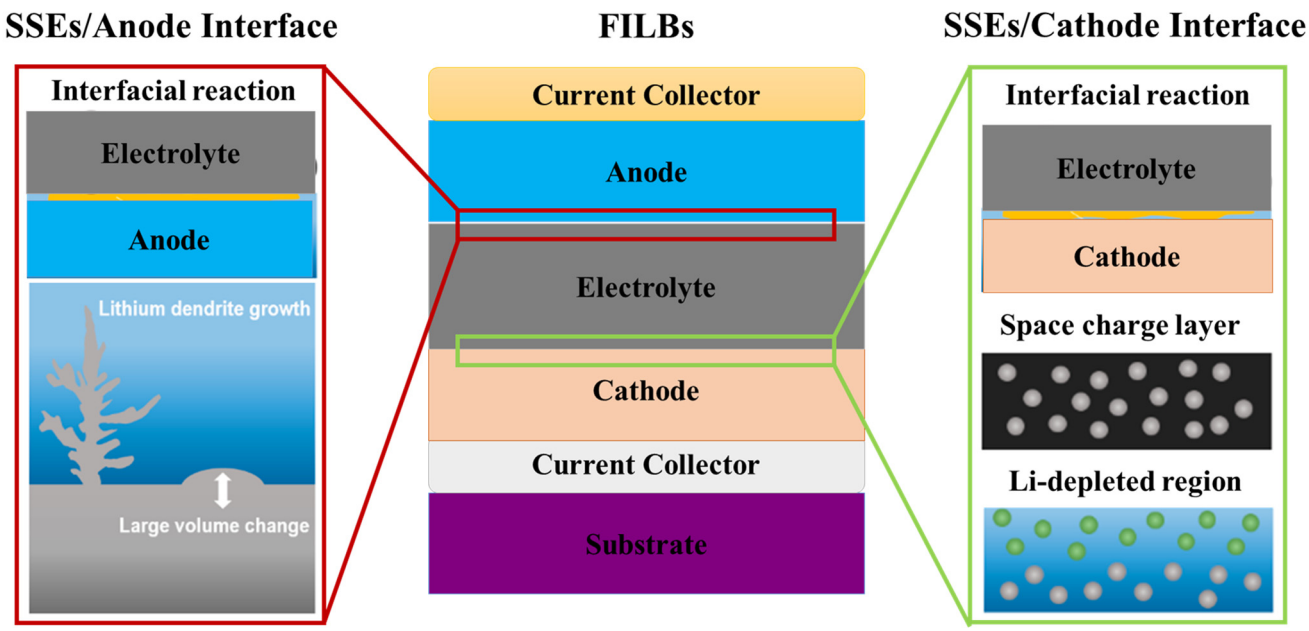

Figure 2. Schematic diagram of TFLIBs and electrode/SSEs interface issues [21].

2.2.3. Energy Density

The energy contained in batteries is a vital indicator of the battery's performance, which directly determines the application fields. When evaluating the energy content of batteries, the specific energy (measured in $Wh \cdot kg^{-1}$) and energy density (measured in $Wh \cdot L^{-1}$) are commonly utilized [52]. TFLIBs exhibit a higher specific capacity, broader working voltage, and longer cycle life than traditional LIBs. However, due to the geometric structure and deposition technology limitations, meeting the energy and power density requirements is a challenging task for rapidly developing micro-medical devices, wireless communications, sensors, and other fields. Achieving high specific energy and energy density in electrode materials necessitates meeting two fundamental requirements: (1) High specific charge ($Ah \cdot kg^{-1}$) and charge density ($Ah \cdot L^{-1}$), indicating that the material contains a large amount of charge carriers per unit mass and volume; (2) A high (for the cathode) and low (for the anode) standard redox potential in their respective electrode redox reactions, which can achieve a high batteries voltage [17]. Additionally, both the positive and negative electrode reactions must be highly reversible to retain the specific charge during numerous cycles in rechargeable batteries. Furthermore, the energy density can be increased by designing thin film structures to improve the active material content and contact area of the electrode material; examples of this are 3D structuring or anode-free thin film Li-metal batteries.

2.2.4. Charging Rate

Recently, the fast charging of battery packs (for example, reaching 80% of the nominal capacity within 15 min) has become an important goal in developing electronic de-

vices [53,54]. The ability to charge at a high rate allows for the rapid recharging of mobile electronic devices, which enhances the user-friendliness. The rate performance of TFLIBs depends mainly on the ions and electrons mobility of the electrodes, electrolyte, and across interfaces. In particular, the electrode's poor ionic and electronic transport is considered a rate-determining step of modern batteries. Therefore, electrodes should meet two criteria for fast charging technology: high ionic and excellent electronic conductivity [55]. Numerous endeavors have been taken to enhance the rate performance of batteries by developing new electrode materials and modifying their structure. However, charging under a high load will accelerate degradation, which leads to a decline in the battery power and capacity. To accelerate the energy development of TFLIBs, it is critical to strike a balance between the rate capacity and energy density.

2.2.5. Manufacturing Cost

Another significant barrier to the widespread application of TFLIBs is the manufacturing cost, including the cost of the raw materials and the deposition processes. Despite the discovery of numerous high-performing electrode and electrolyte materials, high costs are incurred, particularly when preparing thin films. For example, when using PVD to deposit the NCM cathode, it would be costly to prepare the sputtering target. Additionally, one needs to maintain a low deposition rate to produce high-quality films during the deposition process, which is time-consuming. Therefore, it is crucial to lower the cost of producing TFLIBs. Lowering the manufacturing cost of TFLIBs can be achieved by optimizing the materials, designing novel architectures, and optimizing the deposition process.

3. Batteries Materials

TFLIBs can be assessed based on various factors, such as: (1) open-circuit voltage; (2) maximum working current; (3) discharge capacity; and (4) recyclability. Similarly to traditional LIBs, the open-circuit voltage is solely influenced by the electrode materials. The lifetime is determined by the solid interfaces that exist in the whole cell. The maximum working current that batteries can handle is highly dependent on the interfacial condition between the electrodes and SSEs. The electron and ion diffusivities in the materials are also important [17]. Therefore, exploring more promising materials can effectively improve the battery performance. This section reviews the recent developments in advanced materials for TELBs, including current collectors, electrodes, and electrolyte materials.

3.1. Current Collectors

The current collector (CC) not only serves as a conduit for the transportation of electrode materials, but also plays a crucial role in the collection and transportation of the electrons in TFLIBs [56,57]. It plays an essential role in battery's (dis)charge performance. To guarantee excellent battery performance, CCs must satisfy the following requirements in TFLIBs: (1) High electrical conductivity to facilitate the efficient diffusion of the charge carriers within the electrodes [58]; (2) High robustness to improve the electrode stability during consistent charging and discharging procedures [59]; (3) High thermal conductivity to quickly disperse ohmic and chemical reaction heat within the batteries [60]; (4) High chemical inertness to ensure stability alongside the complex electrochemical reactions [61]; (5) Compact size and lightweight to infuse the batteries with high energy and power densities [62]; (6) Low cost to achieve the demands of mass production and commercialization [63].

In recent years, researchers have explored a variety of materials for use as CCs. CCs are typically metallic elements, such as Al, Cu, and Au [64]. In addition, inorganic compounds and metal alloys have been explored, such as TiN, Nickel alloys, stainless steel, etc. The range of the electrochemical stability voltages of CCs directly determines its application for either an anode or cathode. For example, Cu and Al are the standard CCs for anodes and cathodes. The electrochemical stability voltages of these CCs are shown in Table 1. Although various CCs have been developed recently, they are challenging to apply on

an industrial scale due to their poor mechanical strength and (electro)chemical stability. Poor adhesion between the surface of CCs and the electrode materials is also a significant contribution. The next generation of TFLIBs is aimed at achieving a higher capacity, longer lifespan, environmental protection, and economic price. This requires CCs to exhibit higher electrochemical stability, higher conductivity, lighter weight, and lower price. To enhance the performance of CCs, various approaches have been explored, including the design of an artificial layer on the CC's surface, the optimization of materials, and the structure of CCs.

Table 1. Various thin film current collectors for different electrodes.

Current Collectors	Electrode	Electrolyte	Voltage Window	Reference
Au	cathode	1 M $LiClO_4$ in PC 1 M $LiPF_6$ in EC/DMC	3–5 3–4.4	[65]
Ag	cathode	1 M $LiClO_4$ in PC 1 M $LiPF_6$ in EC/DMC	3–3.7	[66]
Al	cathode	1 M $LiClO_4$ in PC 1 M $LiPF_6$ in EC/DMC	1.5–5.5 1.5–5	[65]
Ni	cathode	1 M $LiPF_6$ in EC/DMC	3–4.5	[67]
Stainless steel	cathode	1 M $LiPF_6$ in EC/DMC	3–4.5	[68]
Stainless steel	cathode	1 M $LiPF_6$ in EC/DMC	1.5–5.5	[69]
Cr	cathode/anode	1 M $LiPF_6$ in EC/DMC	0–4	[70]
Ti	cathode/anode	1 M $LiPF_6$ in EC/DMC	0–4	[70]
TiN	cathode/anode	1 M $LiPF_6$ in EC/DMC	0–4.12	[69]
Carbon fiber paper	cathode/anode	1 M $LiPF_6$ in EC/DMC	1.5–3	[71]
Stainless steel	cathode/anode	1 M $LiPF_6$ in EC/DMC	2–3.4	[72]
Fe	anode	1 M $LiPF_6$ in EC/DMC	0–3.2	[70]
Cu	anode	1 M $LiPF_6$ in EC/DMC	0–3	[70]

3.1.1. Surface Coatings

The coating is a simple method to enhance the conductivity and corrosion resistance of CCs to obtain a better performance. Surface coatings have been extensively studied to protect CCs from corrosion. Compared to adding a corrosion inhibitor to the electrolyte, coating layers can provide better protection because thicker layers can be formed on the current collector surface by controlling the deposition process and composition. However, the coating may result in higher contact resistance between the electrodes and the CC surface. The coating should inhibit corrosion and prevent the increase in contact resistance. Recently, many materials have served as a coating on CC surfaces to improve the performance, such as carbon [73], Ag [74], Ni [75], ZnO [76], and CuO [77]. Carbon materials are excellent coating layers; they enhance the rate performance, reduce the internal resistance, and maintain long-term cycling capacity retention, while also providing corrosion protection and significantly improving the thermal conductivity [73].

Large-area few-layer graphene films were also coated on an Al current collector by CVD to achieve a LIB with a higher rate performance and cycling stability [78]. $LiCoO_2$ (LCO) was papered as an active material to measure the electrochemical performance. It was found that three-layered graphene demonstrated the highest electrochemical performance and corrosion resistance, and the capacity retention is 82.9% after 100 cycles, which is a substantial increase over the Al current collector (75.8%). Graphene film was also coated on Cu current collectors via LPCVD. The graphene-Cu composite was demonstrated to effectively decrease the internal resistance, as well as enhance the $Li_4Ti_5O_{12}$ (LTO) anode material's utilization efficiency. This improves the specific discharge capacity, rate capability,

and cycle life, particularly at high current densities [79]. At a high C-rate (10 C), the LTO electrode achieved a capacity retention of 32%, with a modified current collector higher than LTO with bare Cu. Additionally, metals and metal oxides are good candidates to serve as coating layers.

3.1.2. Alloyed Current Collectors

In addition to the surface modification of the original collector, many new collector materials with excellent performance have been recently explored. The exploration of new-type current collector materials is mainly divided into three directions:

(1) Alloy CCs with transition metals, such as Ni, Cr, and Fe, to improve the mechanical strength and stability and to have a wider range of electrochemical stability voltages. TiN has emerged as a potential candidate for current collectors and can be produced through the magnetron sputtering of a Ti target under a nitrogen-argon atmosphere. Researchers have noted that TiN is a promising cathode current collector for high-voltage LIBs and has demonstrated superior oxidative stability in $LiPF_6$ and lithium bis(fluorosulfonyl)imide (LIFSI) electrolytes compared to other current collectors, such as Al or stainless steel [76,80].

(2) Enhance the ability of electrode materials to accommodate volume changes in order to maintain better contact with the electrode material, thereby improving the cyclability. TiNi alloys have recently received considerable attention because of their super-elastic and shape memory properties [81]. The super-elasticity of TiNi alloys is attributed to a stress-induced reversible martensitic transformation. A 50.3Ti–49.7Ni thin film prepared by DC sputtering was utilized as a current collector for Si film electrodes. The designed Si/TiNi electrode demonstrated a high initial columbic efficiency of 87%. Furthermore, the Si/TiNi film electrode achieve a high-capacity retention (46% for the first cycle) for up to 50 cycles, compared to Si film using a Cu current collector (28%). In addition, the electrochemical properties, cycle performance, and structural stability of the Si/TiNi electrode were significantly improved compared to Si electrodes using conventional Cu foil current collectors.

(3) Exploring low-density current collectors with high conductivity and a large surface area to improve the specific energy density. Carbon-based materials are of interest due to their lower density, superior flexibility, and chemical stability compared to metals. For this reason, several carbon-based CCs have been proposed, including reduced graphene-oxide films, carbon nanotube films, and graphene-coated films, to enhance the energy density and cycle stability [82]. Shichun Mu et al. developed a flexible, lightweight graphite film (GF) through the direct carbonization and graphitization of polyimide films (PI) (Figure 3a) [83]. The GF possesses an extraordinary planar conductivity ultrahigh electrical conductivity, of $1.07 \cdot 10^{-6}$ $S \cdot m^{-1}$, and low surface sheet resistance, resulting from its high planar oriented structure. It displayed an outstanding cycling performance (142.31 $mAh \cdot g^{-1}$ at 2.0 C), with a capacity retention of 71.80% after 1000 cycles in the CSi half-cell, showing a 13.82% improvement over that using the Cu collector. In addition to maintaining the same stable cycling performance as metal current collectors, the extremely light weight of graphite films also resulted in a more than 25% improvement in the electrode gravimetric energy density (332 $Wh \cdot kg^{-1}$) than that (260 $Wh \cdot kg^{-1}$) of $LiCoO_2$ | | CSi full-cell with Cu and Al current collectors (Figure 3b).

3.1.3. 3D-Current Collectors

The surface of the CC exhibits a high specific surface area to enhance the adhesion of electrode materials to the CCs and increase the contact area. The CC's surface should not be flat and should be modified to increase its surface area. To enlarge the surface area of CCs, surface treatment methods with different surface morphology have been developed. The 3D surface structures were fabricated using an anodization process, chemical etching, and microscale lithographic technology. The honeycomb-like surface of the aluminum current collector is etched by an anodization process in sulfuric acid and phosphoric acid mixed solution to achieve sufficient electrical contact between the electrodes and CCs [85].

It was shown that the contact between the cathode and Al CCs improved by 23% after anodization. After the surface treatment, the corrosion current peak reduces from 0.267 to 0.022 mA·cm^{-2}. The capacity retention of the $LiCoO_2$ electrode with an oxidation-treated aluminum current collector is 6.3% higher than with untreated aluminum foil at 5 C after 500 cycles. In addition, dendritic copper current collectors have been prepared by hydrogen evolution reactions (Figure 3c) [84]. The high surface structure of the dendritic copper collector promotes the migration of Li-ions, intending to inhibit the growth of Li dendrites. Compared to the planar copper foil, the dendrite copper foil exhibits low interface resistance and the stable Li-electrodeposition dendritic copper current collector showed low voltage hysteresis when driven stably without short circuit issues. A long cycle life of 500 h at 1 mAh·cm^2 was achieved in a symmetric performance, which resulted in a good cycling performance and cycle stability. A Li-metal anode with the cell also showed an excellent full-cell cycling performance during 40 cycles.

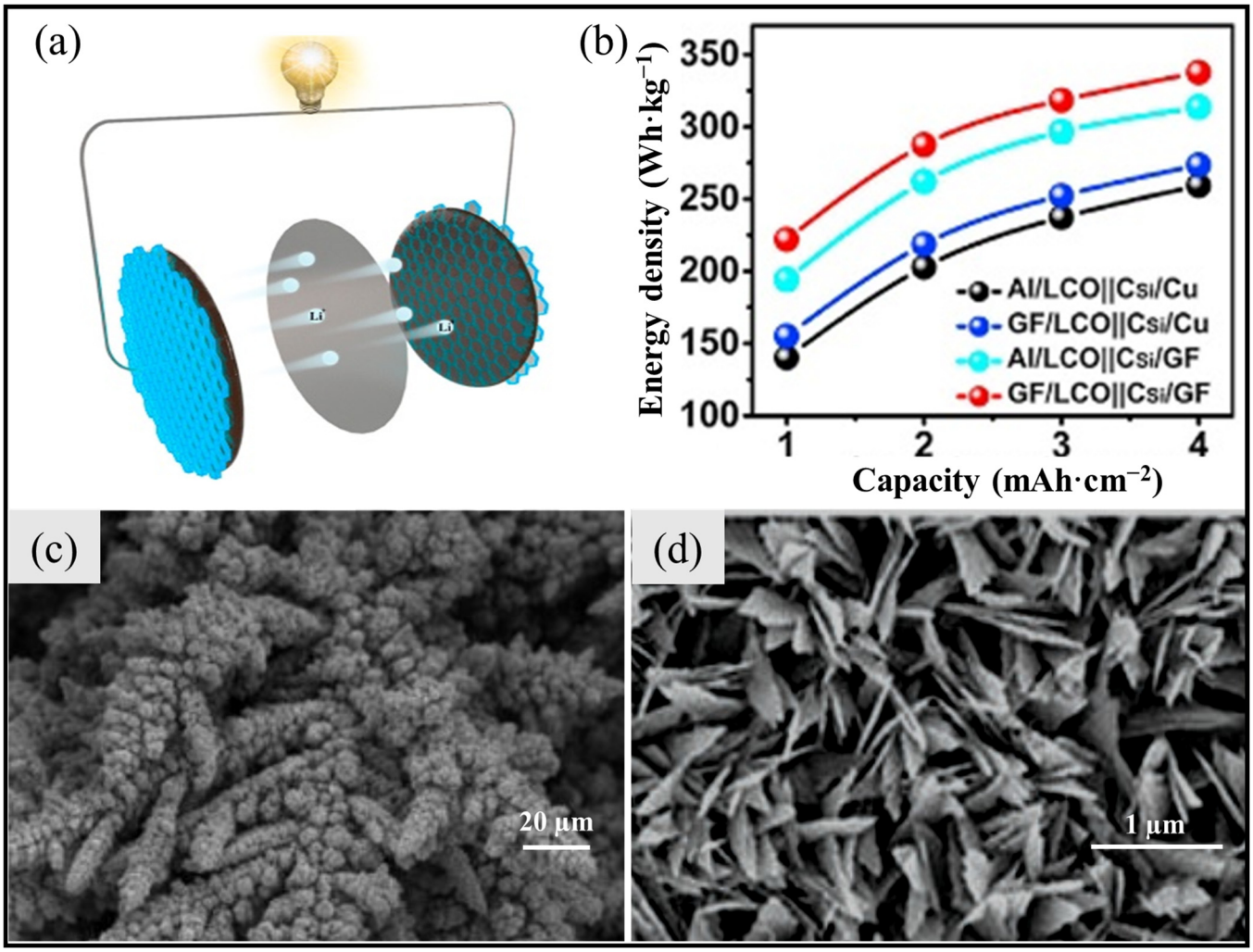

Figure 3. (**a**) Schematic diagram of graphite film | | Li cells; (**b**) Electrode energy density change with increasing area capacity of $LiCoO_2$ | | Csi full-cells with different current collectors [83] (**c**) Scanning electron microscopy images of a dendritic copper current collector [84]. (**d**) Top and side views of VA-CuO-Cu current collectors [77].

Chemical etching is also an effective treatment for current collectors to achieve a rough surface and better performance. Yang et al. designed vertically aligned CuO nanosheets on planar Cu CCs by simple wet chemical reaction (Figure 3d) [77]. The integration of the CuO array and Cu ensures good electron transfer. The vertical arrangement of channels

between CuO nanosheets ensures the rapid diffusion of ions and reduces the local current density. The nanosheet structure of CuO remains unchanged and keeps good contact with the Cu collector during the cycle. An average CE of 94% can be maintained for 180 cycles in a VA-CuO-Cu | | Li half-cell. The average CE of 92% can still be maintained with a CuO-Cu current collector with a high current density of 3 $mA \cdot cm^{-2}$. An assembled full cell with a $LiFePO_4$ cathode and Li@VA-CuO-Cu as the anode delivered a capacity retention of 81.3% over 300 cycles.

In recent years, micro-scale lithography technology has been widely applied to produce three-dimensional surface structures. This technique can accurately control the surface morphology and etching rate. A surface-patterned cellular Cu@CuO composite current collector with a hexagonal blind hole array has been synthesized by lithography and solution immersion [86]. The results show that the batteries with the cellular Cu@CuO current collector maintain a reversible charge capacity of 354.1 $mAh \cdot g^{-1}$ at 100 $mA \cdot g^{-1}$, even after 200 cycles. Compared to the Cu-based CCs with a hexagonal blind hole array and bare Cu current collector, the new pattern gains a performance improvement in the reversible capacity, respectively, by 27.9% and 153.2%. The improved electrochemical property of the cellular Cu@CuO current collector is ascribed to the strengthened adhesion with the active materials, reduced contact resistance, and improved Li-ion diffusion capability. Fabricating a 3D collector is an efficient method to obtain excellent collector materials that can effectively improve the stability and enlarge the contact area between the current collector and the electrodes. This, in turn, improves the (dis)charge rate of the batteries. More importantly, the 3D collector can be applied to fabricate 3D batteries, which will significantly improve the energy density.

3.2. Anode Materials

The anode material influences the first cycle efficiency and cycling performance of TLIBs and directly determines the batteries' capacity. The development goals of anode materials are an impressive specific capacity, excellent cycling stability, and low price. Based on the underlying reaction mechanism, anodes can be divided into three groups [87]: intercalation, alloying, and conversion materials.

(1) Intercalation anodes lead to an outstanding cycling ability as the volume change during the reaction is not apparent. However, their capacities are relatively low. The most typical intercalation anode material is carbon. Carbon materials combine good electrical conductivity with high crystallinity and stable charging and discharging behavior. It is currently the most commercialized anode material for LIBs.

(2) Alloying anodes can deliver a very large capacity, but the volume expansion during cycling limits their cycling ability. They mainly include metal anodes, such as Si, Ge, Sn etc.

(3) Conversion anodes mainly refer to transition metal oxides, sulfides, nitrides, phosphides, and fluorides, such as Fe, Mn, Co, Ni, Cr, and Cu. There is no place for Li-ion insertion and extraction in their spatial structure. Therefore, they do not conform to the traditional Li-ion insertion and extraction mechanism. The reaction with Li-metal at room temperature has been considered irreversible. However, conversion anodes provide specific capacities, around 1000 $mAh \cdot g^{-1}$ or even larger, nearly twice that of graphite. In this part, we will review the most popular anode materials of recent years.

3.2.1. Li-Based Anodes

Li-metal has long been recognized as an optimal anode material for rechargeable batteries, owing to its exceptionally high theoretical capacity (3860 $mAh \cdot g^{-1}$) and its extremely low negative electrochemical potential (−3.040 V vs. SHE) [88]. Unfortunately, Li-metal is prone to precipitate as dendrites during charging when used as an anode material. The formed Li-dendrites pose a significant risk of short circuits because they can penetrate the separator to cause short circuits. Moreover, isolated Li-metal will be produced during the discharging process, which inevitably reduces the performance [89]. The formed Li-dendrites cause many severe problems, mainly including (Figure 4a): (1) Cell

short circuits; (2) Aggravation of adverse reactions; (3) Dead-Li growth; (4) Increased polarization; and (5) Large volume changes [90]. Many approaches have been put forward to make Li-metal anodes feasible in LIBs, including electrolyte additives [91], solid-state electrolytes [92], artificial solid electrolyte interphase (SEI) [93], and structured anodes [94]. In the past, many reviews have systematically summarized how to improve the Li-metal anode performance. In this section, the most recent progress in the surface modification of Li-metal and Li-alloyed anodes will be reviewed.

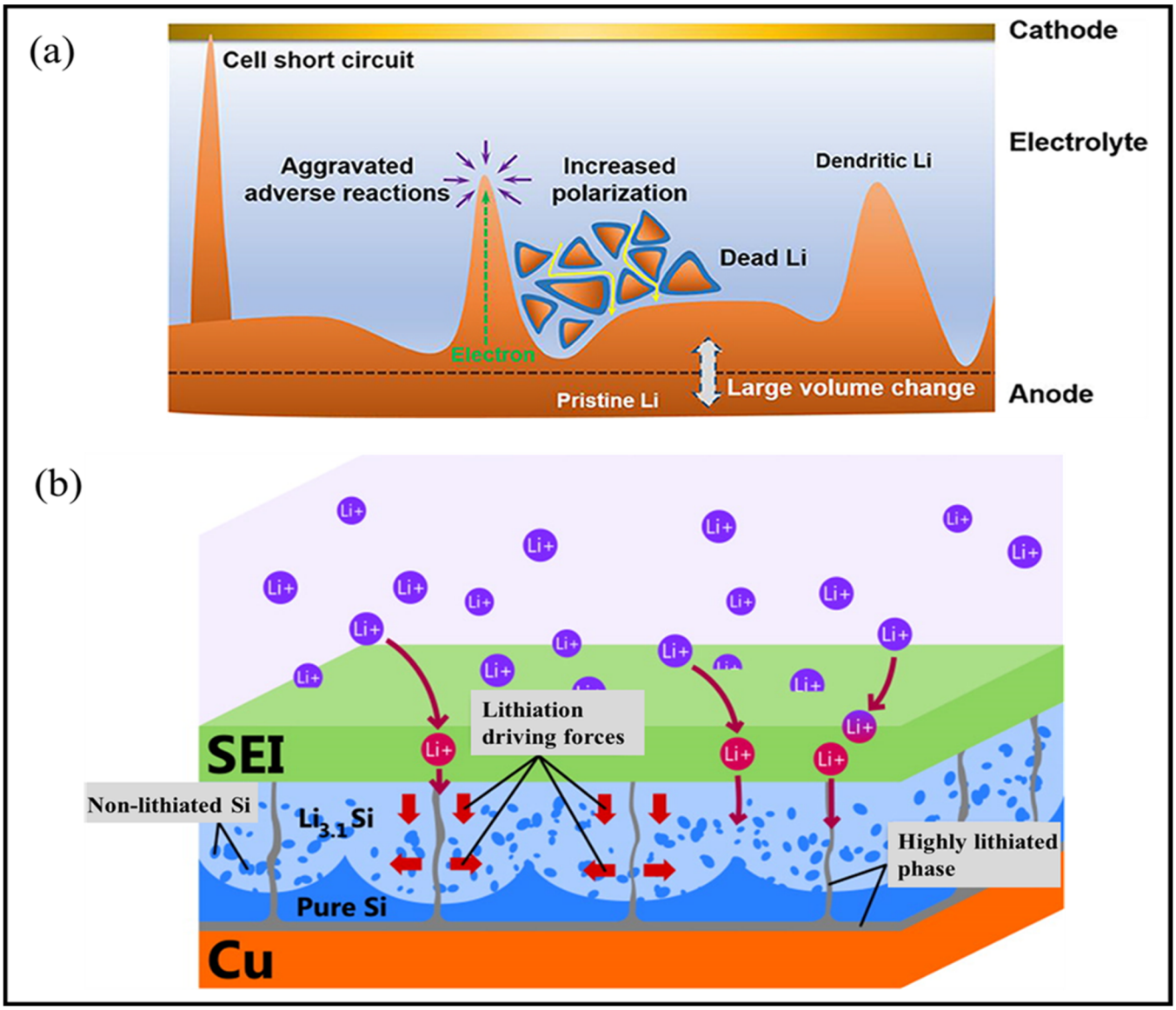

Figure 4. Scheme of the dilemma of Li-metal anodes (**a**) [90]; and Si thin film anodes (**b**) in rechargeable batteries [95].

Surface Modification of Li-Anodes

Many methods have been developed for TFLIBs to prepare a robust artificial film before cell operation. These methods have been proven in practical approaches to improve SEI layers and suppress the Li-dendrites formation. Chemical and physical methods can be used to construct artificial SEI layers. The chemical approaches mainly include gas and liquid treatments. Koch et al. have shown that a passivation layer Li_3N can be deposited on the Li-metal surface by reacting with N_2 at room temperature. The formed Li_3N layer exhibits better stability and forms good protection for Li-metal [96]. In addition to gas

treatment, liquid treatment is another effective method to coat a protective film on the surface of the Li-anode. Li et al. prepared an artificial SEI layer with a uniform distribution of Li_3PO_4 through an in-situ reaction of polyphosphoric acid with Li-metal and its native film [97]. The Li_3PO_4 layer can promote the Li-ions' transportation between the Li-metal anode and SSE's interface and induce a smooth surface with a high Young's modulus. This is sufficient to hinder the growth of Li-dendrites by mechanical protection.

Advanced thin film manufacturing methods, such as PVD, CVD, and ALD, can minimize the corrosion of Li-metal in the air during processing and meet the challenge of the low melting point of Li-metal. This is promising to control the coating thickness, uniformity, consistency, and defect density more accurately. Many inorganic materials with strong mechanical strength have been deposited as artificial SEI films, such as carbon [98], Al_2O_3 [93], BN [99], and LiF [100]. Carbon is the most common inorganic material used as artificial SEI films, which result in the formation of a stable and durable SEI film, which effectively reduces the growth of the Li-dendrites [98]. Al_2O_3 films have often been fabricated by spin-coating or ALD. The Al_2O_3 films prepared through different physical approaches possess different structures and morphologies and have demonstrated the effective suppression of Li-dendrite growth [101]. Applying chemical vapor deposition provides another effective way to improve the interface stability of Li-metal anodes. 2D boron nitride (BN) coated on the surface of the Li-metal anode is an excellent interfacial protection layer. Dendrite-free Li-morphology is realized because its flexibility, chemical stability, and mechanical strength come from its strong interlayer bonds and ultra-thin thickness [99]. Thus, physical coating represents a straightforward and effective approach to protecting Li-metal anodes.

Li-Alloyed Anodes

It has been discovered that using inorganic materials that react with Li-metal anodes to form alloys significantly reduces the interfacial resistance. Furthermore, ultra-thin and conformal alloy coatings can enhance the solid electrolyte wettability to Li-metal. It eliminates the separation between the solid electrolytes and Li-metal [102]. The alloying reactions of Li-metal with metallic elements, such as Mg [103], Al [104], Ge [105], Sn [106], Ag [107], and Au [108], or semi-metallic elements such as C [98] and Si [104], have been explored in recent decades. Al-coated garnet deposited by electron-beam evaporation exhibits excellent wettability to Li-metal through the reaction to form an Li_xAl alloy, resulting in reduced interfacial resistance [104]. A thin Au layer is sputtered onto the polished surface of SSEs to flatten the interface further, reducing the resistance and preventing short-circuiting [108]. In addition to metallic elements, some nonmetallic elements can also react with Li-alloys. For example, a 10 nm Si coating is deposited on a garnet electrolyte by PECVD. The silicon layer is in perfect contact with the garnet and reacts with the Li-metal to create a lithiumphilic surface, which significantly reduces the interfacial resistance between the garnet electrolyte and Li-metal anode [104]. The alloying interfacial layers can effectively decrease the interfacial resistance and block the side reaction between the SSEs and Li-metal. In addition, many compounds also exhibit a high reactivity with Li-metal anode. For example, with the ultrathin, conformal ZnO film coatings, ZnO can react with Li-metal during cycling to create better contact with the garnet electrolyte surface, which leads to a significant reduction in the interface resistance [13].

3.2.2. Si-Based Anodes

Pure Si Anodes

Pure amorphous and crystalline Si both serve as negative electrode materials. However, it is reported that the crystal structure is inactive before it becomes amorphous, followed by the initial alloying with Li-ion. Obrovac et al. [109] carried out one of the earliest clarification works. They used XRD to investigate *c*-Si and observe its conversion to partially lithiated *a*-Si in the initial lithiation process. The *c*-Si was transformed into partially lithiated a-Si. Then *a*-Si crystallized to $Li_{15}Si_4$, and the fully lithiated material

existed at room temperature when the voltage decreased to 50 mV. The formed phase is known to cause high internal stresses, particle cracking, poor electrical contact, and capacity fading. However, numerous experiments and calculation results have demonstrated that the cycling performance of the Si film electrode can be improved by reducing its thickness [110–112]. Ohara et al. found the best performance of a Si thin film when the thickness was 50 nm, which maintained a high specific capacity of approximately 3100 mAh·g^{-1} and a high coulombic efficiency of 100% at 12 C after 1000 cycles [113]. This was early research on the electrochemical performance of Si thin film anodes. However, there are still some problems with pure silicon thin film anodes. The main research question is how to manage and limit the effects of the total volume change. In addition, a highly lithiated phase forms between the Si electrode and Cu CCs at the onset of the lithiation process. The fast-diffusion paths and non-lithiated Si regions are both being filled with Li^+ ions at the same time. (Figure 4b). However, pure Si films exhibit poor intrinsic electronic conductivity of 10^{-3} S·cm^{-1} and a low Li-ion diffusion rate (diffusion coefficient between 10^{-14} and 10^{-13} cm^2·s^{-1}). This limits the Li-ion diffusion rate in the whole process. Therefore, it is also important to improve the effective conductivity of silicon layers to improve the power performance of TFLIBs.

In recent years, many proposed solutions and strategies have been put forward for controlling and buffering the problems of the high-volume expansion of silicon anodes, as shown in Figure 5a. Modifying the substrate surface is very important to obtain long-term cycle stability for a pure Si thin film system. For example, the copper foil is roughened with sandpaper to enlarge the contact area with the deposited amorphous Si film and help the film with a higher tolerance with the volume changes [114]. In addition, many chemical etching methods have been used to modify the surface of silicon anodes. A substrate was etched in $FeCl_3$, which can accommodate volume changes and enhance the capacity of the Si anodes [115]. Another original method is to treat the substrate through plasma-immersion-lanthanum-ion implantation so that the capacity retention rate of the silicon film anode can reach 93% in the 80th cycle [110]. Electrodeposition, also used to obtain copper foil with a rough surface, has been utilized to enhance the performance of a-Si thin film anodes. Unfortunately, it was demonstrated that the capacity retention of the anode is only 42% after the first discharge [116].

Although the above methods can effectively modify the surface of silicon films, their shape and etching thickness cannot be accurately controlled. Therefore, patterned films obtained by lithography are an excellent surface modification strategy to accommodate the volumetric changes. The electrochemical characteristics of Si film anodes have been improved by designing a variety of novel patterns and structures. For example, lozenge-shaped tiles (Figure 5b) [118] are produced by covering the mask on the substrate surface during deposition. As a result of the good stress suppression effect between the Si tiles, the good adhesion, and the improved mechanical stability of the patterned Si anodes during (de)lithiation, a high capacity retention of 91% can be achieved after 100 cycles. The study and comparison of planar and shaped Si nanostructures clearly show the advantages of the 3D patterned electrodes, including the high specific surface area, increased current density, and improved mechanical stability. In our group, we have designed an n-type doped a-Si honeycomb structure utilizing lithography (Figure 5c). The voltage distribution of the Si anode is displayed in Figure 5d, with inserted SEM images that correspond to different Li-contents. The mechanical deformation of the honeycomb wall is caused by the internal stress generated in the lithiation process [119]; 3D patterned Si anodes can accommodate the volumetric changes effectively to maintain high capacity and improve the energy density of TFLIBs. However, there are still many aspects to be improved, including the design of the pattern shapes and the optimization of the size, which will be an excellent opportunity to design even better pure-silicon thin film anodes.

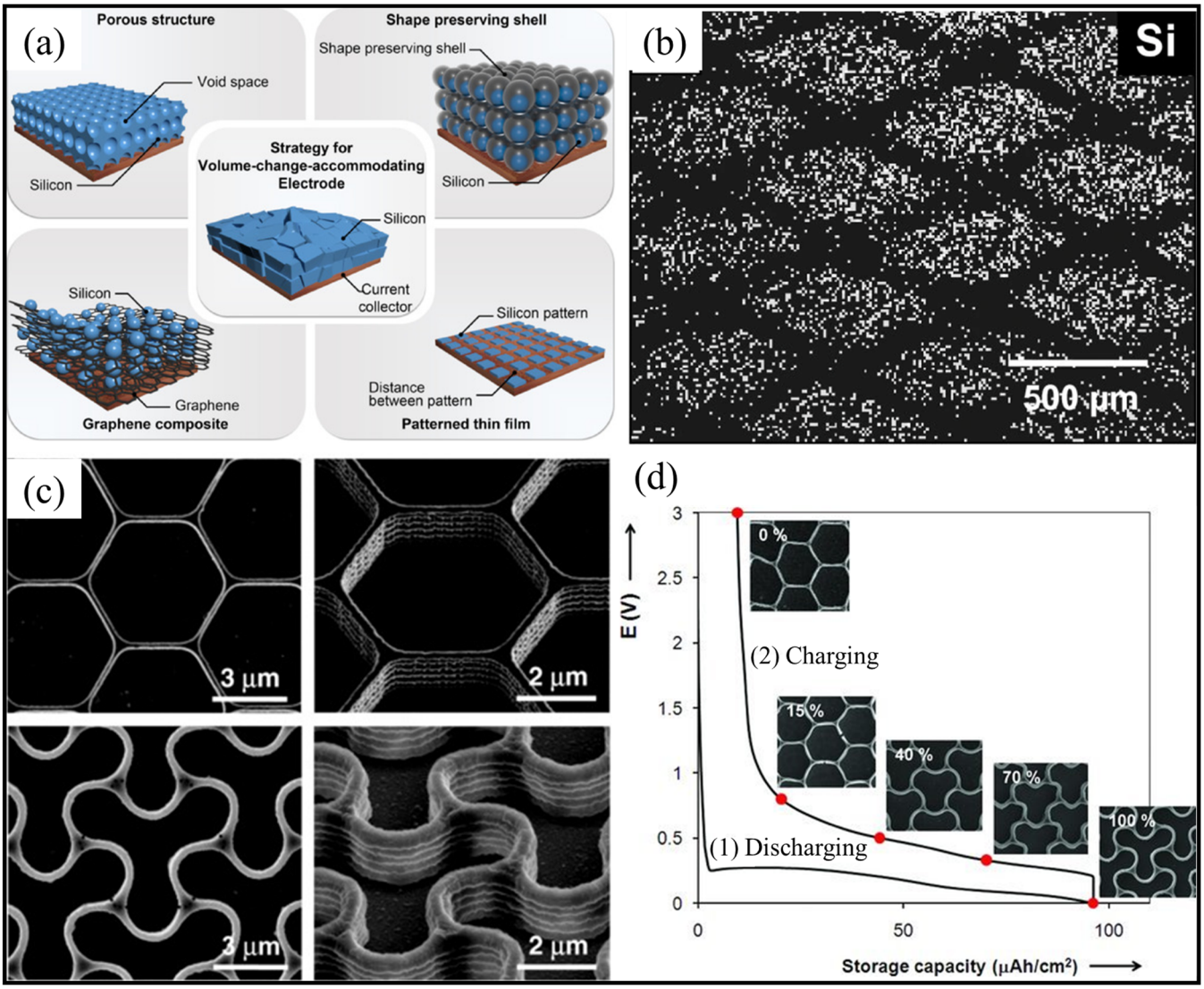

Figure 5. (**a**) Representative strategies for volume-change-accommodating Si electrode [117], (**b**) SEM photographs of patterned Si film electrodes [118], (**c**) SEM top and tilted view photographs of as-prepared (top) and fully lithiated silicon honeycomb structure (bottom). (**d**) Morphological changes of the Si honeycomb structure as a function of Li-content [119].

Composition modification is also an excellent promising approach to enhance the performance of Si electrodes. This could significantly reduce the expansion and contraction of Si anodes during (dis)charging and improve the conductivity. In recent years, there have been numerous investigations into combining active Si anodes with other elements, such as Cu [120], Mo [121], Fe [122], Al [123], B [124], Y [125], and Ti [126]. The formed metal silicide (Si-Mo, Si-Cu, Si-B, Si-Ti) films reduce the resistance, and improve the mechanical properties due to the additional chemical bonds.

It was also found that a SiN layer coated on a Si surface can effectively enhance the electrochemical performance of Si anodes. Forming a Li_3N film at the surface improves both the storage capacity and ionic conductivity. In addition, a thinner SiNx layer was more effective because SiN prevents the transport of Li^+ and the decline in capacity [127].

A conductive and mechanical buffer multilayered structure of Si anodes with interlayers of Fe, Al, Y, and Ti can accommodate volumetric changes. It is favorable for the loner cycle life of the electrodes. Sputtered Au-Ti/Si/LIPON/SnO_2 multilayered anodes with a LiPON/SnO_2 layer acting as a porous SEI layer showed no visible capacity loss over 200 cycles [128]. However, the challenge with multilayered Si-based anodes is optimizing

the thickness, density, and quantity of layers. A sufficient amount of active Si must be available, while keeping a good Li^+ diffusion rate and high CE. Although the capacity of silicon alloys and silicon composite is slightly lower than that of pure silicon, it is still higher than most other anode materials. Applying such materials can effectively enhance the ion conductivity of Si and reduce the influence of volume changes, thus improving the cycling performance.

Recently, Si oxide (SiO_x, $0 \leq x \leq 2$) has attracted much attention in developing high-performance LIBs because of its ultrahigh theoretical Li-storage capacity, low working potential, earth-abundancy, and good cycle life [129]. Si-oxide materials, including SiO, SiO_2, and nonstoichiometric SiO_x, have various electrochemical properties. The theoretical capacities of SiO and SiO_2 are 2600 and 1965 $mAh \cdot g^{-1}$, respectively [130,131]. The Li-storage capacity decreases gradually with the oxygen content in SiO_x. In addition, the volume changes of SiO and SiO_2 are smaller than that of pure silicon during (dis)charging. The SiO anode shows a small volume change of 150% after lithiation. The volume change is decreased from 300% for Si to 100% for SiO_2. With the increase in the oxygen content in silicon-based materials, the volume changes during (dis)charging decreases, and the cycle stability improves gradually.

3.2.3. Metal Oxides Anodes

Metal oxides are of great interest for TFLIBs because they can store Li-ions [132]. In addition, some metal oxides, such as iron and manganese, are naturally abundant and, thus, low-cost. The size, morphology, and orientation of metal oxide nanostructures can also be easily adjusted. This makes it possible to systematically investigate the relationship between their structure and electrochemical properties. Metal oxides can be reversibly reduced and oxidized by the following general equation:

$$M_xO_y + 2yLi^+ + 2ye^- \rightarrow xM + yLi_2O \quad (1)$$

According to the crystal structure of metal oxides, the electrochemical mechanisms of these anode materials can be classified into three types [133]: (i) Intercalation reaction: intercalated compounds, such as Li_3VO_4, LiV_3O_8, $Li_4Ti_5O_{12}$, and TiO_2; (ii) Alloy reaction: oxides, such as SiO_2, SnO_2, GeO_2, and their mixed oxide derivatives; (iii) Conversion reaction: metal oxides, such as Co_3O_4, MoO_2, Fe_2O_3, V_2O_5, and NiO. In recent years, various oxide-thin film anodes with high electrochemical performance have been synthesized for TFLIBs (Table 2). However, using metal oxides also brings several unpleasant difficulties, such as poor electrical conductivity, poor ion transportation [134], and severe volume changes [135] over the (dis)charging process. All of these factors result in the pulverization of thin film electrodes. Further efforts should be made to develop thin film metal oxide anodes to address these concerns and exploit high-efficiency electrochemical energy-storage devices.

Table 2. Various anode materials for TFLIBs.

Metal Oxides Anode	Reaction Mechanism	Initial Discharge Capacity ($mAh \cdot g^{-1}$)	Coulomb Efficiency	Reference
LTO	intercalation	313	95.0%	[136]
$TiNb_2O_7$(TNO)	intercalation	398	92.0%	[137]
$TiNb_2O_7$	intercalation	460	99.0%	[138]
$SrLi_2Ti_6O_{14}$	intercalation	175	91.4%	[139]
SnO_2	alloy	650	99.5%	[140]
LNVO	conversion	871	98.5%	[141]
$NiFe_2O_4$	conversion	849	67.7%	[142]
Co_2O_3	conversion	1235	56.0%	[143]
Fe_2O_3	conversion	951	100%	[144]

Table 2. *Cont.*

Metal Oxides Anode	Reaction Mechanism	Initial Discharge Capacity (mAh·g^{-1})	Coulomb Efficiency	Reference
MoO_2	conversion	1510	-	[145]
ZnO	conversion	1200	-	[146]
MoO_x	conversion	1118	81.8%	[147]
RuO_2	conversion	1200	33.0%	[148]
ZnOS	conversion	1271	64.1%	[149]
In_2O_3	conversion	1083	81.5%	[150]

3.3. Cathode Materials

The cathode films used in the early TFLIBs were mainly composed of binary compounds without Li-element, such as TiS_2 [151], MoO_3 [152], and V_2O_5 [153]. The preparation conditions are relatively simple, but the cycle performance is poor. They are classified as first-generation cathode films. Later, intercalation compounds were developed, such as $LiCoO_2$ [154], spinel $LiMn_2O_4$ [155], and olivine $LiFePO_4$ [156]. They have a higher voltage and show good cycling behavior. The application of these materials in TFLIBs is rapidly growing at present. The cathode films made of intercalation compounds are called second-generation cathode films. $LiCoO_2$ is widely applied in mobile electronic devices as a commercial cathode material. However, further advancement is necessary to meet the pressing demand for energy storage systems featuring high energy density and rapid charging rates. The industry requires electrode materials that demonstrate high voltage, specific capacity, and exceptional rate performance. This should be achieved through doping, exploration, and structural adjustment in the second-generation cathode materials.

3.3.1. High Voltage Cathodes

In recent years, the energy density of LIBs has been significantly improved, mainly through boosting the batteries' materials and optimally engineering the design. The energy density of LIBs is calculated by integrating the operating voltage with respect to the storage capacity. As a result, enhancing the working voltage has become a critical approach to boosting the energy density of TFLIBs. As the anode materials work at low potentials near to Li-metal, increasing the total battery voltage highly depends on the cathode materials [157]. Dependent on the voltage range, three classes of materials can be considered for cathode host materials: (1) the 3-V cathodes, e.g., MnO_2, $LiFePO_4$; (2) the 4-V cathodes, e.g., $LiCoO_2$, $LiCo_{1-y-z}Ni_yAl_zO_2$, $LiNi_{1/3}Mn_{1/3}Co_{1/3}O_2$, $LiMn_2O_4$; (3) and the 5-V cathodes such as spinel $LiNi_{0.5}Mn_{1.5}O_4$ (LMNO) and its related doped structures, olivine $LiCoPO_4$, inverse spinel $LiNiVO_4$, and fluorophosphate Li_2CoPO_4F [158]. Only when 5 V cathode materials are used, the energy density of Li-ion batteries can reach the industrial requirement of 500 Wh·kg^{-1}. This section reviews the recent development of LMNO and $LiCoPO_4$, the most commonly used high-voltage cathode materials.

Spinel $LiNi_{0.5}Mn_{1.5}O_4$ (LMNO) is considered to be an excellent cathode for next-generation TFLIBs for EV and grid-scale electric device applications because of its impressive working voltage of ~4.7 V (vs. Li^+/Li), low price, long cycle life, and excellent rate performance [159]. However, several issues and challenges continue to be significant in the development of LMNO: (1) the unstable SEI formation at high operating voltages; (2) the dissolution of Mn during electrochemical cycling; and (3) the structural transition from the LiM_2O_4-type spinel structure to M_3O_4-type spinel, and rock-salt structures at the surfaces [160]. Numerous endeavors have been undertaken to enhance the electrochemical characteristics of LMNO, such as doping, controlling morphology, particle size, the degree of cation ordering, and surface modification [161].

Among these solutions, surface modification is the most efficient and simple way to prevent harmful side reactions upon the electrochemical cycling of thin-film LMNO, which enhances the overall capacity and cycle life. An efficient surface passivation layer prevents the direct contact of the active particles with the electrolyte. It suppresses the phase

transition and side reactions at the particle surface, thus significantly enhancing the electrochemical performance of the cathode materials. The coating compound materials mainly include metal oxides (Al_2O_3 [162], TiO_2 [163], ZnO [164]), metal fluorides (MgF_2 [165], AlF_3 [166], CeF_2 [167]), polyanionic compounds (Li_3PO_4 [168], $LiFePO_4$ [169], Li_2SiO_3 [170], LiPON [171]), and carbon-based materials (carbon [172], graphene oxide [173]). The coating layers minimize the harmful side reactions between LNMO and the electrolyte to enhance the reversible (de)intercalation of Li-ions in the (dis)charge process. For example, an Al_2O_3-modified LMNO thin-film electrode prepared by PLD exhibits excellent (dis)charge performances when elevated at room temperatures. It delivers a discharge capacity of 126.3 mAh·g^{-1} after 100 cycles at 25 °C, corresponding to 95.4% of its initial value. Even at 55 °C, 84.1% of its initial discharge capacity can be maintained at the 100th cycle, and the rate capability has also been improved substantially [162]. The coating can also increase the ionic conductivity of LMNO. Lv et al. [171] coated an ~15 nm amorphous LiPON thin film onto an LNMO thin film electrode by magnetron sputtering. It was shown that the LNMO/LiPON electrode exhibited stable reversible capacities (higher than 105 mAh/g) following cycling to 4.9 V after 150 cycles. LiPON serves as the artificial interface film, allowing Li-ions to diffuse through and suppress the formation of a thick insulating surface. EIS studies of such electrodes show lower interface and charge transfer resistances with lower electrode polarization. The uniformly distributed LiPON film on the LNMO cathode surface can separate the direct contact between the LNMO and electrolyte, inhibit the side reactions of Mn dissolution, and provide a stable interface for ionic transport. The LiPON coating on LNMO formed a space charge layer, maintaining a slightly higher manganese ion valence state.

Doping is also an excellent approach to enhance the Li-ion conductivity and structural stability by introducing different ions in the cathode host materials [174], mainly including metal cations such as Al^{3+} [175], Cr^{3+} [176], Co^{3+} [177], Fe^{3+} [177], and Ru^{4+} [178]. It was found that doping different ions will have different effects. For example, Mg-doped LNMO is reported to possess lower polarization, enhance Li-ion conductivity at room temperature, and induce good stability upon cycling, even at high C-rates. Cr-doped material results in better chemical and structural stability with less Jahn–Teller distortion for the Cr-doped spinel materials. Due to it having a smaller lattice parameter, the co-doped LNMO has more improved electrochemical properties than LNMO. Fe doping can promote the enrichment of specific surfaces and suppress the formation of thick SEI films, significantly enhancing the electrochemical performance of 5 V spinel cathode materials. In addition to doping metal ions, the performance of LNMO can also be improved by substituting anions for O. It was shown that fluorine doping can improve the electrochemical properties. It can suppress the formation of NiO impurity and simultaneously reduce the voltage polarization [179].

Olivine-structured $LiCoPO_4$ (LCP) has attracted considerable interest as a potential cathode material for LIBs due to its high redox potential (4.8 V vs. Li^+/Li) and theoretical capacity (167 mAh·g^{-1}) [180]. However, LCP exhibits some unsatisfactory characteristics, including low specific capacity, poor cycle stability, and poor rate performance. Through surface modification, ion doping, particle size reduction, and morphology control [181–183], great efforts have been taken to enhance the electronic and ionic conductivity of $LiCoPO_4$. Surface modification is a common strategy to enhance the cycling stability of the LCP cathode by protecting the LCP from direct contact with electrolytes. This inhibits surface degradation caused by the HF attack induced by electrolyte decomposition [184]. Many materials have been used to modify the surface of LCP to enhance its electronic conductivity and electrode stability; examples of this are carbon [185], NiO [186], and AlF_3 [187]. An LCP was coated with an 8–10 nm continuous NiO layer, which can reduce the volumetric stresses and strains that occur during Li^+ insertion and extraction.

3.3.2. High-Capacity Cathodes

Cathode materials essentially limit the battery's storage capacity because many high-capacity anode materials already exist, such as Li-metal and Si. To improve the output

capacity of TFLIBs, it is therefore essential to explore new promising high-capacity cathode materials. Recently, many novel crystal structure cathodes have been reported, as shown in Figure 6 [188]. Layered transition metal (TM) oxides are considered very promising cathode materials, with high energy density, owing to their high theoretical capacity (~280 mAh·g^{-1}) compared with that of olivine (~170 mAh·g^{-1}) or spinel (~150 mAh·g^{-1}) [189,190]. The most common layered cathode material is $LiCoO_2$ (140 mAh·g^{-1}). However, an $LiCoO_2$-layered oxide can only provide a limited practical capacity due to its narrow potential window (~4.3 V vs. Li/Li$^+$). Recently, Li- and Ni-rich layered oxide materials have received more attention compared to other layered cathodes, owing to their high capacities. The capacities of Li-rich and Ni-rich layered materials are between approximately 1.25 and 1.5 times higher than that of the relatively low Ni content layered materials, such as the commercialized $LiNi_{1/3}Co_{1/3}Mn_{1/3}O_2$ (160 mAh·g^{-1}) [188]. In recent years, many high-capacity thin-film cathode materials have been explored. An overview is given in Table 3.

Table 3. Various cathode materials for TFLIBs.

Metal Oxides Anode	Crystal Structure	Capacity	Voltage Range (V)	Rate Performance	Reference
V_2O_5	Layer	142 mAh·g^{-1}	2.5–4.0	86.7 mAh·g^{-1} at 56 C	[191]
LiV_2O_5		36 μAh·cm^{-2}·μm^{-1}	2.4–3.6		[192]
HT-$LiCoO_2$	Layer	135 mAh·g^{-1}	3.0–4.2	103 mAh·g^{-1} at 10 C	[193]
$LiNiO_2$	Layer	23 μAh·cm^{-2}·μm^{-1}	2.8–4.2		[194]
$LiNi_{0.8}Co_{0.2}O_2$	Layer	125 mAh·g^{-1}	2.8–4.4		[195]
Li_2MnO_3	Layer	267 mAh·g^{-1}	2.0–4.8	147.84 mAh·g^{-1} at 9.3 C	[196]
$LiNi_{0.8}Co_{0.15}Al_{0.05}O_2$ (NCA)	Layer	197 mAh·g^{-1}	2.5–4.2		[197]
$LiNi_{1/3}Co_{1/3}Mn_{1/3}O_2$ (NMC333)	Layer	177 mAh·g^{-1}	2.8–4.5	60 mAh·g^{-1} at 2 C	[198]
$LiNi_{0.5}Mn_{0.3}Co_{0.2}O_2$ (NMC532)	Layer	167 mAh·g^{-1}	3.0–4.5		[199]
$LiNi_{0.6}Mn_{0.2}Co_{0.2}O_2$ (NMC622)	Layer	79 mAh·g^{-1}	2.5–4.5		[200]
$Li_{1.2}Mn_{0.55}Ni_{0.15}Co_{0.1}O_2$	Layer	250 mAh·g^{-1}	2.0–4.8		[201]
$LiMn_2O_4$ (LMO)	Spinel	82 mAh·g^{-1}		67 mAh·g^{-1} at 348 C	[202]
$Li_{0.92}Co_{0.65}Mn_{1.35}O_4$	Spinel	340 mAh·g^{-1}	1.6–4.5	268 mAh·g^{-1} at 10 C	[203]
$LiCoMnO_4$	Spinel	107 mAh·g^{-1}	3.0–5.0		[204]
$LiNi_{0.5}Mn_{1.5}O_4$	Spinel	117 mAh·g^{-1}	3.0–5.0	108 mAh·g^{-1} at 10 C	[205]
$LiMnPO_4$	Olivine	24 mAh·g^{-1}	3.5–4.4		[206]
$LiFePO_4$	Olivine	159 mAh·g^{-1}	3.0–4.0	153 mAh·g^{-1} at 7.5 C	[207]

Li-rich oxides (Figure 6a) possess higher specific capacities (>250 mAh·g^{-1}) and energy densities (>900 Wh·kg^{-1}), which meet the requirements of the next-generation rechargeable TFLIBs [208]. The high capacity is provided by the accumulated cation and anion redox reactions of the Li-rich oxides. The high manganese content ensures good safety and low cost. Li-rich oxides are a group of lithium transition metal oxides ($Li_{1+x}TM_{1-x}O_2$) with a Li/TM ratio greater than 1 ($0 < x < 1$), such as Li_2MnO_3 (200 mAh·g^{-1}) [209], Li_2RuO_3 (270 mAh·g^{-1}) [210] and Li_3IrO_4 (340 mAh·g^{-1}) [211]. In recent years, a lot of novel materials with high capacity have been designed and synthesized by partially replacing the Li and TM elements in Li-rich oxides, such as $Li_{1.9}Cr_{0.3}Mn_{0.8}O_3$ (250 mAh·g^{-1}) [212] and $Li_{1.144}Ni_{0.136}Mn_{0.544}Co_{0.136}O_2$ (301 mAh·g^{-1}) [213]. However, layered Li-rich cathode materials still face severe problems, such as a low initial coulombic efficiency, severe

voltage decay, significant capacity losses, poor rate capability, and transitional metals dissolution [214]. In recent years, a variety of approaches have been explored for improving the electrochemical performance of Li-rich oxide cathodes. Substitution/doping and coating are two of the main strategies to improve the electrochemical performance. Different elements and radicals, such as Mg [215], Al [216], Ti [217], Zn [218], Sn [219], Y [220], B [221], F [222], and Cl [223], have been introduced into the framework of layered Li-rich oxides. Both TM-site substitution and surface substitution/doping improve the initial CE, rate capability, and cycling stability. For example, substitution/doping with ions that possess a large ionic radius (e.g., K^+) or high electronegativity (e.g., F^-) can hamper the migration of the TM ions, and thus mitigate the voltage decline. In addition to doping, a great variety of materials have been selected to modify the surface of layered Li-rich oxides, such as oxides [105], fluorides [224], phosphate [225], and silicates [226]. The main function of such protective coatings is to reduce the direct contact between the cathode and electrolytes, thus reducing the parasitic electrolyte oxidation and TM dissolution. It has also been observed that the coatings in the layered Li-rich oxides can delay the structural changes near the surface. As a result, such coatings usually result in longer cycle life materials.

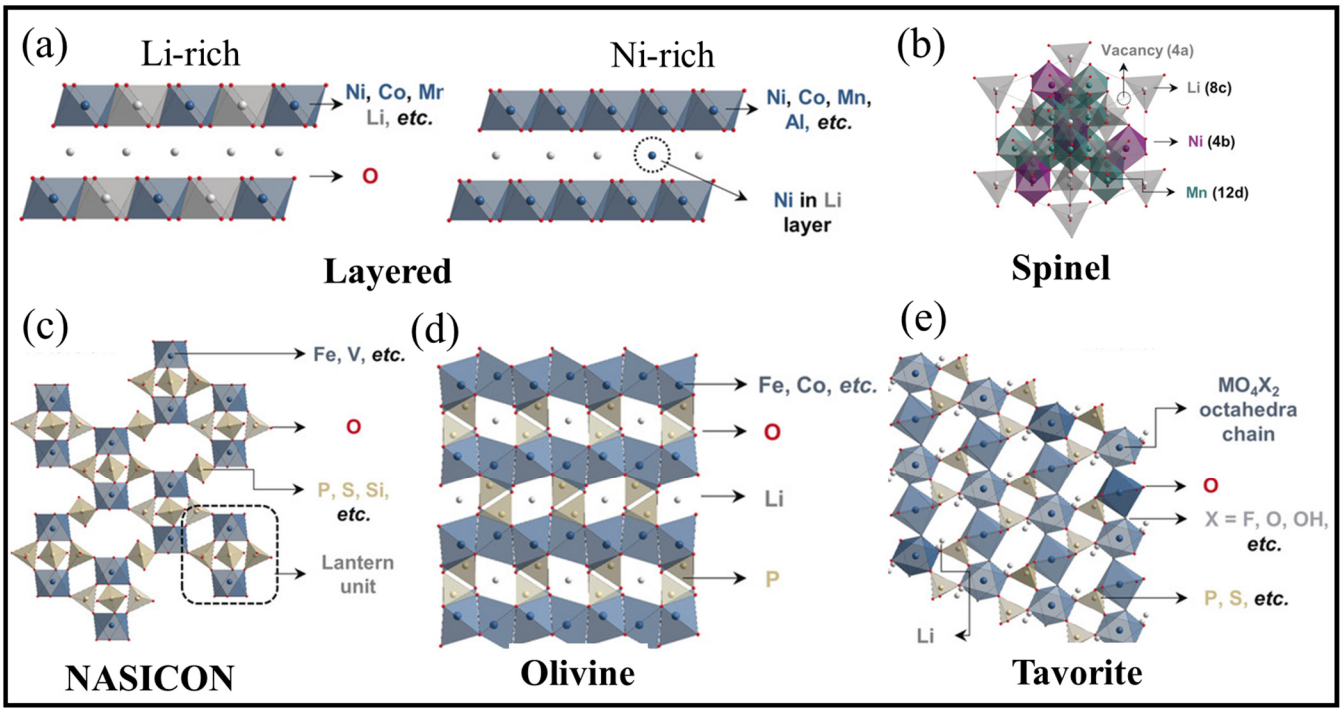

Figure 6. Schematic representation of the crystal structure of various cathode materials: (**a**) layered, (**b**) spinel, (**c**) NASICON, (**d**) Olivine, and (**e**) Tavorite [188].

Ni-rich layered oxide is another interesting cathode material for high-capacity TFLIBs, and has attracted significant attention. $LiNiO_2$ is the most typical representative of Ni-rich layer oxides. It shows a higher discharge capacity of >220 mA·h g^{-1} and a lower cost than $LiCoO_2$ [227]. However, the difficulty in synthesis, serious Li/Ni cationic mixing, and poor thermal stability of $LiNiO_2$ hinder its commercialization. Many transition-metal dopings have been developed to partially replace Ni and resolve the problems of $LiNiO_2$ [228]. The most successful solutions are ternary layered oxides, $LiNi_xCo_yMn_{1-x-y}O_2$ (NCM) [229], or $LiNi_xCo_yAl_{1-x-y}O_2$ (NCA) [230]. They generally exist in particles and are essential as high-performance cathode materials. During the charging (oxidation) process, the oxidation of NCM starts with Ni^{2+} to Ni^{3+}, followed by Ni^{3+} to Ni^{4+}, and finally, Co^{3+} to Co^{4+}. For Mn^{4+}, it remains electrochemically inactive. In general, the oxidation of Ni^{2+} to Ni^{3+}/Ni^{4+} occurs at relatively low operating potentials (<4.3 V vs. Li^+/Li). The oxidation of Co^{3+} to Co^{4+} only appears above 4.3 V [231]. As the applied upper cut-off

voltage is often below 4.3 V, Ni-rich layered oxides' capacity mainly originates from Ni's redox chemistry [232]. Therefore, by increasing the Ni content and reducing the Co and Mn content, Ni-rich layered oxides provide higher capacity (e.g., $LiNi_{0.6}Mn_{0.2}Co_{0.2}O_2$ (NCM622): ∼180 mAh·g^{-1}, $LiNi_{0.8}Mn_{0.1}Co_{0.1}O_2$ (NCM811): ∼200 mAh·g^{-1}). However, this occurs at the expense of the capacity retention and thermal stability [233].

Although these Ni-rich layered oxides exhibit high capacities, many problems and challenges hinder their practical applications. It can be summarized as follows [234]: (1) Residual Li-compounds. The existence of residual Li compounds leads to the gelation of polyvinylidene difluoride binders during electrode preparation; (2) Microcracking of particles. During the (dis)charging process, the microcracks are caused by anisotropic lattice distortion and mechanical strain related to the different phase transitions, especially in Ni-rich layered oxides with more than 80% nickel content; (3) Rock-salt phase formation. The electrolyte infiltrates the microcracks and forms an excessive interface layer between the positive electrode and electrolyte. These problems result in the loss of the active transition metals (decreased capacity and working voltage) and the migration of the transition-metal ions to the anode. This affects the optimized capacity ratio of the cathode and anodes and increases the impedance of the solid electrolyte interphase.

To date, many methods have been used to solve the issues of Ni-rich layered oxides and improve their electrochemical performance, including primary particle engineering, surface coatings, doping, and concentration gradient designs. For thin-film battery systems, surface coatings are a simple and effective method. Introducing coating materials onto the surface of Ni-rich layered oxides avoids direct contact with the electrolyte, thus minimizing the parasitic reactions. It also sets a kinetic barrier to O_2 evolution. Different types of surface coating materials, such as oxides (Al_2O_3, ZrO_2, TiO_2, and Co_3O_4), fluorides (AlF_3), and phosphates (Li_3PO_4), have been reported [235].

Moreover, the electrochemical inactive coating materials inevitably reduce Ni-rich layered oxides' capacity and energy density. In addition, advanced technologies to deposit these coating materials also need to be improved to enhance the quality of the coatings. Similarly to surface coatings, bulk doping is also an effective and straightforward approach for regulating the structure of Ni-rich layered oxides and, thus, their electrochemical performance. To date, doping with a single cation, doping with a single anion, and co-doping with multiple ions have been reported to modify Ni-rich layered oxides. However, this is mainly conducted for powder batteries. It is more complicated to apply these approaches in thin-film batteries.

3.4. Electrolytes

The electrolyte is sandwiched between the positive and negative electrodes, which is critical for the optimal electrochemical stability of batteries during long-term operation. A good performance requires an impressive ionic conductivity, Li^+ transference number, and electrochemical and thermal stability. Significant mechanical strength is also desired. Until recently, the absence of liquid electrolytes working with electrochemical windows above 5 V limited the application of electrode materials. However, the recent breakthroughs in exploring inorganic solid electrolytes have opened up new possibilities for using alternative electrode materials. Excellent inorganic solid electrolytes can help gain thermal and chemical stability, impressive ionic conductivity, and prolonged cycle life [236]. The preparation method, however, strongly influences the performance of solid electrolyte films.

Moreover, the deposition rate of various elements may vary considerably. However, a stable ion-conducting structure requires various elements, generating some deposition challenges. Solid electrolytes can be divided into three development stages, according to the complexity of preparation [17,237]. The early solid electrolytes were clearly limited by the preparation methods, mostly binary compounds and their composites [238], such as Li_3N, Li_2S, and Li_2S-SiS_2-P_2S_5. Although solid-state electrolyte systems, such as GeS_2, exhibit a conductivity higher than 10^{-5} S·cm^{-1}, they are highly reactive in the humid air. Subsequently, more stable oxygen-containing inorganic salts have been developed;

examples are amorphous borate (Li_2O-B_2O_3-SiO_2), silicate (Li_2O-V_2O_5-SiO_2), and other systems called first-generation solid-state electrolytes. Although these systems are relatively easy to synthesize, they are all highly alkaline, absorb water easily and are challenging to operate. In addition, they have a low ion conductivity, which limits the development of TFLIBs.

With the development of new reactive deposition technologies, a second-generation solid electrolyte film, based on LiPON, with excellent performance has been developed [17]. TFLIBs have made considerable progress, and various battery systems and structures have been developed. With these new thin film preparation methods, which facilitate greater control of the thin-film components, such as PLD and ALD, many thin-film oxide-based electrolytes with excellent performance have gradually been obtained. These inorganic film systems can mainly be divided into four structural types: (1) Perovskite structure: $LiO_{0.33}La_{0.56}TiO_3$ ($Li_3xLa_{2/3-x}TiO_3$, x = 0.1–1) with high ionic conductivity; (2) NASICON structure: $Li_{1+x}A_xTi_{2-x}(PO_4)_3$ (LATP) with high chemical compatibility with Li-metal [239]; (3) LISICON and Thio-LISICON structure; (4) Garnet structure: $Li_7La_3Zr_2O_{12}$ (LLZO) with higher environmental stability [240]; (5) Sulfides: $Li_{10}GeP_2S_{12}$ and $Li_{9.54}Si_{1.74}P_{1.44}S_{11.7}Cl_{0.3}$ with high conductivity $1.2{\cdot}10^{-2}$ and $2.5{\cdot}10^{-2}$ $S{\cdot}cm^{-1}$ [241]. The crystal structures of these inorganic solid electrolytes are shown in Figure 7, which are regarded as third-generation solid electrolyte membrane systems.

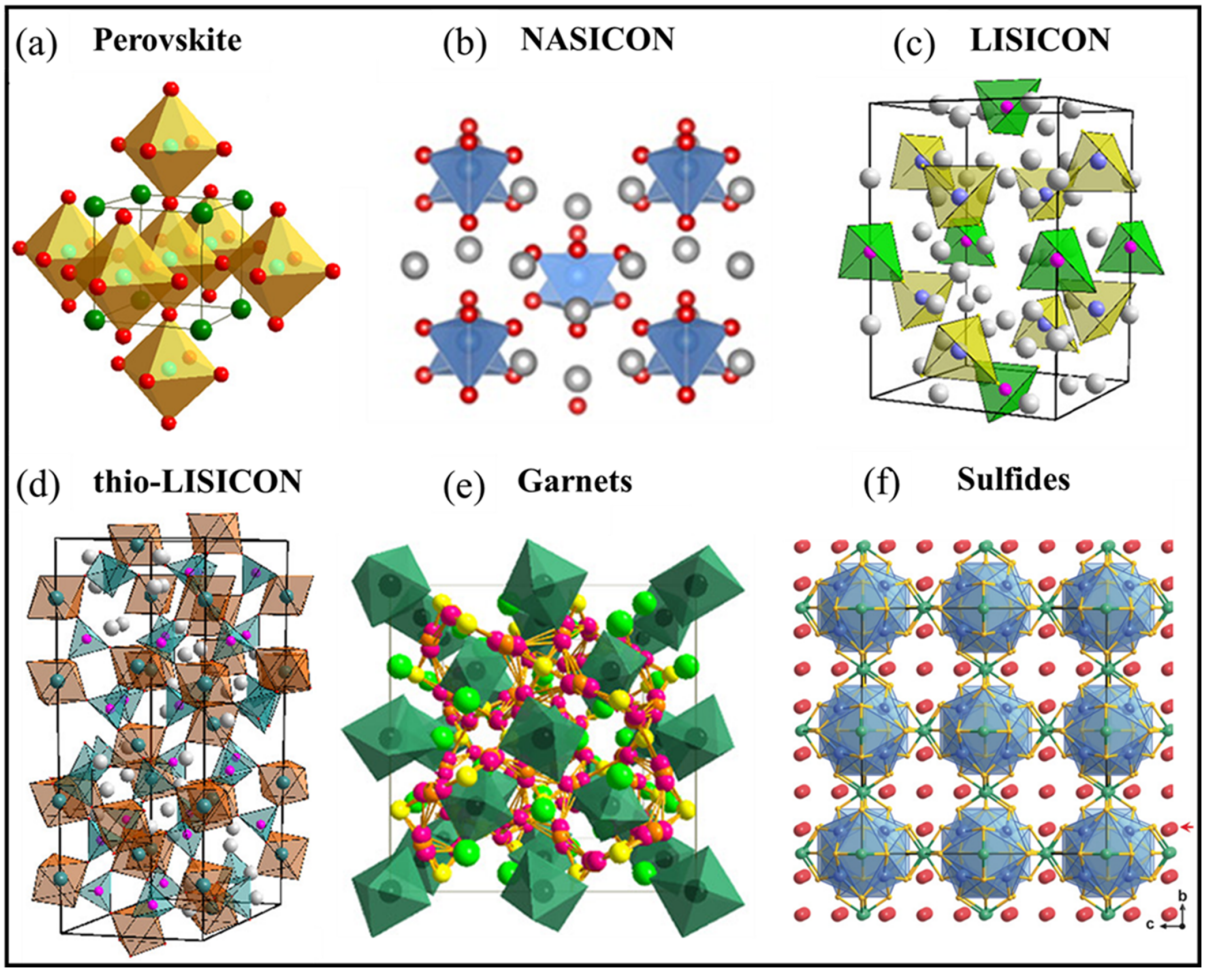

Figure 7. Schematic illustration of the crystal structure of electrolytes: (**a**) Perovskite; (**b**) NASICON [239]; (**c**) LISICON; (**d**) Thio-LISICON; (**e**) Garnets [240]; (**f**) Sufides [241].

3.4.1. Perovskites

In 1971, Takahashi et al. [242] first reported perovskite-type solid electrolytes with the common formula ABO_3 (A=La, Sr, or Ca; B=Al or Ti). Perovskite has a face-centered cubic structure (Figure 7a), where A is at the top corner of the cube, B is at the body center, and O is located at the face center [243]. The perovskite-type $Li_{2/3-x}La_{3x}TiO_3$ (LLT) has been extensively studied in TFLIBs. It is a promising electrolyte and one of the most conductive oxide electrolytes available because of its impressive crystalline conductivity at room temperature. However, LLT is plagued by high grain boundary resistance, significant electronic conductivity, and a tendency to react with Li-metal anode (reduction in the Ti^{4+}) [244]. LLT has been successfully deposited on MgO and $SrTiO_3$ substrates by PLD and reactive sputtering [245,246]. In 2002, Ohta et al. deposited a predominantly single-crystalline LLT film onto (001)-oriented $SrTiO_3$. At 190 °C, the deposited LLT film demonstrated a high conductivity of $2.5{\cdot}10^{-2}$ S·cm^{-1}, with an activation energy of 0.37 eV, which is similar to the bulk LLT. The extrapolated results suggest that it has a conductivity of $1.5{\cdot}10^{-4}$ S·cm^{-1} at 25 °C. Moreover, PLD has also been employed to deposit amorphous LLT films [247,248]. Ahn and Yoon optimized the thermal processing conditions to achieve maximum conductivity while maintaining its amorphous structure [247]. The ion conductivities of the deposited films at 500 °C exceeded $1{\cdot}10^{-5}$ S·cm^{-1} measured at 25 °C. However, when LLT is deposited directly onto LCO at a deposition temperature of over 400 °C, less Li-ion capacities are obtained galvanostatically. This is due to the interfacial reactions and inter diffusion that occur when deposited at a high temperature. However, rapid thermal annealing can induce the crystallization of the LCO film and maintain its amorphous structure, which can effectively increase its capacity [248]. Other perovskite-structured solid electrolytes have also been used in TFLIBs, see Table 4.

Table 4. Various solid electrolyte materials for TFLIBs.

Electrolyte	Crystal Structure	Deposition Method	E_a (eV)	Ionic Conductivity (S·cm^{-1})	Reference
LiPON		PLD		$1.5{\cdot}10^{-8}$	[249]
Li_xNb_yO		ALD	0.62	$6.4{\cdot}10^{-8}$	[250]
$Li_{0.33}La_{0.56}TiO_3$ (LLTO)	Perovskite	PLD	0.35	$3.5{\cdot}10^{-5}$	[251]
epitaxial $Li_{0.33}La_{0.56}TiO_3$	Perovskite	PLD	0.34	$6.7{\cdot}10^{-4}$	[252]
$Li_{0.17}La_{0.61}TiO_3$	Perovskite	PLD	0.25	$3.8{\cdot}10^{-4}$	[253]
$Li_{0.5}La_{0.5}TiO_2$	Perovskite	PLD		$1.1{\cdot}10^{-5}$	[248]
Li_3OCl	anti-perovskite	PLD	0.36	$8.9{\cdot}10^{-6}$	[254]
$Li_{1+x}Al_xGe_{2-x}(PO_4)_3$ (LAGP)	NASICON	sputtering		$>10^{-4}$	[255]
$Li_{1.5}Al_{0.5}Ge_{1.5}(PO_4)_3$	NASICON	sputtering	0.25	$1.29{\cdot}10^{-6}$	[256]
$Li_{0.5}Al_{0.29}Ti_{1.35}P_{2.9}$ (LATP)	NASICON	sputtering		$6.5{\cdot}10^{-6}$	[257]
Li_2O-SiO_2	LISICON	PLD		$4.1{\cdot}10^{-7}$	[258]
$Li_{3.25}Ge_{0.25}P_{0.75}S_4$	thio-LISICON	PLD	0.38	$1.7{\cdot}10^{-4}$	[259]
$Li_7La_3Zr_2O_{12}$ (LLZO)	Garnet	CVD	0.50	$4.2{\cdot}10^{-6}$	[260]
Al-doped LLZO	Garnet	ALD	0.63	$1.0{\cdot}10^{-8}$	[261]
$Li_6BaLa_2Ta_2O_{12}$	Garnet	PLD	0.42	$2.0{\cdot}10^{-6}$	[262]
Li_2O-V_2O_5-SiO_2(LVSO)		PLD	0.54	$2.5{\cdot}10^{-7}$	[263]
$LiAlF_4$		ALD		$3.5{\cdot}10^{-8}$	[264]
$LiAl_{0.3}S$		ALD	0.48	$2.5{\cdot}10^{-7}$	[265]
Li_2S-P_2O_5		PLD	0.45	$7.9{\cdot}10^{-5}$	[266]
Li_3PS_4		PLD	0.47	$5.3{\cdot}10^{-4}$	[267]

3.4.2. NASICON

The general formula of an NASICON-type solid electrolyte is MA_2 $(BO_4)_3$ (M=Li, Na, K or Ag; A=Ti, Zr, Ge or V; B=P, Si or Mo) (Figure 7b) [268]. In 1976, Goodenough et al. [269] obtained NASICON-type $Na_{1+x}Zr_2P_{3-x}Si_xO_{12}$ by a solid-state reaction method at a high-temperature. It comprises the common vertex of the PO_4 tetrahedron and ZrO_6 octahedron [270]. Li-ion solid electrolytes with a NASICON structure can be obtained by replacing Na with Li. Compared with other M ions, $LiTi_2(PO_4)_3$ and $LiGe_2(PO_4)$ have a higher ionic conductivity, which is, however, still very low. In order to further increase the ionic conductivity, Ti is partially substituted. $Li_{1+x}Al_xTi_{2-x}$ $(PO_4)_3$ (LATP) and $Li_{1+x}Al_xGe_{2-x}$ $(PO_4)_3$ (LAGP) were obtained by partially substituting Ti and Ge with Al. This can achieve a high conductivity of 10^{-4}–10^{-3} S·cm^{-1} at room temperature [271]. The investigation of RF magnetron sputtering has been carried out to achieve high conductivity in the thin film form for these materials. The amorphous films possess an ion conductivity of approximately $3{\cdot}10^{-6}$ S·cm^{-1}, which is equivalent to the LIPON film.

However, the electronic conductivity is noteworthy as it measures at about 10^{-14} S·cm^{-1}. Elevating the substrate temperature to 300 °C during the sputtering deposition would significantly enhance the conductivity to $2.5{\cdot}10^{-5}$ S·cm^{-1} at 25 °C, which is ascribed to the formation of more compact films. Additionally, introducing nitrogen through a N_2 plasma is another approach for enhancing the conductivity of films derived from NASICON targets, similar to LiPON deposition. The resulting amorphous films have reported room temperature conductivities of 10^{-5} S·cm^{-1} [272]. Other amorphous $LiZr_2(PO_4)_3$ films with a NASICON structure have been deposited by sputtering [273]. The deposited films had a large ohmic resistance and behaved similarly to an insulator. However, the film underwent partial crystallization and transformed into small particles after annealing above 800 °C, leading to a reduced room-temperature ionic conductivity of $1.3{\cdot}10^{-7}$ S·cm^{-1}. In addition, the chemical compatibility of NASICON materials with metallic Li is a crucial challenge. The Li-metal is highly reactive, which can react with Ti^{4+} to form highly resistive interphases [274]. It has been reported that bulk $LiZr_2$ $(PO_4)_3$ is unstable when in contact with Li-metal, resulting in a low-resistance interlayer [275]. Therefore, addressing the (electro)chemical compatibility of NASICON electrolyte films in contact with Li-metal is urgent.

3.4.3. LISICON and Thio-LISICON

Bruce and West first described LISICON $Li_{14}ZnGe_4O_{16}$ and related systems (Li_{2+2x} $Zn_{1-x}GeO_4$) in 1983 [276,277]. The LISICON framework is related to the γ-Li_3PO_4 crystal structure (Figure 7c), which exhibits a relatively low ionic conductivity. Even in doped compounds, such as γ-$Li_{14.4}V_{1.6}Ge_{2.4}O_{16}$, the room-temperature ionic conductivity remains relatively low, at about 10^{-6} S·cm^{-1}. Furthermore, LISICON $Li_{14}ZnGe_4O_{16}$ is highly reactive with metallic Li and atmospheric CO_2, and the conductivity decreases with time.

It was found that the oxygen ions are replaced by larger and more easily polarized sulfides in the framework, which improves the mobility of Li^+. Kanno et al. first introduced the Thio-LISICON family to enhance the Li^+ conductivity [278,279]. Many Thio-LISICON structured solid electrolytes with high conductivity are obtained by aliovalent substitution in solid solutions. Among them, the highest conductivity is apparently observed with $Li_{3.25}Ge_{0.25}P_{0.75}S_4$. Ohta et al. used PLD to deposit the Thio-LISICON-structured $Li_{3.25}Ge_{0.25}P_{0.75}S_4$ electrolytes (Figure 7d), which demonstrated an incredibly high room temperature conductivity of 10^{-4} S·cm^{-1} [259], which is roughly an order of magnitude lower than the bulk conductivity of the material. Such behavior was ascribed to the enrichment of Li-content in the deposited films, which leads to a reduction in the number of vacancies available to increase the mobility of Li-ions. However, this material is unstable in bulk form. Later, Ge was replaced by Si to improve its stability and ionic conductivity. The new Thio-LISICON $Li_{3.4}Si_{0.4}P_{0.6}S_4$ exhibits an even higher ionic conductivity of $6.4{\cdot}10^{-4}$ S·cm^{-1} at 25 °C [279].

3.4.4. Garnets

The chemical formula of the garnet structure is A_3B_2 $(XO_4)_3$ (A=Ca, Mg, Fe, Mn; B=Al, Fe, Cr, Ti, Zr, V), where A, B, and X have 8, 6, and 4 oxygen coordination (Figure 7e). In 2003, Thangadurai et al. [280] first produced $Li_5La_3M_2O_{12}$ (M=Ta or Nb), exhibiting a conductivity of only 10^{-5} S·cm^{-1} and an activation energy of 0.6 eV. In 2007, Weppner's group obtained the cubic phase $Li_7La_3Zr_2O_{12}$ (LLZO) through the doping substitution of the M-site elements, which exhibits high Li-ion conductivity $3{\cdot}10^{-4}$ S·cm^{-1} and compatibility with Li-metal [281]. Therefore, LLZO has become a highly promising solid-state electrolyte, which has led to extensive research for high-energy LIBs [106]. LLZO can crystallize into two different types of crystals: a low-temperature tetragonal symmetry ($\sim 10^{-6}$ S·cm^{-1}) and a high-temperature cubic symmetry ($\sim 10^{-4}$ S·cm^{-1}). Numerous techniques have been used to stabilize the high-temperature cubic phase because of the high Li^+ conductivity. The aliovalent substitutions at the cation site are an illustrative example [239,282]. In the last decade, LLZO has been synthesized with different cationic substitutions via vacuum deposition approaches.

For example, LLZO films were fabricated by pulsed laser annealing and high process temperatures without elemental substitutions. The obtained LLZO films exhibited a conductivity of $1.61{\cdot}10^{-6}$ S·cm^{-1} at 25 °C [283]. The Al-doped LLZO films have also been deposited by PLD to study the impact of the Al^{3+} concentration on the conductivity of the material in this paper. The LLZO film with (111) orientation and a moderate level of Al^{3+} incorporation (less than 0.6 moles replacement for Li^+) exhibited a room temperature conductivity close to $1{\cdot}10^{-5}$ S·cm^{-1}. In addition, Saccoccio et al. deposited LLZO films doped with Ta element on MgO (100) substrates [284]. The cubic phase films can be synthesized at 50 °C. However, the deposition rate is slow, despite the enhanced conductivity achieved at high laser fluence, extrapolated to $4.4{\cdot}10^{-6}$ S·cm^{-1} at 25 °C. In addition to PLD, many other deposition technologies also have been used to synthesize LLZO thin films, such as CVD, ALD, and PVD. Kalita et al. synthesized an amorphous LLZO film with an exceptional conductivity of $4{\cdot}10^{-7}$ S·cm^{-1}, which is very smooth, dense, and homogeneous [285]. After being doped with Al and Ta, the LLZO films exhibit an impressive conductivity of $1.2{\cdot}10^{-4}$ S·cm^{-1} and an activation energy of 0.47 eV, making them a promising candidate for LIBs [286]. Garnet electrolytes have emerged as the most extensively investigated and promising inorganic SSEs for the next-generation commercial TFLIBs.

3.4.5. Sulfides

Sulfide-based materials possess the highest conductivity among all solid electrolyte materials, such as $Li_{10}GeP_2S_{12}$ and $Li_{9.54}Si_{1.74}P_{1.44}S_{11.7}Cl_{0.3}$, with ionic conductivities of $1.2{\cdot}10^{-2}$ and $2.5{\cdot}10^{-2}$ S·cm^{-1} at 25 °C, respectively, which are comparable to the traditional alkyl carbonate liquid electrolytes in LIBs [11,287]. These high conductivities result from the weak bonds between the less electronegative sulfur anions and Li^+ coupled with a more accessible microstructural framework [288]. Recently, the sulfide-based electrolytes $Li_{3+2x}PS_{4+x}$ have been successfully applied in TFLIBs. $Li_{3.42}PS_{4.21}$ was designed by introducing an excess of Li_2S in Li_3PS_4 by PLD, which showed the most impressive ionic conductivity of $5{\cdot}10^{-4}$ S·cm^{-1}. They were combined with LCO and Li to establish the $LiCoO_2$ | | $Li_{3.42}PS_{4.21}/Li_3PO_4$ | | Li full TFLIBs. These batteries were able to cycle reversibly at 10 C. The sulfide electrolyte has been demonstrated to be fairly stagnant when in contact with Li-metal because Li_3PS_4 can react with Li-metal to synthesize the electronically insulating Li_3P and Li_2S interphase layers [289]. However, the main issue with sulfide electrolytes is their high reactivity with air and moisture. The entirety of the examined sulfide electrolytes that have been referenced required the operation in glovebox-integrated vacuum deposition equipment. This requirement brings more challenges to the ultimate scale-up and the processing of these electrolytes.

4. Architecture Designs

In addition to the performance of the component materials, the structure of the batteries also greatly impacts the performance. The construction structure of batteries determines the efficient surface contact of the active materials and the diffusion length of Li-ions. That highly influences storage capacity and Li^+-ion kinetics. The optimization of architecture is an essential condition for designing high-performance TFLIBs.

4.1. Planar TFLIBs

A schematic cross-section of typical thin-film batteries described by Bates is shown in Figure 8a [290]. A wide variety of materials can be used as the substrate if they are stable during the subsequent thin-film deposition and heat treatment. They also should have a relatively smooth surface. Each component of the thin-film batteries, current collector, cathode, anode, and electrolyte is deposited from the vapor phase. A final protective film is needed to prevent the Li-metal from reacting with air when the batteries are exposed to the environment. The typical energy densities that can be achieved for these thin-film cells are 3.6 $J \cdot cm^{-2}$ (1 $mWh \cdot cm^{-2}$). With the demand for high-energy devices, it is necessary to expand the deposited film area by folding or stacking the batteries into an optimized volume [291]. However, before Li-ion and Li-free cells can be considered for applications, other problems must be solved. As Li-metal is an anode material, the entire battery must be insulated from oxygen and water vapor during testing and use. Consequently, the packaging requirements are high.

Due to the structural limitations requiring complex mask systems to prepare functional layers of different shapes, Nakazawa et al. designed a vertical FLIB structure by DC sputtering and radio frequency sputtering methods. Li-free batteries are a special type of Li-ion battery that have recently been demonstrated by Neudecker. In such batteries, the Li-anode is formed in situ during activation. This is achieved by electroplating a Li-film at the interface between the current collector (e.g., Cu) and electrolyte (LiPON) [292]. These batteries exhibit high discharge rates and reversible capacities similar to the LIBs with a $c$$LiCoO_2$ cathode. In addition, the fabrication, handling, and storage of these batteries are greatly simplified. They do not degrade due to solder reflow, a typical electronic mounting technique, including a short heating cycle to 250 °C. However, due to the small distance between the electrodes and SSEs, the probability of short circuits in the vertical battery structure is relatively high. Therefore, the current research commonly used is the classic cross-section thin film structure to prepare planar TFLIBs. In order to solve the problems of the cross-section structure thin film batteries and improve the energy density, many high-performance anode films and other component film materials have been used to replace Li-metal.

4.2. Bipolar TFLIBs

A bipolar architecture of ASSBs can offer substantial benefits in the battery performance and cost compared to conventional LIBs. The bipolar design refers to the battery configuration, in which unit cells are in direct contact with each other and are connected in series in a batteries module without using external electrical connections (Figure 8b) [293]. The bipolar design allows a simple series connection of multiple batteries to establish the total output voltage and shorten the electronic path in the module, which leads to an increase in power capability [295]. Moreover, the bipolar design can avoid a number of the passive components and parts required for packaging; The external electrical connections are also absent. Without these components, the bipolar ASSBs design can reach the energy density of large-scale battery systems and save costs. The idea of bipolar battery stacking originates from the voltaic pile at the advent of electrochemical science. In 1897, Tribelhorn patented the first bipolar lead-acid batteries, in which a stack of cup-shaped electrodes was separated by glass balls [296]. Kapitza then constructed a bipolar Pb-acid battery in 1923 by immersing Pb plates in an H_2SO_4 solution and achieved a maximum power density of 35 $kW \cdot L^{-1}$ and 6 $kW \cdot kg^{-1}$ [297]. However, the advancement of bipolar lead-acid batteries

with liquid electrolytes has been hindered by short-circuiting problems until advanced electrolyte technology was designed to fix acids in gel or absorbent glass mats.

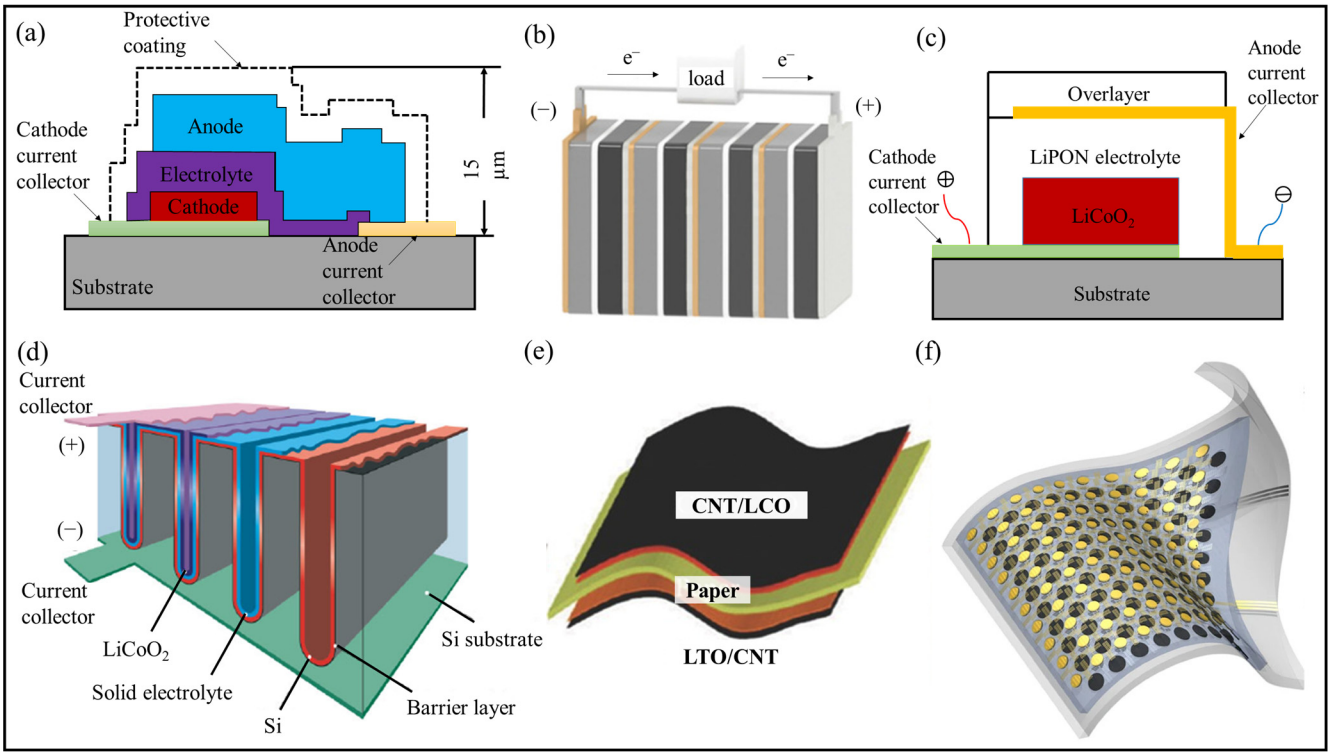

Figure 8. Scheme of different batteries architectures. (**a**) Planar TFLIBs; (**b**) Bipolar LIBs [293]; (**c**) Anode-free TFLIBs; (**d**) 3D TFLIBs [112]; (**e**) Flexible and (**f**) stretchable LIBs [294].

Inspired by this, bipolar solid-state LIBs have attracted broad interest in recent years. They can improve the output voltage and power density of the batteries. The SEs can eliminate the internal short-circuiting problem of bipolar batteries caused by electrolyte leakage. Shen and Halpert studied the potential advantages of bipolar cell structures from electrode thickness, porosity, bipolar plate thickness, and conductivity [298]. Their calculations indicated that bipolar batteries could exhibit ~40% higher energy and power densities than monopolar batteries. This was mainly due to the volume and weight saving of the passive materials. However, the development of bipolar battery structures still faces some technical challenges, such as the possibility of internal short-circuits between cells, the corrosion sensitivity of the bipolar plates, and the complex manufacturing process for accurate and reliable cell stacking. In order to realize bipolar LIBs, a series of effective strategies are proposed. First, developing SEs with high Li^+ conductivity and wide electrochemical windows is very important; then, a stable conformal interface (i.e., by interface engineering) between SEs and active electrodes must be built [299]. In addition to developing highly conductive selenium, the biggest challenge is to form a stable conformal Li^+ interface to promote the transport between the selenium and active electrode materials. Moreover, a bipolar SSLB construction requires electrically conductive bipolar plates (current collectors) that work as an electrical interconnection and partition between the adjacent cells [298]. The bipolar plates may be electrically insulated around their edges to prevent internal short-circuiting between cells.

Although these strategies can significantly enhance the electrochemical performance of the cells, stacking multiple cells in a single package is very challenging. There are only a few reports on bipolar LIBs. The stacking strategies of bipolar LIBs reported in the literature can be roughly divided into the lamination of free-standing SE sheets and the printing of SE slurries. For example, Gambe et al. reported bipolar LIBs via lamination of the $LiFePO_4$ composition and Li-anode with a quasi-SE composed of a Li–glyme complex and

oxide nanoparticles (SiO_2, CeO_2, Al_2O_3, and ZrO_2) [300]. Coin-type bipolar LIBs were constructed by stacking the cells with SUS bipolar plates (Figure 9a). The two- and three-cell stacks exhibited plateau voltages of 6.8 and 10.2 V, respectively. They delivered capacities as high as ~156 mAh·g^{-1} at 35 °C and 0.1 C, implying a positive electrode utilization of ~91% (Figure 9b). Furthermore, bipolar LIBs showed high CE (~99%) and excellent cycling stability (91% after 200 cycles). This has primarily been attributed to the forming of Li^+-conductive interfaces between $LiFePO_4$ and quasi-SE in the composite positive electrode.

The printing processes of slurries (inks) are simple, low-cost, and easily scalable. Moreover, the printable slurry readily adapts to the shape of the substrate. Then, a novel battery architecture can be implemented with various shapes, shape factors, and functions. This is suitable for the manufacturing of bipolar architectures [290]. Yoshima et al. [301] proved that 12 V-class bipolar LIBs assembled with a thin hybrid SE composed of LLZO and PAN-based gel polymer (GP). $LiMn_{0.8}Fe_{0.2}PO_4$–PAN-GP (Cathode) and $Li_4Ti_5O_{12}$–PAN-GP (Anode) layers were formed via slurry coating on opposite sides of an Al bipolar plate. A thin hybrid SE layer of ~3 μm thickness was then fabricated by spray-coating a slurry of LLZO (94 wt.%), PVDF binder (2 wt.%), and PAN-GP (4 wt.%) on the cathode and anode (Figure 9c). The Li^+ conductivity of the hybrid SE is ~6.0·10^{-3} S·cm^{-1} at 25 °C, which is near to the conductivity of liquid electrolytes. The results show that the coulomb efficiency of bipolar LIBs is over 99.8%, and a stable cycle performance of 85% over 200 cycles is obtained. It also exhibited capacity retentions of ~100% and ~50% at 80 °C and 40 °C, respectively, with respect to the nominal capacity at 25 °C. This demonstrated a successful operation in a wide temperature range (Figure 9d). The bipolar architecture of TFLIBs is a promising solution to improve both the voltage and energy density, thus leading to the development of high-energy batteries in the next generation. However, the development activities in bipolar TFLIBs are still in their early stage. Many technical challenges, such as the stacking design and its manufacturing process, remain to be improved.

4.3. Anode-Free TFLIBs

Li metals can easily react with electrolytes due to their high reactivity. This implies electrolyte consumption, continuous corrosion, uncontrollable dendrite growth, and the formation of irreversible SEI passivation layers [302]. These issues seriously affect the safety, coulombic efficiency, and deteriorate cycling life of batteries. Furthermore, the excessive Li-metal used in the anode decreases the actual specific and volumetric capacity. Inspired by the Li-free batteries structure proposed by Neudecker, anode-free or anode-less rechargeable batteries (Figure 8c) that eliminate the use of excess Li-metal have gained significant attention in the field of LIBs due to their high energy and power density [303,304]. In addition, they bring significantly reduced costs and simplified manufacturing procedures due to the absence of anodes. For example, Zhang's group further designed anode-free rechargeable Li-metal batteries (Al||$LiFePO_4$||Cu). They highlighted the promising prospects for their practical applications [305]. Inspired by their fascinating merits, especially their high-energy density, anode-free batteries have sparked the scientific community's interest.

Dahn's group [303] recently developed dual-salt LiDFOB/$LiBF_4$ electrolytes for high-performance anode-free Li-metal pouch cells. Zhang et al. [304] published news and views in Nat. Energy clarifying the fascinating prospects and significant research value of anode-less batteries. Despite numerous advantages, a limited Li source in anode-free batteries is a huge challenge. Woo et al. [306] assembled a $LiNi_{1/3}Mn_{1/3}Co_{1/3}O_2$||Cu anode-free cell. However, in the initial cycle, only 23% of the extracted Li-ion recovered back into the $Li_{1-x}Ni_{1/3}Mn_{1/3}Co_{1/3}O_2$ cathode. The sharp capacity loss is mainly attributed to the successive formation of SEI film, "dead" Li-metal, and high impedance interfacial layer. All these processes exhaust the limited Li sources [307]. Therefore, the coulombic efficiency is a crucial challenge for anode-free Li-metal batteries. Recently, several strategies have been developed to enhance the coulombic efficiency and to extend the lifetime of anode-free batteries; this also includes optimizing the current collector and electrolytes, designing favorable protocols, etc.

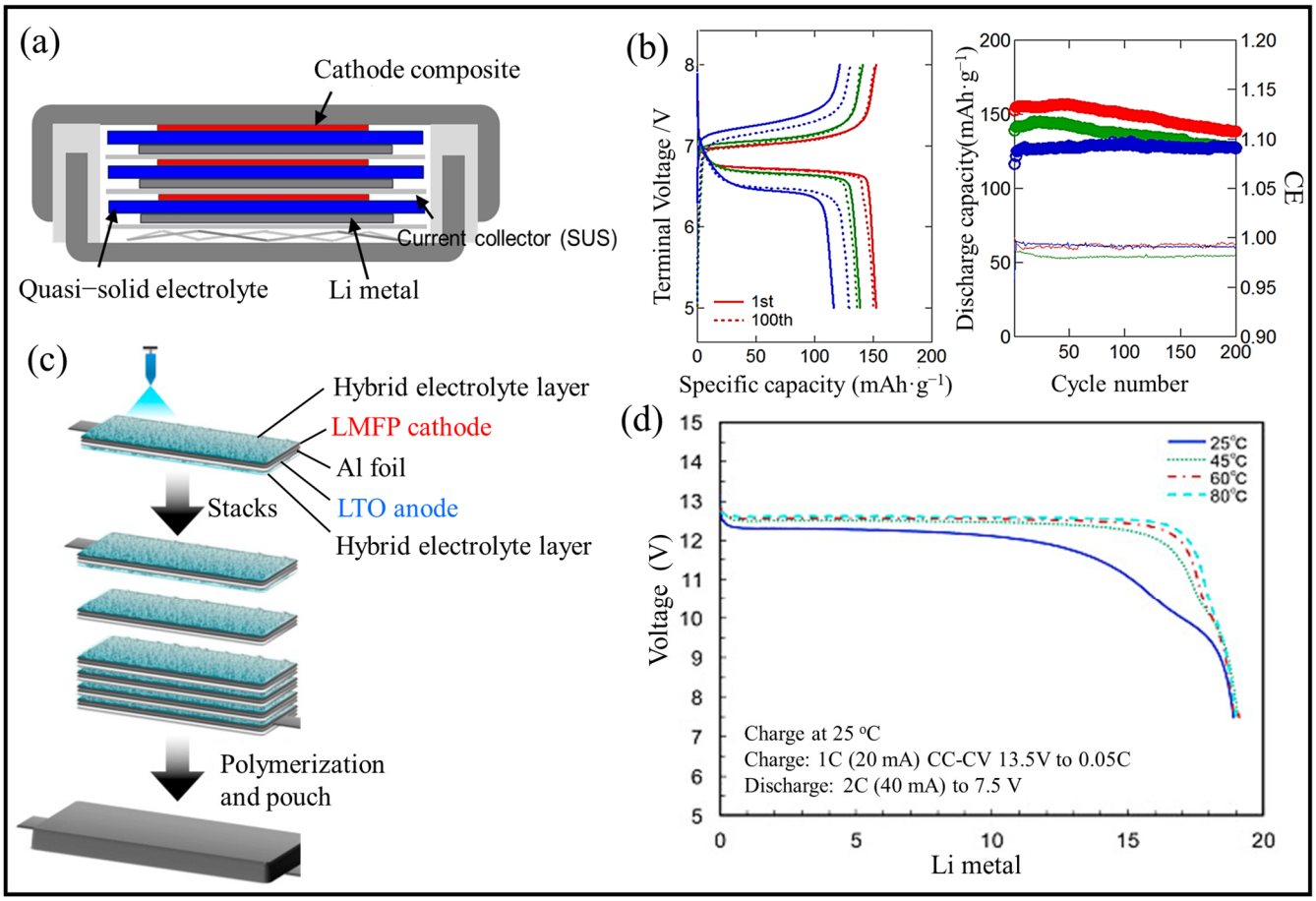

Figure 9. (**a**) Structure of a triple-layered bipolar stacked all-solid-state LIBs; (**b**) 1st and 100th charge-discharge profiles (left) and cycling properties of double-layered all-solid-state LIBs at 35 °C at 0.1 C (red), 0.2 C (green) and 0.5 C (blue) rates (right) [300]; (**c**) Schematic process for the preparation of bipolar batteries (**d**) Discharge curves of a 12 V bipolar batteries at high temperatures [301].

Assegie et al. [308] successfully grew ultrathin graphene artificial layers on Cu through a more common CVD method. The multilayer-graphene (MLG) film on the Cu is an artificial SEI layer. It stabilizes the electrode interface, encapsulates the deposited Li-metal, and effectively suppresses Li-dendrite formation. This is attributed to MLG films effectively relieving the infinite volume change induced upon cycling. Based on this new design, the anode-free cell with MLG and $LiFePO_4$ cathodes (areal mass loading: 12 mg·cm^{-2}) can deliver a capacity retention of 61% after 100 round-trip cycles, which exhibited a 16% higher retention than the full batteries housing a bare Cu electrode. In addition to constructing an artificial SEI layer or function layer on CCs, pursuing alternative current collectors, such as Li-alloyed CCs, to replace Cu or Al completely and designing 3D structure CCs are also effective methods to improve the coulombic efficiency.

Developing outstanding functional electrolytes is also essential for advancing anode-free LIBs. The SSE is still plagued by premature short-circuiting and huge interfacial resistance attributed to poor contact between the Li-metal and electrolytes. As discussed in the previous section, introducing the interlayer is the most common method to improve the electrochemical performance. Kim et al. [309] explored the impact of the geometry, interlayer, and interlayer species on the LLZO solid electrolyte surface on the plating/striping behavior and performance of anode-free batteries. By contrast, LLZO with a thin Au layer formed a Li–Au alloy layer, inducing fast diffusion. Lithiophilic interlayers on solid electrolytes can effectively induce uniform electric fields and Li-ion flux.

Moreover, the interlayer species (i.e., Au, Ag, and Si) influence the Li-ion distribution and subsequent deposition morphology due to the kinetics of the alloying and precipitation

reactions. The interlayer would decrease the interfacial energies by developing a chemically compatible interface. This interface can serve as a buffer layer for Li-ion redistribution and a seed layer for Li-precipitation. Hence, to induce a uniform deposition and alleviate the dendrite problems, solid electrolytes with a uniform morphology and lithiophilic interlayer are needed.

4.4. 3D TFLIBs

Developing new materials and architectures offers an approach to achieving higher energy density in planar TFLIBs. However, it still cannot provide enough power for various small-size applications due to geometric limitations. For conventional 2D planar TFLIBs, it is very complex to combine high power with a high energy performance due to the limited footprint area and volume in cross-section planar TFLIBs. Two routes can be followed to obtain high storage capacities. One is to enlarge the footprint area of 2D all-solid-state LIBs. However, this is not compatible with the small size of integrated devices. Another way is to increase the thickness of the battery's electrodes, which will significantly increase the diffusion path of Li^+, limiting the power [310]. Considering these limitations, new architectures are proposed, which are all based on exploring a three-dimensional (3D) geometry (Figure 8d) [112].

One of the advantages of 3D batteries is that the internal surface area between the cathode, electrolyte, and anode is enlarged. This means that much higher currents can be applied, with almost the same amount of packaging and substrate material. Thus, higher power is achieved. Compared with planar solid-state thin film batteries, the 3D TFLIBs improve the volumetric storage capacity, energy density, and rate capability. In addition, the 3D TFLIB architecture introduces a vertical structure into one or both of the anode and cathode. The vertical structures provide electronic bridges, minimizing the ionic migration distance. This enables operation with high power densities, while the volumes of electrode material are still large, and the energy density is high. Introducing 3D structures also reduces the local current density at a given C rate; this improves the performance by reducing the overpotentials and improving the charge transport. In recent years, many 3D structures have been designed for 3D LIBs to improve the energy density. This section will discuss the manufacturing technologies of novel 3D structures and the recent progress in 3D TFLIBs.

The electrochemical performance of microbatteries is highly dependent on the inherent properties of the electrochemically active cathode and anode materials. Compared to conventional planar batteries, the homogeneity of the battery layers is the most critical problem in the three-dimensional case. The poor adhesion between the electrodes and electrolyte layers caused by the fabrication and assembling of the batteries is a serious obstacle [311]. Hence, ALD has become a popular choice for fabricating 3D thin-film electrodes due to the benefit of having high-quality and conformal thin-film electrodes. The following section will review the recent progress of novel 3D structured electrodes, solid electrolytes, and full thin-film batteries.

4.4.1. 3D Cathodes

The previous section introduced the excellent cathode materials for planar TFLIBs, such as layered $LiCoO_2$, high-voltage cathode materials LMn_2O_4, and high-capacity NCM cathode materials. The cathode materials applied in 3D TFLIBs are similar to conventional cathode materials. The active cathode materials have been applied in 3D TFLIBs, including $LiFePO_4$, $LiCoO_2$, $LiMn_2O_4$, $LiNi_xCo_yMn_{1-x-y}O_2$ layered oxides, V_2O_5, MoS, and others. Among them, $LiCoO_2$ is the most widely used. Shaijumon et al. [312] first designed vertical arrays of Al nanorods directly grown onto Al foil using the pulsed-potential electrodeposition technique. A 30 nm $LiCoO_2$ thin film was deposited through the thermal decomposition of sol-gel precursors evenly spray-coated onto Al nanorods (Figure 10a). The 3D $LiCoO_2$ electrode exhibits a high capacity (120 $\mu Ah \cdot cm^{-2}$ at C/5), excellent capacity retention, and negligible structural deformation during cycling. The 3D matrix of electrodes

meets both the requirements of short transport lengths and large capacity. Later, an even higher footprint capacity for a Li-free 3D electrode was achieved using amorphous VO_2 deposited by ALD on a Pt/TiN-coated Si micropillar array (Figure 10b). A capacity of 130 μAh·cm^{-2} at a rate of 0.7 C was observed for such a configuration [313]. Remarkably, rate-performance experiments have indicated that around 40% of the capacity was accessible with a current density of 40 C (50 μAh·cm^{-2}). In addition, Labyedh et al. [314] recently prepared LMO thin films on Ni-coated silicon pillar arrays using the solid-state conversion technique (Figure 10c). The LMO thin films on 3D electrodes reached a volumetric capacity of 1200 Ah·L^{-1}, which is close to the theoretical capacity of spinel $LiMn_2O_4$. It also showed an impressive rate performance in contrast to the planar film. In addition, a 21 times higher capacitance was achieved with the 3D LMO thin film than with the planar one due to the area enhancement offered by the microstructured substrate. In addition to these periodic 3D structured cathode thin film materials, aperiodic 3D structures have also been researched. Shui et al. [315] conducted a synthesis and comparison of sponge-like porous, fractal-like porous, and compact $LiMn_2O_4$ thin films on Pt foils. The results show that the mesoporous spongy film exhibits the best performance due it having the highest surface area. Wang et al. [191] presented their discovery of 3D porous V_2O_5 nanoparticles with a "multideck cage" structure. The specific capacity of the cathode is 142 mAh·g^{-1} at 0.5 C and 86.7 mAh·g^{-1} at 56 C within a voltage window of 2.5 to 4.0 V (corresponding to one Li-intercalation).

4.4.2. 3D Anodes

The active anode materials include graphite, Si, tin and its alloys, and LTO. The most widely reported 3D thin-film anode is TiO_2. The highest footprint capacity for a 3D TiO_2 thin film was achieved by Létiche et al. [317], who combined a Si-microtube array with 155 nm of TiO_2 and covered it with a Li_3PO_4 SSE film. They obtained 370 μAh·cm^{-2} at a rate of C/16. Unfortunately, only about 20% was accessible at an applicable rate of 2 C. A slightly lower footprint capacity was achieved using chlorine-doped TiO_2 deposited on Si pillars (242 μAh·cm^{-2}). In this case, about 80% was accessible at 2 C; only 37% was accessible at a current rate of 20 C [318]. The higher rate performance is ascribed to the inherently faster Li-ion kinetics due to chlorine doping. This shows the importance of obtaining a large specific capacity with an enlarged surface area and using high-rate performance electrode materials. Therefore, silicon and tin are also widely used in 3D thin film batteries.

As early as 2011, a honeycomb 3D silicon anode material was designed by Notten's group [119]. The Si honeycombs can retain a stable capacity close to the expected value. The result showed that a suitable 3D structure (Figure 5c) could increase the capacity and improve the Si anode's stability during cycling. Apparently, such structures can adapt to the stress caused by volume expansion. By optimizing the 3D structure of the Si anode, the high capacity of Si can be maintained, and the stability can be improved. This provides an effective strategy for the practical application of a Si thin film anode. Kim et al. proposed a 3D Si electrode structure formed on check-patterned Cu current collectors with microscale periods fabricated using wire electrical discharge machining (Figure 10d) [316]. The findings indicated that the capacity and cycling performance of the Si electrodes with patterns were relatively high, which could be attributed to the stress relief of the Si anode. In addition, various high-capacity conversion anodes have been deposited on 3D current collectors via ALD, such as RuO_2 [148], MoO_x [147], Fe_2O_3 [265], and ZnO [319]. Dhara et al. developed 3D CNTs@MoOx composites, enabling a much higher areal capacity, about 27 times higher than planar MoO_x. They also found that the thinner MoO_x shows better cycling stability. The optimized MoO_x (300 cycles, ~25 nm)/CNTs could display a stable reversible capacity of 915 mAh·g^{-1} (areal capacity of 645 μAh·cm^{-2}) with an excellent capacity retention after 50 cycles (97.5% compared to the second cycle) [147].

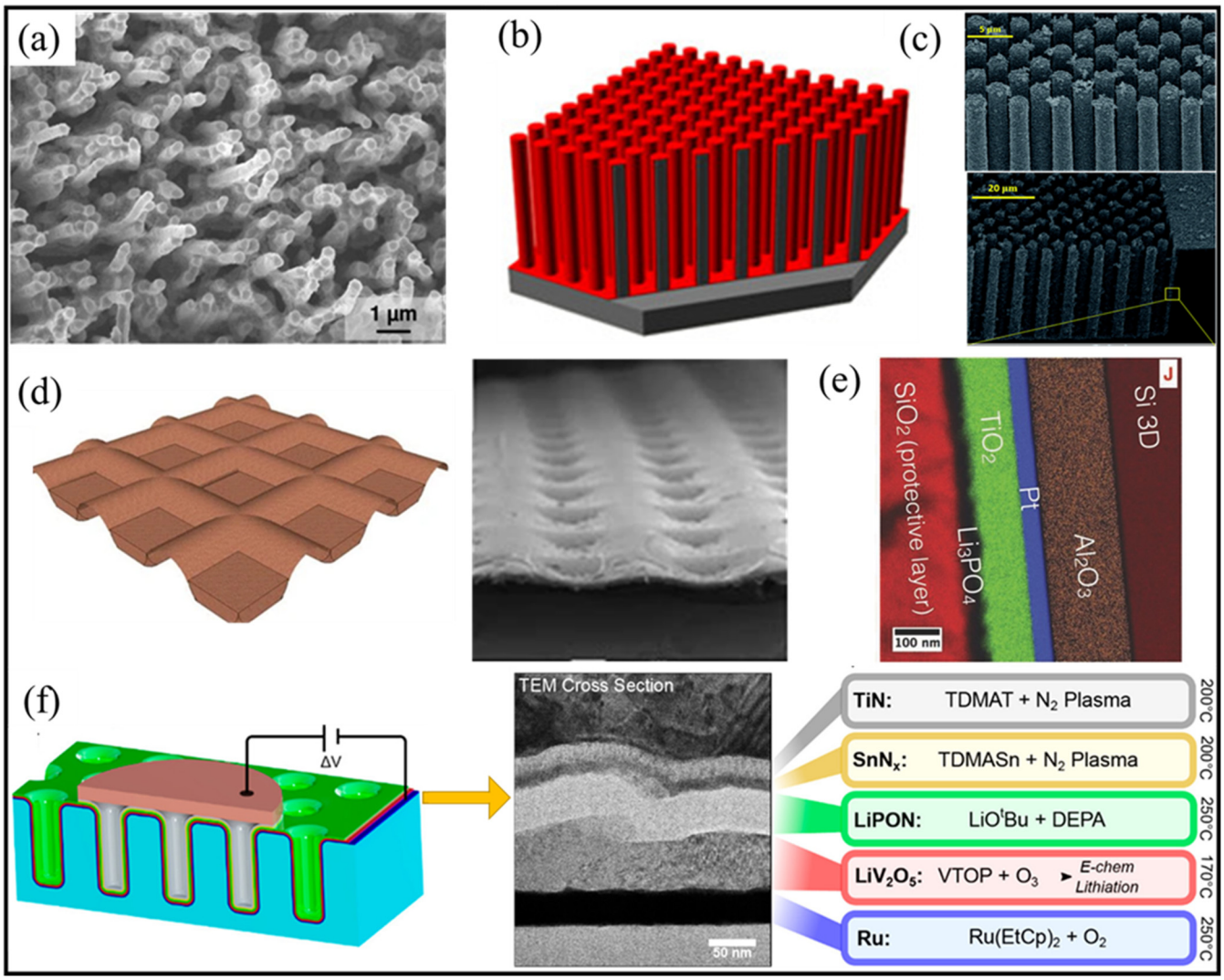

Figure 10. 3D structures. (**a**) SEM image of aluminum nanorods directly grown on Al substrate [312]; (**b**) 3D VO_x film on Si pillars [313]; (**c**) SEM images of Ni/LMO on the TiN-coated Si microstructured substrate [314]; (**d**) 3D schematic illustration of the as-fabricated check-patterned Cu foil (left) and SEM images of Si electrodes on patterned Cu foil (right) [316]; (**e**) Layer interfaces EDX-STEM elemental map of the stacked layers consisted of Si-3D/Al_2O_3/Pt/TiO_2/Li_3PO_4/SiO_2-Li_3PO_4 layer [317]; (**f**) Batteries testing through contact with the top electrode and cathode current collector layers (left), cross-sectional TEM image and overview of all-ALD solid-state batteries with 40 nm Ru/70 nm LiV_2O_5/50 nm Li_2PO_2N/10 nm SnN_x/25 nm TiN (right) [192].

4.4.3. 3D Electrolytes

Solid electrolytes are one of the most crucial components in 3D TFBs. Electrolyte layers provide electrical insulation between the positive and negative electrodes while promoting Li-ion transportation. The material conformality and uniform thickness are critical for uniform resistance over the whole stack. Moreover, a single pinhole will short-circuit the cell, making it useless. Therefore, a suitable thickness that guarantees its proper functioning must be chosen. On the other hand, the electrolyte layer does not contribute to the cell energy density. Therefore, any reduction in the thickness will thus result in an increased energy density. A self-limiting technique is required to achieve good conformality; the most common method used for this is ALD. The conformality originates from self-limiting surface reactions that are separated in time. Many SSE materials deposited by ALD and their most relevant properties have been reported. Among them, the most commonly utilized solid electrolyte for 3D TFLIBs is LiPON. It has a wide electrochemical stability window

(0 to 5 V vs. Li^+/Li), low electronic leakage (<10^{-14} S·cm^{-1}), and good ionic conductivity (10^{-6} S·cm^{-1}). It can be scaled down to nanometer thicknesses while maintaining good insulating properties [320].

In 2015, Nisula et al. [321] fabricated high-quality LiPON films on a 3D-microstructured silicon substrate by thermal ALD. The ionic conductivity of the LiPON electrolyte deposited at 330 °C was measured to be $6.6 \cdot 10^{-7}$ S·cm^{-1} at room temperature. In addition, LiPON was also applied to full 3D thin film batteries, indicating it is a promising electrolyte for 3D TFLIBs. However, there are still some problems that hinder its application, including its reactivity with air, which results in the creation of Li_2CO_3 and increased resistance. Another problem is its temperature stability. LiPON is only a good conductor in the amorphous state and cannot withstand high temperatures. Therefore, other high-performance solid electrolytes have been investigated in 3D TFLIBs, such as LLZO and LLTO. Kazyak et al. [261] deposited LLZO on a Si trench substrate by ALD. The resulting LLZO layer had a uniform thickness throughout the entire depth of the trenches, with a step coverage of over 95%. This provided a pathway toward 3D TFLIBs based on the superionic garnet SSEs. As deposition technologies continue to evolve, numerous high-performance solid-state electrolytes can be more effectively integrated into 3D TFLIBs, further enhancing the performance.

4.4.4. 3D Thin-Film Batteries

Despite the significant work exploring the growth and electrochemical performance of individual battery components for 3D batteries, there are few published reports of full 3D solid-state thin film batteries. Various active materials have different chemical properties, and the deposition conditions are also different. Depositing another substance on one active material may cause a chemical reaction at the interface with the active material, thereby affecting the battery performance. In addition, it is also a severe problem to ensure the conformality of each active material, especially for solid-state electrolytes, which may short-circuit the batteries. To date, only a few 3D all-TFLIBs have been reported. Létiche et al. designed the first 3D lithium-ion all-TFLIBs [317]. They created a 3D TiO_2 thin-film electrode with a Li_3PO_4 SSE film coated on the surface. The structure and performance of this 3D thin-film electrode are shown in Figure 10e. The 3D substrate is a double-microtube structure made of Si wafers using a standard photolithography process. An Al_2O_3 barrier was deposited on Si microtubes. Then, Pt is deposited on top of it as a current collector. TiO_2 and Li_3PO_4 films were deposited by ALD. The electrochemical performance shows that this is one of the highest footprint capacities reported for 3D thin-film batteries, with a good cycle capacity of 370 μAh·cm^{-2} at a C/16 rate. Unfortunately, applying a higher C rate will significantly reduce the accessible capacity, with only 20% accessible at 2 C. This has been attributed to the poor rate performance of the anatase TiO_2 and the low ionic conductivity of Li_3PO_4. The following significant development are the full complete conformal 3D solid-state TFLIBs made by Pearse et al., as shown in Figure 10f [192]. It was constructed by five conformal layers grown via ALD. The 3D substrate was a periodic array of microholes etched in a silicon wafer. The 3D TFB consisted of 40 nm Ru (current collector), 70 nm V_2O_5 (cathode), which was electrochemically pre-lithiated to form crystalline LiV_2O_5, Li_2PO_2N (SSE), 10 nm SnN_x (anode), and 25 nm TiN (second current collector). Cu dots were deposited on top of the stack using electron beam deposition. Planar solid-state batteries made from the LiV_2O_5-SnN_x couple exhibit stable capacities of 2.6 μAh·cm^{-2} (37 μAh·cm^{-2}·μm^{-1} normalized to the cathode thickness) for hundreds of cycles. By integrating with 3D substrates, the surface discharge capacity of these cells has been expanded to 9.3 times that of planar cells. Most importantly, the 3D structure improves the rate performance and coulombic efficiency while increasing the footprint capacity. These results indicate that the 3D architectures simultaneously increase the energy and power density, which are intrinsic to planar architectures with the trade-off between energy and power. 3D all-solid-state TFLIBs can indeed effectively increase the energy density due to the enlarged surface area. However, there are still significant obstacles to

overcome before these batteries can be used in commercial applications. More research and development are necessary to address the remaining challenges. Among them, the choice of composition materials, 3D structures, and deposition technology must be further optimized.

4.5. Other Novel TFLIBs

At present, flexible and stretchable Li-ion batteries (Figure 8e,f) are the ideal power sources for wearable electronics, owing to their high energy density, long cycle life, and excellent rate capability [322]. Flexible batteries have a similar principle to conventional batteries because each contains an anode, cathode, separator, and electrolyte. However, conventional batteries with rigid and fragile planar structures cannot effectively meet the requirements of wearable electronics. Therefore, it is crucial to produce flexible batteries with substantial flexibility while maintaining a high energy density and long-term stability [323]. So far, several approaches have been proposed for developing flexible micro batteries using different configurations, such as a paper-like configuration [324], bridge-island batteries designs [325], sponge/porous configurations [326], and wavy structures [327]. Paper-based TFLIBs use the surface roughness and porous structure of paper and textiles, which are ideal for ion transportation. At the same time, the flexibility of paper and textiles makes it possible for batteries to bend. Cui and co-workers [328] demonstrated the first flexible-paper LIBs, which employed paper as the separator and independent carbon nanotube (CNT) films as the CCs for both the anode and cathode. These microbatteries showed good electrochemical and mechanical performances. It displayed a specific capacity of 122 $mAh \cdot g^{-1}$. The coulomb efficiency in the first cycle is 85%, which increases to 93% after 20 cycles. It exhibited an excellent mechanical performance after manually bending the device down to 6 mm for 50 times without failure.

Graphene is a 2D carbon nanostructure with covalently bonded honeycomb array materials. It has been investigated as a material to produce LIB flexible electrodes. Wang et al. [329] reported the first graphene paper LIB in 2009. In this work, they prepared graphene aqueous dispersions from commercial graphite. A super-paper material with a smooth surface and glossy two sides was formed through the vacuum filtration of graphene aqueous dispersion. Microbatteries using graphene paper as the cathode and a Li-metal foil as the anode delivered a discharge capacity of 528 $mAh \cdot g^{-1}$. Later, Zhao et al. [330] designed a soft Si/graphene electrode for LIBs using acid-sonication treatment to create graphene with carbon vacancies. This composite material showed a reversible capacity of 3200 $mAh \cdot g^{-1}$ at 1 $A \cdot g^{-1}$ and high stability over 150 cycles. In addition to these examples, numerous other electrode materials for flexible batteries have been developed [331], including transition metal oxides [332] and sulfides [333]. Other flexible configurations have also been designed for LIBs, such as sponge structures [294]. Optimizing the flexible configuration will significantly improve thin-film batteries' stability and energy density.

5. Outlook

All solid-state thin-film batteries (TFLIBs) have been produced by various deposition techniques. These techniques efficiently avoid microscopic defects at the solid-solid interface and minimize barriers at the junctions. TFLIBs exhibit high stability, a long cycle life, a wide operating temperature range, and a low self-discharge rate. Recently, fruitful progress has been achieved in TFLIBs. Some TFLIBs have been employed in wearable electronics and low-power microdevices. However, the demand for thinner, lighter, space-saving, and flexible-shaped batteries continues to increase. At present, commercialized TFLIBs cannot fulfill these requirements. Consequently, the creation of high-performance TFLIBs is required to be developed. In this review, the research advances made in recent years for developing high-performance TFLIBs have been outlined. Primary attention was devoted to component materials optimization and cell architecture design.

Exploring novel materials and optimizing the present materials are critical to developing high-performance TFLIBs with improved storage capacity and recyclability. For the

anode side, the electrode films should have low redox potential with the limited volume change, low interface resistance, and a high-capacity retention rate. Developing multiple-compound systems, including complex alloys, pre-lithiated anodes, and in-situ deposited Li anodes are also promising strategies for future TFLIBs' anodes. On the cathode side, the electrode films should, in contrast, have high redox potential with stable and high capacity. Enhancing the stability and enlarging the capacity for high-voltage cathode materials is an indispensable direction to enhance the energy density and cycling life of TFLIBs. The electrolyte films should be highly ionically conductive, lithiophilic, and compatible with both the cathode and anode. In addition, the electrolyte films should be stable to operate at a wide range of voltages. The current collectors should be highly electronically conductive and compatible with the electrode materials. More novelties, such as memory and liquid alloys, should be explored to build superior current collectors for TFLIBs.

With the development of various advanced deposition technologies, such as CVD, PVD, PLD, ALD, 3D printing, surface modification, doping, and nano-structuring, are several common methods to improve the performance of these component materials. Although many advanced composite materials have been reported, few commercially available materials are still available. The high cost of manufacturing TFLIBs is an important issue hindering their widespread use in commercial applications. The following techniques are available to lower the cost of manufacturing TFLIBs: (1) Roll-to-Roll Manufacturing: This technique involves the continuous fabrication of TFLIBs on a roll of substrate material, allowing for high-volume and low-cost production; (2) Low-cost substrate materials: TFLIBs can be produced on numerous substrate materials, such as glass, metal foils, and polymer films. Using cost-effective and widely available substrate materials can reduce the overall manufacturing cost of TFLIBs; (3) Improving Manufacturing Processes: Improving deposition efficiency can reduce manufacturing costs. 3D printing technologies enable the fabrication of TFLIBs using low-cost, high-throughput methods; (4) Materials recycling: Recycling the component materials during the fabrication of TFLBs can also reduce the cost. Lowering the manufacturing cost of TFLBs will make them more purchasable, thus facilitating their widespread adoption in a broad range of applications.

The architecture of the batteries will also significantly affect their properties. Designing 3D TFLIBs will increase the areal energy and power densities. Various 3D methodologies have been proposed to increase the batteries' storage capacity, while keeping the same footprint area. In this review, the research progress on 3D component materials and complete 3D thin film batteries in recent years has been investigated in detail. Although many achievements have been made in 3D TFLIBs, they have not yet achieved commercial success. Many problems remain, such as the conformity of the 3D thin films, optimizing 3D structures, and lowering the manufacturing costs. Future efforts in material development and micro-manufacturing technology are still needed to realize commercial 3D TFLIBs.

Reliability is a critical factor for TFLIBS and is affected by various factors. The mechanical integrity of TFLIBs is one of the main issues. TFLIBs are very vulnerable to mechanical load, leading to cracking or delamination of the layers within the battery and further performance fade. Advanced materials with higher mechanical stability will help suppress crack and delamination formation in the battery layers. High power is also a reliability concern for thin-film lithium batteries. The cell should be able to operate at a high current to achieve a high energy transformation rate. Working with a high current would lead to overheating, increased resistance, and electrode degradation. This results in a reduced capacity, shorter cycle life, and potential safety hazards such as thermal runaways. Therefore, it is crucial to design TFLIBs with the appropriate electrode materials, thickness, and structure to handle high currents. The optimization of the manufacturing process to ensure uniformity and consistency is also important. In addition, it is desirable to improve the thermal management. The cycling process of the battery must be conducted mindfully to avoid exposure to excessive power demands. This can prolong the lifespan of the battery and reduce safety risks.

With the continuous advancements in high energy density and reliability, TFLIBs can be widely applied in life in wearable devices, medical implants, or smart cards. We anticipate that this review will provide useful direction for the creation of high-energy-density and stable TFLIBs, enabling them to be used in an even wider variety of real-world scenarios.

Author Contributions: Writing—original draft preparation, B.W.; writing—review and editing, C.C.; writing—review and editing, D.L.D.; writing—review and editing, P.H.L.N.; supervision, project administration, R.-A.E. All authors have read and agreed to the published version of the manuscript.

Funding: This research received no external funding.

Data Availability Statement: The data presented in this study are available on request from the corresponding author.

Acknowledgments: The author Baolin Wu gratefully acknowledges fellowship support by the China Scholarship Council.

Conflicts of Interest: The authors declare no known competing financial interest or personal relationships that could have appeared to influence the work reported in this paper.

Abbreviations

Notation	Definition
ASSBs	All-solid-state batteries
TFLIBs	All-solid-state thin-film Li-ion batteries
LIBs	Li-ion batteries
SSEs	Solid-state electrolytes
PVD	Physical vapor deposition
CVD	Chemical vapor deposition
PLD	Pulsed Laser Deposition
ALD	Atomic Layer Deposition
PECVD	Plasma-enhanced chemical vapor deposition
LPCVD	Low-pressure chemical vapor deposition
MOCVD	Metal-Organic Chemical Vapour Deposition
CCs	Current collector
3D	Three-dimensional
SEI	Solid electrolyte interphase
RT	Room temperature
EC	Ethylene carbonate
PC	Propylene carbonate
DEC	Diethyl carbonate
DMC	Dimethyl carbonate
LLT	Lithium lanthanum titanates
LLZO	$Li_7La_3Zr_2O_{12}$
LLCZN	$Li_7La_{2.75}Ca_{0.25}Zr_{1.75}Nb_{0.25}O_{12}$
LMNO	$LiNi_{0.5}Mn_{1.5}O_4$
LiPON	Lithium phosphorus oxynitride
LCP	$LiCoPO_4$
NCM532	$LiNi_{0.5}Mn_{0.3}Co_{0.2}O_2$
NCM111	$LiNi_{0.3}Mn_{0.3}Co_{0.3}O_2$
NCM811	$LiNi_{0.8}Mn_{0.1}Co_{0.1}O_2$
NCM622	$LiNi_{0.6}Mn_{0.2}Co_{0.2}O_2$
LATP	$Li_{1+x}Al_xTi_{2-x}(PO_4)_3$
LAGP	$Li_{1+x}Al_xGe_{2-x}(PO_4)_3$
SSE	Solid-state electrolytes
LLZTO	$Li_{6.75}La_3Zr_{1.75}Ta_{0.25}O_{12}$
MLG	multilayer-graphene

LTO	$Li_4Ti_5O_{12}$
LCO	$LiCoO_2$
TNO	$TiNb_2O_7$
GF	Graphite film

References

1. Palacín, M.R. Recent advances in rechargeable battery materials: A chemist's perspective. *Chem. Soc. Rev.* **2009**, *38*, 2565–2575. [CrossRef] [PubMed]
2. Armand, M.; Tarascon, J.M. Building better batteries. *Nature* **2008**, *451*, 652–657. [CrossRef] [PubMed]
3. Chen, L.; Huang, Y.-F.; Ma, J.; Ling, H.; Kang, F.; He, Y.-B. Progress and Perspective of All-Solid-State Lithium Batteries with High Performance at Room Temperature. *Energy Fuels* **2020**, *34*, 13456–13472. [CrossRef]
4. Peljo, P.; Girault, H.H. Electrochemical potential window of battery electrolytes: The HOMO–LUMO misconception. *Energy Environ. Sci.* **2018**, *11*, 2306–2309. [CrossRef]
5. Arbizzani, C.; Gabrielli, G.; Mastragostino, M. Thermal stability and flammability of electrolytes for lithium-ion batteries. *J. Power Sources* **2011**, *196*, 4801–4805. [CrossRef]
6. Takehara, Z.-i. Future prospects of the lithium metal anode. *J. Power Sources* **1997**, *68*, 82–86. [CrossRef]
7. Takeda, Y.; Yamamoto, O.; Imanishi, N. Lithium Dendrite Formation on a Lithium Metal Anode from Liquid, Polymer and Solid Electrolytes. *Electrochemistry* **2016**, *84*, 210–218. [CrossRef]
8. Yang, J.; Wang, X.; Zhang, G.; Ma, A.; Chen, W.; Shao, L.; Shen, C.; Xie, K. High-Performance Solid Composite Polymer Electrolyte for all Solid-State Lithium Battery Through Facile Microstructure Regulation. *Front. Chem.* **2019**, *7*. [CrossRef]
9. Chen, J.; Huang, X.; Zhu, Y.; Jiang, P. Cellulose Nanofiber Supported 3D Interconnected BN Nanosheets for Epoxy Nanocomposites with Ultrahigh Thermal Management Capability. *Adv. Funct. Mater.* **2017**, *27*, 1604754. [CrossRef]
10. Hou, H.; Xu, Q.; Pang, Y.; Li, L.; Wang, J.; Zhang, C.; Sun, C. Efficient Storing Energy Harvested by Triboelectric Nanogenerators Using a Safe and Durable All-Solid-State Sodium-Ion Battery. *Adv. Sci.* **2017**, *4*, 1700072. [CrossRef]
11. Kato, Y.; Hori, S.; Saito, T.; Suzuki, K.; Hirayama, M.; Mitsui, A.; Yonemura, M.; Iba, H.; Kanno, R. High-power all-solid-state batteries using sulfide superionic conductors. *Nat. Energy* **2016**, *1*, 16030. [CrossRef]
12. Gür, T.M. Review of electrical energy storage technologies, materials and systems: Challenges and prospects for large-scale grid storage. *Energy Environ. Sci.* **2018**, *11*, 2696–2767. [CrossRef]
13. Gittleson, F.S.; El Gabaly, F. Non-Faradaic Li^+ Migration and Chemical Coordination across Solid-State Battery Interfaces. *Nano Lett.* **2017**, *17*, 6974–6982. [CrossRef]
14. Wang, Z.; Lee, J.Z.; Xin, H.L.; Han, L.; Grillon, N.; Guy-Bouyssou, D.; Bouyssou, E.; Proust, M.; Meng, Y.S. Effects of cathode electrolyte interfacial (CEI) layer on long term cycling of all-solid-state thin-film batteries. *J. Power Sources* **2016**, *324*, 342–348. [CrossRef]
15. Lobe, S.; Dellen, C.; Finsterbusch, M.; Gehrke, H.G.; Sebold, D.; Tsai, C.L.; Uhlenbruck, S.; Guillon, O. Radio frequency magnetron sputtering of $Li_7La_3Zr_2O_{12}$ thin films for solid-state batteries. *J. Power Sources* **2016**, *307*, 684–689. [CrossRef]
16. Joshi, B.; Samuel, E.; Kim, Y.-i.; Yarin, A.L.; Swihart, M.T.; Yoon, S.S. Progress and potential of electrospinning-derived substrate-free and binder-free lithium-ion battery electrodes. *Chem. Eng. J.* **2022**, *430*, 132876. [CrossRef]
17. Patil, A.; Patil, V.; Wook Shin, D.; Choi, J.-W.; Paik, D.-S.; Yoon, S.-J. Issue and challenges facing rechargeable thin film lithium batteries. *Mater. Res. Bull.* **2008**, *43*, 1913–1942. [CrossRef]
18. Lin, J.; Lin, L.; Qu, S.; Deng, D.; Wu, Y.; Yan, X.; Xie, Q.; Wang, L.; Peng, D. Promising Electrode and Electrolyte Materials for High-Energy-Density Thin-Film Lithium Batteries. *Energy Environ. Mater.* **2022**, *5*, 133–156. [CrossRef]
19. Fenech, M.; Sharma, N. Pulsed Laser Deposition-based Thin Film Microbatteries. *Chem. Asian J.* **2020**, *15*, 1829–1847. [CrossRef]
20. Liang, X.; Tan, F.; Wei, F.; Du, J. Research progress of all solid-state thin film lithium Battery. *IOP Conf. Ser. Earth Environ. Sci.* **2019**, *218*, 012138. [CrossRef]
21. Yang, G.; Abraham, C.; Ma, Y.; Lee, M.; Helfrick, E.; Oh, D.; Lee, D. Advances in Materials Design for All-Solid-state Batteries: From Bulk to Thin Films. *Appl. Sci.* **2020**, *10*, 4727. [CrossRef]
22. Clement, B.; Lyu, M.; Sandeep Kulkarni, E.; Lin, T.; Hu, Y.; Lockett, V.; Greig, C.; Wang, L. Recent Advances in Printed Thin-Film Batteries. *Engineering* **2022**, *13*, 238–261. [CrossRef]
23. Xia, Q.; Zan, F.; Zhang, Q.; Liu, W.; Li, Q.; He, Y.; Hua, J.; Liu, J.; Xu, J.; Wang, J.; et al. All-Solid-State Thin Film Lithium/Lithium-Ion Microbatteries for Powering the Internet of Things. *Adv. Mater.* **2023**, *35*, 2200538. [CrossRef] [PubMed]
24. Pasta, M.; Armstrong, D.; Brown, Z.L.; Bu, J.; Castell, M.R.; Chen, P.; Cocks, A.; Corr, S.A.; Cussen, E.J.; Darnbrough, E.; et al. 2020 roadmap on solid-state batteries. *J. Phys. Energy* **2020**, *2*, 032008. [CrossRef]
25. Hull, M.N. Recent progress in the development of solid electrolyte batteries. *Energy Convers.* **1970**, *10*, 215–226. [CrossRef]
26. Liang, C.C.; Bro, P. A High-Voltage, Solid-State Battery System: I. Design Considerations. *J. Electrochem. Soc.* **1969**, *116*, 1322. [CrossRef]
27. Megahed, S.; Scrosati, B. Lithium-ion rechargeable batteries. *J. Power Sources* **1994**, *51*, 79–104. [CrossRef]
28. Bates, J.B.; Dudney, N.J.; Gruzalski, G.R.; Zuhr, R.A.; Choudhury, A.; Luck, C.F.; Robertson, J.D. Electrical properties of amorphous lithium electrolyte thin films. *Solid State Ion.* **1992**, *53–56*, 647–654. [CrossRef]

29. West, W.C.; Whitacre, J.F.; White, V.; Ratnakumar, B.V. Fabrication and testing of all solid-state microscale lithium batteries for microspacecraft applications. *J. Micromech. Microeng.* **2002**, *12*, 58. [CrossRef]
30. Notten, P.H.L.; Roozeboom, F.; Niessen, R.A.H.; Baggetto, L. 3-D Integrated All-Solid-State Rechargeable Batteries. *Adv. Mater.* **2007**, *19*, 4564–4567. [CrossRef]
31. Cras, F.L.; Pecquenard, B.; Dubois, V.; Phan, V.-P.; Guy-Bouyssou, D. All-Solid-State Lithium-Ion Microbatteries Using Silicon Nanofilm Anodes: High Performance and Memory Effect. *Adv. Energy Mater.* **2015**, *5*, 1501061. [CrossRef]
32. Garbayo, I.; Struzik, M.; Bowman, W.J.; Pfenninger, R.; Stilp, E.; Rupp, J.L.M. Glass-Type Polyamorphism in Li-Garnet Thin Film Solid State Battery Conductors. *Adv. Energy Mater.* **2018**, *8*, 1702265. [CrossRef]
33. Guo, Y.; Wu, S.; He, Y.-B.; Kang, F.; Chen, L.; Li, H.; Yang, Q.-H. Solid-state lithium batteries: Safety and prospects. *eScience* **2022**, *2*, 138–163. [CrossRef]
34. Zheng, Y.; Yao, Y.; Ou, J.; Li, M.; Luo, D.; Dou, H.; Li, Z.; Amine, K.; Yu, A.; Chen, Z. A review of composite solid-state electrolytes for lithium batteries: Fundamentals, key materials and advanced structures. *Chem. Soc. Rev.* **2020**, *49*, 8790–8839. [CrossRef]
35. Tong, L.; Wang, P.; Fang, W.; Guo, X.; Bao, W.; Yang, Y.; Shen, S.; Qiu, F. Interface Engineering of Silicon/Carbon Thin-Film Anodes for High-Rate Lithium-Ion Batteries. *ACS Appl. Mater. Interfaces* **2020**, *12*, 29242–29252. [CrossRef]
36. Larcher, D.; Tarascon, J.M. Towards greener and more sustainable batteries for electrical energy storage. *Nat. Chem.* **2015**, *7*, 19–29. [CrossRef] [PubMed]
37. Kang, Y.; Deng, C.; Chen, Y.; Liu, X.; Liang, Z.; Li, T.; Hu, Q.; Zhao, Y. Binder-Free Electrodes and Their Application for Li-Ion Batteries. *Nanoscale Res. Lett.* **2020**, *15*, 112. [CrossRef]
38. Aliofkhazraei, M.; Ali, N. 7.04—PVD Technology in Fabrication of Micro- and Nanostructured Coatings. In *Comprehensive Materials Processing*; Hashmi, S., Batalha, G.F., Van Tyne, C.J., Yilbas, B., Eds.; Elsevier: Oxford, UK, 2014; pp. 49–84. [CrossRef]
39. Putkonen, M.; Aaltonen, T.; Alnes, M.; Sajavaara, T.; Nilsen, O.; Fjellvåg, H. Atomic layer deposition of lithium containing thin films. *J. Mater. Chem.* **2009**, *19*, 8767–8771. [CrossRef]
40. Li, Y.; Sun, Y.; Pei, A.; Chen, K.; Vailionis, A.; Li, Y.; Zheng, G.; Sun, J.; Cui, Y. Robust Pinhole-free Li3N Solid Electrolyte Grown from Molten Lithium. *ACS Cent. Sci.* **2018**, *4*, 97–104. [CrossRef]
41. Tian, C.; Lin, F.; Doeff, M.M. Electrochemical Characteristics of Layered Transition Metal Oxide Cathode Materials for Lithium Ion Batteries: Surface, Bulk Behavior, and Thermal Properties. *Acc. Chem. Res.* **2018**, *51*, 89–96. [CrossRef]
42. Pan, Q.; Barbash, D.; Smith, D.M.; Qi, H.; Gleeson, S.E.; Li, C.Y. Correlating Electrode–Electrolyte Interface and Battery Performance in Hybrid Solid Polymer Electrolyte-Based Lithium Metal Batteries. *Adv. Energy Mater.* **2017**, *7*, 1701231. [CrossRef]
43. Zhang, W.; Schröder, D.; Arlt, T.; Manke, I.; Koerver, R.; Pinedo, R.; Weber, D.A.; Sann, J.; Zeier, W.G.; Janek, J. (Electro)chemical expansion during cycling: Monitoring the pressure changes in operating solid-state lithium batteries. *J. Mater. Chem. A* **2017**, *5*, 9929–9936. [CrossRef]
44. Koerver, R.; Zhang, W.; de Biasi, L.; Schweidler, S.; Kondrakov, A.O.; Kolling, S.; Brezesinski, T.; Hartmann, P.; Zeier, W.G.; Janek, J. Chemo-mechanical expansion of lithium electrode materials—On the route to mechanically optimized all-solid-state batteries. *Energy Environ. Sci.* **2018**, *11*, 2142–2158. [CrossRef]
45. Koerver, R.; Aygün, I.; Leichtweiß, T.; Dietrich, C.; Zhang, W.; Binder, J.O.; Hartmann, P.; Zeier, W.G.; Janek, J. Capacity Fade in Solid-State Batteries: Interphase Formation and Chemomechanical Processes in Nickel-Rich Layered Oxide Cathodes and Lithium Thiophosphate Solid Electrolytes. *Chem. Mater.* **2017**, *29*, 5574–5582. [CrossRef]
46. Bucci, G.; Talamini, B.; Renuka Balakrishna, A.; Chiang, Y.-M.; Carter, W.C. Mechanical instability of electrode-electrolyte interfaces in solid-state batteries. *Phys. Rev. Mater.* **2018**, *2*, 105407. [CrossRef]
47. Zhang, W.; Richter, F.H.; Culver, S.P.; Leichtweiss, T.; Lozano, J.G.; Dietrich, C.; Bruce, P.G.; Zeier, W.G.; Janek, J. Degradation Mechanisms at the $Li_{10}GeP_2S_{12}/LiCoO_2$ Cathode Interface in an All-Solid-State Lithium-Ion Battery. *ACS Appl. Mater. Interfaces* **2018**, *10*, 22226–22236. [CrossRef]
48. Morimoto, H.; Awano, H.; Terashima, J.; Shindo, Y.; Nakanishi, S.; Ito, N.; Ishikawa, K.; Tobishima, S.-i. Preparation of lithium ion conducting solid electrolyte of NASICON-type $Li_{1+x}Al_xTi_{2-x}(PO_4)_3$ (x = 0.3) obtained by using the mechanochemical method and its application as surface modification materials of $LiCoO_2$ cathode for lithium cell. *J. Power Sources* **2013**, *240*, 636–643. [CrossRef]
49. Richards, W.D.; Miara, L.J.; Wang, Y.; Kim, J.C.; Ceder, G. Interface Stability in Solid-State Batteries. *Chem. Mater.* **2016**, *28*, 266–273. [CrossRef]
50. Okumura, T.; Nakatsutsumi, T.; Ina, T.; Orikasa, Y.; Arai, H.; Fukutsuka, T.; Iriyama, Y.; Uruga, T.; Tanida, H.; Uchimoto, Y.; et al. Depth-resolved X-ray absorption spectroscopic study on nanoscale observation of the electrode–solid electrolyte interface for all solid state lithium ion batteries. *J. Mater. Chem.* **2011**, *21*, 10051–10060. [CrossRef]
51. Bron, P.; Roling, B.; Dehnen, S. Impedance characterization reveals mixed conducting interphases between sulfidic superionic conductors and lithium metal electrodes. *J. Power Sources* **2017**, *352*, 127–134. [CrossRef]
52. Löbberding, H.; Wessel, S.; Offermanns, C.; Kehrer, M.; Rother, J.; Heimes, H.; Kampker, A. From Cell to Battery System in BEVs: Analysis of System Packing Efficiency and Cell Types. *World Electr. Veh. J.* **2020**, *11*, 77. [CrossRef]
53. Heubner, C.; Nikolowski, K.; Reuber, S.; Schneider, M.; Wolter, M.; Michaelis, A. Recent Insights into Rate Performance Limitations of Li-ion Batteries. *Batter. Supercaps* **2021**, *4*, 268–285. [CrossRef]
54. Liu, Y.; Zhu, Y.; Cui, Y. Challenges and opportunities towards fast-charging battery materials. *Nat. Energy* **2019**, *4*, 540–550. [CrossRef]

55. Zhu, G.-L.; Zhao, C.-Z.; Huang, J.-Q.; He, C.; Zhang, J.; Chen, S.; Xu, L.; Yuan, H.; Zhang, Q. Fast Charging Lithium Batteries: Recent Progress and Future Prospects. *Samll* **2019**, *15*, 1805389. [CrossRef] [PubMed]
56. Yang, Y.; Yuan, W.; Zhang, X.; Ke, Y.; Qiu, Z.; Luo, J.; Tang, Y.; Wang, C.; Yuan, Y.; Huang, Y. A review on structuralized current collectors for high-performance lithium-ion battery anodes. *Appl. Energy* **2020**, *276*, 115464. [CrossRef]
57. Rehnlund, D.; Lindgren, F.; Böhme, S.; Nordh, T.; Zou, Y.; Pettersson, J.; Bexell, U.; Boman, M.; Edström, K.; Nyholm, L. Lithium trapping in alloy forming electrodes and current collectors for lithium based batteries. *Energy Environ. Sci.* **2017**, *10*, 1350–1357. [CrossRef]
58. Deng, W.; Zhu, W.; Zhou, X.; Liu, Z. Graphene nested porous carbon current collector for lithium metal anode with ultrahigh areal capacity. *Energy Stor. Mater.* **2018**, *15*, 266–273. [CrossRef]
59. Li, S.; Church, B.C. Electrochemical stability of aluminum current collector in aqueous rechargeable lithium-ion battery electrolytes. *J. Appl. Electrochem.* **2017**, *47*, 839–853. [CrossRef]
60. Ma, T.; Xu, G.-L.; Li, Y.; Wang, L.; He, X.; Zheng, J.; Liu, J.; Engelhard, M.H.; Zapol, P.; Curtiss, L.A.; et al. Revisiting the Corrosion of the Aluminum Current Collector in Lithium-Ion Batteries. *J. Phys. Chem. Lett.* **2017**, *8*, 1072–1077. [CrossRef]
61. Jiang, X.; Chen, J.; Yang, Y.; Lv, Y.; Ren, Y.; Li, W.; Li, C. Corrosion Protection of Copper Current Collector Of Lithium- Ion Batteries by Doped Polypyrrole Coatings. *Int. J. Electrochem. Sci.* **2020**, *15*, 2667–2676. [CrossRef]
62. Du, J.; Liu, Y.; Mo, X.; Li, Y.; Li, J.; Wu, X.; Ouyang, M. Impact of high-power charging on the durability and safety of lithium batteries used in long-range battery electric vehicles. *Appl. Energy* **2019**, *255*, 113793. [CrossRef]
63. Killer, M.; Farrokhseresht, M.; Paterakis, N.G. Implementation of large-scale Li-ion battery energy storage systems within the EMEA region. *Appl. Energy* **2020**, *260*, 114166. [CrossRef]
64. Whitehead, A.H.; Schreiber, M. Current Collectors for Positive Electrodes of Lithium-Based Batteries. *J. Electrochem. Soc.* **2005**, *152*, A2105. [CrossRef]
65. Kanamura, K.; Toriyama, S.; Shiraishi, S.; Takehara, Z.i. Studies on Electrochemical Oxidation of Nonaqueous Electrolytes Using In Situ FTIR Spectroscopy: I. The Effect of Type of Electrode on On-Set Potential for Electrochemical Oxidation of Propylene Carbonate Containing 1.0 mol dm−3. *J. Electrochem. Soc.* **1995**, *142*, 1383. [CrossRef]
66. Huang, S.; Chen, Y.; Liu, Q. Electrochemical behavior and application of a silver electrode in a 1 M LiPF6 solution. *J. Alloys Compd.* **2018**, *758*, 1–4. [CrossRef]
67. Gu, Y.; Federici, J.F. Fabrication of a Flexible Current Collector for Lithium Ion Batteries by Inkjet Printing. *Batteries* **2018**, *4*, 42. [CrossRef]
68. Fredriksson, W.; Edström, K. XPS study of duplex stainless steel as a possible current collector in a Li-ion battery. *Electrochim. Acta* **2012**, *79*, 82–94. [CrossRef]
69. Shironita, S.; Ihsan, N.; Konakawa, K.; Souma, K.; Umeda, M. Investigation of nitriding treated Ni-free stainless steel as current collector for 5 V-class Li-ion secondary cell. *Electrochim. Acta* **2019**, *295*, 1052–1056. [CrossRef]
70. Myung, S.-T.; Sasaki, Y.; Sakurada, S.; Sun, Y.-K.; Yashiro, H. Electrochemical behavior of current collectors for lithium batteries in non-aqueous alkyl carbonate solution and surface analysis by ToF-SIMS. *Electrochim. Acta* **2009**, *55*, 288–297. [CrossRef]
71. Gao, T.; Qu, Q.; Zhu, G.; Shi, Q.; Qian, F.; Shao, J.; Zheng, H. A self-supported carbon nanofiber paper/sulfur anode with high-capacity and high-power for application in Li-ion batteries. *Carbon* **2016**, *110*, 249–256. [CrossRef]
72. Myung, S.-T.; Sasaki, Y.; Saito, T.; Sun, Y.-K.; Yashiro, H. Passivation behavior of Type 304 stainless steel in a non-aqueous alkyl carbonate solution containing $LiPF_6$ salt. *Electrochim. Acta* **2009**, *54*, 5804–5812. [CrossRef]
73. Zhu, P.; Gastol, D.; Marshall, J.; Sommerville, R.; Goodship, V.; Kendrick, E. A review of current collectors for lithium-ion batteries. *J. Power Sources* **2021**, *485*, 229321. [CrossRef]
74. Doberdò, I.; Löffler, N.; Laszczynski, N.; Cericola, D.; Penazzi, N.; Bodoardo, S.; Kim, G.-T.; Passerini, S. Enabling aqueous binders for lithium battery cathodes-Carbon coating of aluminum current collector. *J. Power Sources* **2014**, *248*, 1000–1006. [CrossRef]
75. Lu, L.-L.; Zhang, Y.; Pan, Z.; Yao, H.-B.; Zhou, F.; Yu, S.-H. Lithiophilic Cu–Ni core–shell nanowire network as a stable host for improving lithium anode performance. *Energy Stor. Mater.* **2017**, *9*, 31–38. [CrossRef]
76. Hou, Z.; Yu, Y.; Wang, W.; Zhao, X.; Di, Q.; Chen, Q.; Chen, W.; Liu, Y.; Quan, Z. Lithiophilic Ag Nanoparticle Layer on Cu Current Collector toward Stable Li Metal Anode. *ACS Appl. Mater. Interfaces* **2019**, *11*, 8148–8154. [CrossRef] [PubMed]
77. Zhang, C.; Lv, W.; Zhou, G.; Huang, Z.; Zhang, Y.; Lyu, R.; Wu, H.; Yun, Q.; Kang, F.; Yang, Q.-H. Vertically Aligned Lithiophilic CuO Nanosheets on a Cu Collector to Stabilize Lithium Deposition for Lithium Metal Batteries. *Adv. Energy Mater.* **2018**, *8*, 1703404. [CrossRef]
78. Kim, S.Y.; Song, Y.I.; Wee, J.-H.; Kim, C.H.; Ahn, B.W.; Lee, J.W.; Shu, S.J.; Terrones, M.; Kim, Y.A.; Yang, C.-M. Few-layer graphene coated current collectors for safe and powerful lithium ion batteries. *Carbon* **2019**, *153*, 495–503. [CrossRef]
79. Jiang, J.; Nie, P.; Ding, B.; Wu, W.; Chang, Z.; Wu, Y.; Dou, H.; Zhang, X. Effect of Graphene Modified Cu Current Collector on the Performance of Li4Ti5O12 Anode for Lithium-Ion Batteries. *ACS Appl. Mater. Interfaces* **2016**, *8*, 30926–30932. [CrossRef]
80. Baggetto, L.; Verhaegh, N.A.M.; Niessen, R.A.H.; Roozeboom, F.; Jumas, J.-C.; Notten, P.H.L. Tin Nitride Thin Films as Negative Electrode Material for Lithium-Ion Solid-State Batteries. *J. Electrochem. Soc.* **2010**, *157*, A340. [CrossRef]
81. Cho, G.-b.; Kim, B.-m.; Noh, J.-p.; Im, Y.-m.; Lee, S.-h.; Kim, K.-w.; Nam, T.-h. Electrochemical properties of Si film electrodes with TiNi shape memory alloy as a current collector. *J. Alloys Compd.* **2013**, *577*, S190–S194. [CrossRef]
82. Chen, Y.; Fu, K.; Zhu, S.; Luo, W.; Wang, Y.; Li, Y.; Hitz, E.; Yao, Y.; Dai, J.; Wan, J.; et al. Reduced Graphene Oxide Films with Ultrahigh Conductivity as Li-Ion Battery Current Collectors. *Nano Lett.* **2016**, *16*, 3616–3623. [CrossRef] [PubMed]

83. Wu, Q.; Yang, J.; Zhao, Y.; Song, R.; Wang, Z.; Huang, Z.; Shi, M.; Ye, Y.; He, D.; Mu, S. Lifting the energy density of lithium ion batteries using graphite film current collectors. *J. Power Sources* **2020**, *455*, 227991. [CrossRef]
84. Choi, B.N.; Seo, J.Y.; Kim, B.; Kim, Y.S.; Chung, C.-H. Electro-deposition of the lithium metal anode on dendritic copper current collectors for lithium battery application. *Appl. Surf. Sci.* **2020**, *506*, 144884. [CrossRef]
85. Cao, L.; Li, L.; Xue, Z.; Yang, W.; Zou, H.; Chen, S.; Liu, Z. The aluminum current collector with honeycomb-like surface and thick Al_2O_3 film increased durability and enhanced safety for lithium-ion batteries. *J. Porous Mater.* **2020**, *27*, 1677–1683. [CrossRef]
86. Yuan, W.; Qiu, Z.; Huang, Y.; Wang, C.; Tang, Y. Honeycomb-Inspired Surface-Patterned Cu@CuO Composite Current Collector for Lithium-Ion Batteries. *Energy Technol.* **2019**, *7*, 1900445. [CrossRef]
87. Goriparti, S.; Miele, E.; De Angelis, F.; Di Fabrizio, E.; Proietti Zaccaria, R.; Capiglia, C. Review on recent progress of nanostructured anode materials for Li-ion batteries. *J. Power Sources* **2014**, *257*, 421–443. [CrossRef]
88. Feng, X.; Ouyang, M.; Liu, X.; Lu, L.; Xia, Y.; He, X. Thermal runaway mechanism of lithium ion battery for electric vehicles: A review. *Energy Stor. Mater.* **2018**, *10*, 246–267. [CrossRef]
89. Hu, Z.; Li, J.; Zhang, X.; Zhu, Y. Strategies to Improve the Performance of Li Metal Anode for Rechargeable Batteries. *Front. Chem.* **2020**, *8*, 409. [CrossRef]
90. Cheng, X.-B.; Zhang, R.; Zhao, C.-Z.; Zhang, Q. Toward Safe Lithium Metal Anode in Rechargeable Batteries: A Review. *Chem. Rev.* **2017**, *117*, 10403–10473. [CrossRef]
91. Shiga, T.; Kato, Y.; Kondo, H.; Okuda, C.-a. Self-extinguishing electrolytes using fluorinated alkyl phosphates for lithium batteries. *J. Mater. Chem. A* **2017**, *5*, 5156–5162. [CrossRef]
92. Ates, T.; Keller, M.; Kulisch, J.; Adermann, T.; Passerini, S. Development of an all-solid-state lithium battery by slurry-coating procedures using a sulfidic electrolyte. *Energy Stor. Mater.* **2019**, *17*, 204–210. [CrossRef]
93. Kozen, A.C.; Lin, C.-F.; Pearse, A.J.; Schroeder, M.A.; Han, X.; Hu, L.; Lee, S.-B.; Rubloff, G.W.; Noked, M. Next-Generation Lithium Metal Anode Engineering via Atomic Layer Deposition. *ACS Nano* **2015**, *9*, 5884–5892. [CrossRef]
94. Matsuda, S.; Kubo, Y.; Uosaki, K.; Nakanishi, S. Insulative Microfiber 3D Matrix as a Host Material Minimizing Volume Change of the Anode of Li Metal Batteries. *ACS Energy Lett.* **2017**, *2*, 924–929. [CrossRef]
95. Bordes, A.; De Vito, E.; Haon, C.; Secouard, C.; Montani, A.; Marcus, P. Investigation of Lithium Insertion Mechanisms of a Thin-Film Si Electrode by Coupling Time-of-Flight Secondary-Ion Mass Spectrometry, X-ray Photoelectron Spectroscopy, and Focused-Ion-Beam/SEM. *ACS Appl. Mater. Interfaces* **2015**, *7*, 27853–27862. [CrossRef] [PubMed]
96. Koch, S.L.; Morgan, B.J.; Passerini, S.; Teobaldi, G. Density functional theory screening of gas-treatment strategies for stabilization of high energy-density lithium metal anodes. *J. Power Sources* **2015**, *296*, 150–161. [CrossRef]
97. Li, N.-W.; Yin, Y.-X.; Yang, C.-P.; Guo, Y.-G. An Artificial Solid Electrolyte Interphase Layer for Stable Lithium Metal Anodes. *Adv. Mater.* **2016**, *28*, 1853–1858. [CrossRef]
98. Zhang, Y.-j.; Bai, W.-q.; Wang, X.-l.; Xia, X.-h.; Gu, C.-d.; Tu, J.-p. In situ confocal microscopic observation on inhibiting the dendrite formation of a-CN_x/Li electrode. *J. Mater. Chem. A* **2016**, *4*, 15597–15604. [CrossRef]
99. Yan, K.; Lee, H.-W.; Gao, T.; Zheng, G.; Yao, H.; Wang, H.; Lu, Z.; Zhou, Y.; Liang, Z.; Liu, Z.; et al. Ultrathin Two-Dimensional Atomic Crystals as Stable Interfacial Layer for Improvement of Lithium Metal Anode. *Nano Lett.* **2014**, *14*, 6016–6022. [CrossRef]
100. Lu, Y.; Tu, Z.; Archer, L.A. Stable lithium electrodeposition in liquid and nanoporous solid electrolytes. *Nat. Mater.* **2014**, *13*, 961–969. [CrossRef]
101. Zhang, X.-Q.; Cheng, X.-B.; Zhang, Q. Advances in Interfaces between Li Metal Anode and Electrolyte. *Adv. Mater. Interfaces* **2018**, *5*, 1701097. [CrossRef]
102. Park, C.-M.; Kim, J.-H.; Kim, H.; Sohn, H.-J. Li-alloy based anode materials for Li secondary batteries. *Chem. Soc. Rev.* **2010**, *39*, 3115–3141. [CrossRef] [PubMed]
103. Fu, K.; Gong, Y.; Fu, Z.; Xie, H.; Yao, Y.; Liu, B.; Carter, M.; Wachsman, E.; Hu, L. Transient Behavior of the Metal Interface in Lithium Metal–Garnet Batteries. *Angew. Chem. Int. Ed.* **2017**, *56*, 14942–14947. [CrossRef] [PubMed]
104. Fu, K.; Gong, Y.; Liu, B.; Zhu, Y.; Xu, S.; Yao, Y.; Luo, W.; Wang, C.; Lacey, S.D.; Dai, J.; et al. Toward garnet electrolyte-based Li metal batteries: An ultrathin, highly effective, artificial solid-state electrolyte/metallic Li interface. *Sci. Adv.* **2017**, *3*, e1601659. [CrossRef] [PubMed]
105. Liu, Y.; Li, C.; Li, B.; Song, H.; Cheng, Z.; Chen, M.; He, P.; Zhou, H. Germanium Thin Film Protected Lithium Aluminum Germanium Phosphate for Solid-State Li Batteries. *Adv. Energy Mater.* **2018**, *8*, 1702374. [CrossRef]
106. He, M.; Cui, Z.; Chen, C.; Li, Y.; Guo, X. Formation of self-limited, stable and conductive interfaces between garnet electrolytes and lithium anodes for reversible lithium cycling in solid-state batteries. *J. Mater. Chem. A* **2018**, *6*, 11463–11470. [CrossRef]
107. Feng, W.; Dong, X.; Li, P.; Wang, Y.; Xia, Y. Interfacial modification of Li/Garnet electrolyte by a lithiophilic and breathing interlayer. *J. Power Sources* **2019**, *419*, 91–98. [CrossRef]
108. Tsai, C.-L.; Roddatis, V.; Chandran, C.V.; Ma, Q.; Uhlenbruck, S.; Bram, M.; Heitjans, P.; Guillon, O. $Li_7La_3Zr_2O_{12}$ Interface Modification for Li Dendrite Prevention. *ACS Appl. Mater. Interfaces* **2016**, *8*, 10617–10626. [CrossRef]
109. Obrovac, M.N.; Christensen, L. Structural Changes in Silicon Anodes during Lithium Insertion/Extraction. *Electrochem. Solid-State Lett.* **2004**, *7*, A93. [CrossRef]
110. Moon, T.; Kim, C.; Park, B. Electrochemical performance of amorphous-silicon thin films for lithium rechargeable batteries. *J. Power Sources* **2006**, *155*, 391–394. [CrossRef]

111. Omampuliyur, R.S.; Bhuiyan, M.; Han, Z.; Jing, Z.; Li, L.; Fitzgerald, E.A.; Thompson, C.V.; Choi, W.K. Nanostructured Thin Film Silicon Anodes for Li-Ion Microbatteries. *J. Nanosci. Nanotechnol.* **2015**, *15*, 4926–4933. [CrossRef]
112. Oudenhoven, J.F.M.; Baggetto, L.; Niessen, R.A.H.; Knoops, H.C.M.; Donders, M.E.; van Dongen, T.; de Croon, M.H.J.M.; Kessels, W.M.M.; Notten, P.H.L. Towards High Energy Density 3D-integrated Lithium-ion Micro-batteries. *MRS Online Proc. Libr.* **2011**, *1168*, 1. [CrossRef]
113. Ohara, S.; Suzuki, J.; Sekine, K.; Takamura, T. A thin film silicon anode for Li-ion batteries having a very large specific capacity and long cycle life. *J. Power Sources* **2004**, *136*, 303–306. [CrossRef]
114. Deng, H.; Park, M.; Chung, C.Y.; Park, C.-H.; Joo, S.-K. Effect of Substrate Surface Conditions on Electrochemical Performance of Si Thin Film Anode. *ECS Trans.* **2007**, *2*, 105. [CrossRef]
115. Takamura, T.; Ohara, S.; Uehara, M.; Suzuki, J.; Sekine, K. A vacuum deposited Si film having a Li extraction capacity over 2000 mAh/g with a long cycle life. *J. Power Sources* **2004**, *129*, 96–100. [CrossRef]
116. Zhang, T.; Zhang, H.P.; Yang, L.C.; Wang, B.; Wu, Y.P.; Takamura, T. The structural evolution and lithiation behavior of vacuum-deposited Si film with high reversible capacity. *Electrochim. Acta* **2008**, *53*, 5660–5664. [CrossRef]
117. Ko, M.; Chae, S.; Cho, J. Challenges in Accommodating Volume Change of Si Anodes for Li-Ion Batteries. *ChemElectroChem* **2015**, *2*, 1645–1651. [CrossRef]
118. Cho, G.-b.; Noh, J.-p.; Sung, H.-j.; Lee, S.-h.; Im, Y.-m.; Ahn, H.-j.; Kim, K.-w. Patterned Si thin film electrodes for enhancing structural stability. *Nanoscale Res. Lett.* **2012**, *7*, 20. [CrossRef]
119. Baggetto, L.; Danilov, D.; Notten, P.H.L. Honeycomb-Structured Silicon: Remarkable Morphological Changes Induced by Electrochemical (De)Lithiation. *Adv. Mater.* **2011**, *23*, 1563–1566. [CrossRef]
120. Polat, B.D.; Eryilmaz, O.L.; Keleş, O.; Erdemir, A.; Amine, K. Compositionally graded SiCu thin film anode by magnetron sputtering for lithium ion battery. *Thin Solid Film.* **2015**, *596*, 190–197. [CrossRef]
121. Hwang, C.-M.; Lim, C.-H.; Yang, J.-H.; Park, J.-W. Electrochemical properties of negative $SiMo_x$ electrodes deposited on a roughened substrate for rechargeable lithium batteries. *J. Power Sources* **2009**, *194*, 1061–1067. [CrossRef]
122. Kim, J.-B.; Jun, B.-S.; Lee, S.-M. Improvement of capacity and cyclability of Fe/Si multilayer thin film anodes for lithium rechargeable batteries. *Electrochim. Acta* **2005**, *50*, 3390–3394. [CrossRef]
123. Zhang, Q.; Liu, J.; Wu, Z.-Y.; Li, J.-T.; Huang, L.; Sun, S.-G. 3D nanostructured multilayer Si/Al film with excellent cycle performance as anode material for lithium-ion battery. *J. Alloys Compd.* **2016**, *657*, 559–564. [CrossRef]
124. Liu, H.; Zhu, M.; Du, Z.; Obrovac, M.N. The Electrochemistry of Amorphous Si-B Thin Film Electrodes in Li Cells. *J. Electrochem. Soc.* **2016**, *163*, A192. [CrossRef]
125. Li, H.; Bai, H.; Tao, Z.; Chen, J. Si–Y multi-layer thin films as anode materials of high-capacity lithium-ion batteries. *J. Power Sources* **2012**, *217*, 102–107. [CrossRef]
126. Wang, Y.H.; He, Y.; Xiao, R.J.; Li, H.; Aifantis, K.E.; Huang, X.J. Investigation of crack patterns and cyclic performance of Ti–Si nanocomposite thin film anodes for lithium ion batteries. *J. Power Sources* **2012**, *202*, 236–245. [CrossRef]
127. Wu, C.-Y.; Chang, C.-C.; Duh, J.-G. Silicon nitride coated silicon thin film on three dimensions current collector for lithium ion battery anode. *J. Power Sources* **2016**, *325*, 64–70. [CrossRef]
128. Lin, J.; Guo, J.; Liu, C.; Guo, H. Artificial solid electrolyte interphase with in-situ formed porosity for enhancing lithiation of silicon wafer. *J. Power Sources* **2016**, *336*, 401–407. [CrossRef]
129. Jiao, M.; Wang, Y.; Ye, C.; Wang, C.; Zhang, W.; Liang, C. High-capacity SiO_x ($0 \leq x \leq 2$) as promising anode materials for next-generation lithium-ion batteries. *J. Alloys Compd.* **2020**, *842*, 155774. [CrossRef]
130. Lee, J.; Moon, J.; Han, S.A.; Kim, J.; Malgras, V.; Heo, Y.-U.; Kim, H.; Lee, S.-M.; Liu, H.K.; Dou, S.X.; et al. Everlasting Living and Breathing Gyroid 3D Network in Si@SiO_x/C Nanoarchitecture for Lithium Ion Battery. *ACS Nano* **2019**, *13*, 9607–9619. [CrossRef]
131. Tang, C.; Liu, Y.; Xu, C.; Zhu, J.; Wei, X.; Zhou, L.; He, L.; Yang, W.; Mai, L. Ultrafine Nickel-Nanoparticle-Enabled SiO_2 Hierarchical Hollow Spheres for High-Performance Lithium Storage. *Adv. Funct. Mater.* **2018**, *28*, 1704561. [CrossRef]
132. Poizot, P.; Laruelle, S.; Grugeon, S.; Dupont, L.; Tarascon, J.M. Nano-sized transition-metal oxides as negative-electrode materials for lithium-ion batteries. *Nature* **2000**, *407*, 496–499. [CrossRef] [PubMed]
133. Reddy, M.V.; Subba Rao, G.V.; Chowdari, B.V.R. Metal Oxides and Oxysalts as Anode Materials for Li Ion Batteries. *Chem. Rev.* **2013**, *113*, 5364–5457. [CrossRef]
134. Li, N.; Patrissi, C.J.; Che, G.; Martin, C.R. Rate Capabilities of Nanostructured $LiMn_2O_4$ Electrodes in Aqueous Electrolyte. *J. Electrochem. Soc.* **2000**, *147*, 2044. [CrossRef]
135. Li, H.; Wang, Z.; Chen, L.; Huang, X. Research on Advanced Materials for Li-ion Batteries. *Adv. Mater.* **2009**, *21*, 4593–4607. [CrossRef]
136. Cunha, D.M.; Hendriks, T.A.; Vasileiadis, A.; Vos, C.M.; Verhallen, T.; Singh, D.P.; Wagemaker, M.; Huijben, M. Doubling Reversible Capacities in Epitaxial $Li_4Ti_5O_{12}$ Thin Film Anodes for Microbatteries. *ACS Appl. Energy Mater.* **2019**, *2*, 3410–3418. [CrossRef]
137. Daramalla, V.; Penki, T.R.; Munichandraiah, N.; Krupanidhi, S.B. Fabrication of $TiNb_2O_7$ thin film electrodes for Li-ion micro-batteries by pulsed laser deposition. *Mater. Sci. Eng. B* **2016**, *213*, 90–97. [CrossRef]
138. Daramalla, V.; Venkatesh, G.; Kishore, B.; Munichandraiah, N.; Krupanidhi, S.B. Superior Electrochemical Performance of Amorphous Titanium Niobium Oxide Thin Films for Li-Ion Thin Film Batteries. *J. Electrochem. Soc.* **2018**, *165*, A764. [CrossRef]

139. Rambabu, A.; Senthilkumar, B.; Dayamani, A.; Krupanidhi, S.B.; Barpanda, P. Preferentially oriented $SrLi_2Ti_6O14$ thin film anode for Li-ion micro-batteries fabricated by pulsed laser deposition. *Electrochim. Acta* **2018**, *269*, 212–216. [CrossRef]
140. Maximov, M.Y.; Novikov, P.A.; Nazarov, D.V.; Rymyantsev, A.M.; Silin, A.O.; Zhang, Y.; Popovich, A.A. Characterization and Electrochemical Performance at High Discharge Rates of Tin Dioxide Thin Films Synthesized by Atomic Layer Deposition. *J. Electron. Mater.* **2017**, *46*, 6571–6577. [CrossRef]
141. Lee, S.-J.; Lee, H.-Y.; Ha, T.-S.; Baik, H.-K.; Lee, S.-M. Amorphous Lithium Nickel Vanadate Thin-Film Anodes for Rechargeable Lithium Microbatteries. *Electrochem. Solid-State Lett.* **2002**, *5*, A138. [CrossRef]
142. Wei, K.; Zhao, Y.; Cui, Y.; Wang, J.; Cui, Y.; Zhu, R.; Zhuang, Q.; Xue, M. Lithium phosphorous oxynitride (LiPON) coated $NiFe_2O_4$ anode material with enhanced electrochemical performance for lithium ion batteries. *J. Alloys Compd.* **2018**, *769*, 110–119. [CrossRef]
143. Khamlich, S.; Nuru, Z.Y.; Bello, A.; Fabiane, M.; Dangbegnon, J.K.; Manyala, N.; Maaza, M. Pulsed laser deposited Cr_2O_3 nanostructured thin film on graphene as anode material for lithium-ion batteries. *J. Alloys Compd.* **2015**, *637*, 219–225. [CrossRef]
144. Teng, X.; Qin, Y.; Wang, X.; Li, H.; Shang, X.; Fan, S.; Li, Q.; Xu, J.; Cao, D.; Li, S. A Nanocrystalline Fe_2O_3 Film Anode Prepared by Pulsed Laser Deposition for Lithium-Ion Batteries. *Nanoscale Res. Lett.* **2018**, *13*, 60. [CrossRef] [PubMed]
145. Fenech, M.; Lim, S.; Cheung, J.; Sharma, N. Mechanistic insights into the phenomena of increasing capacity with cycle number: Using pulsed-laser deposited MoO_2 thin film electrodes. *Phys. Chem. Chem. Phys.* **2019**, *21*, 25779–25787. [CrossRef]
146. Wang, D.; Li, Y.; Zhao, Y.; Guo, Q.; Yang, S.; Ding, G.; Mei, Y.; Huang, G. Cycling-Induced Capacity Increase of Graphene Aerogel/ZnO Nanomembrane Composite Anode Fabricated by Atomic Layer Deposition. *Nanoscale Res. Lett.* **2019**, *14*, 69. [CrossRef]
147. Dhara, A.; Sarkar, S.K.; Mitra, S. Controlled 3D Carbon Nanotube Architecture Coated with MoOx Material by ALD Technique: A High Energy Density Lithium-Ion Battery Electrode. *Adv. Mater. Interfaces* **2017**, *4*, 1700332. [CrossRef]
148. Gregorczyk, K.E.; Kozen, A.C.; Chen, X.; Schroeder, M.A.; Noked, M.; Cao, A.; Hu, L.; Rubloff, G.W. Fabrication of 3D Core–Shell Multiwalled Carbon Nanotube@RuO2 Lithium-Ion Battery Electrodes through a RuO_2 Atomic Layer Deposition Process. *ACS Nano* **2015**, *9*, 464–473. [CrossRef]
149. Sinha, S.; Ramasamy, H.V.; Nandi, D.K.; Didwal, P.N.; Cho, J.Y.; Park, C.-J.; Lee, Y.-S.; Kim, S.-H.; Heo, J. Atomic layer deposited zinc oxysulfide anodes in Li-ion batteries: An efficient solution for electrochemical instability and low conductivity. *J. Mater. Chem. A* **2018**, *6*, 16515–16528. [CrossRef]
150. Zhou, Y.; Zhang, H.; Xue, M.; Wu, C.; Wu, X.; Fu, Z. The electrochemistry of nanostructured In_2O_3 with lithium. *J. Power Sources* **2006**, *162*, 1373–1378. [CrossRef]
151. Takehara, Z.i.; Ogumi, Z.; Uchimoto, Y.; Endo, E.; Kanamori, Y. Thin Film Solid-State Lithium Batteries Prepared by Consecutive Vapor-Phase Processes. *J. Electrochem. Soc.* **1991**, *138*, 1574. [CrossRef]
152. Ohtsuka, H.; Sakurai, Y. Characteristics of Li/MoO_{3-x} thin film batteries. *Solid State Ion.* **2001**, *144*, 59–64. [CrossRef]
153. Baba, M.; Kumagai, N.; Fujita, N.; Ohta, K.; Nishidate, K.; Komaba, S.; Groult, H.; Devilliers, D.; Kaplan, B. Fabrication and electrochemical characteristics of all-solid-state lithium-ion rechargeable batteries composed of $LiMn_2O_4$ positive and V_2O_5 negative electrodes. *J. Power Sources* **2001**, *97–98*, 798–800. [CrossRef]
154. Chiu, K.F. Lithium cobalt oxide thin films deposited at low temperature by ionized magnetron sputtering. *Thin Solid Films* **2007**, *515*, 4614–4618. [CrossRef]
155. Iriyama, Y.; Nishimoto, K.; Yada, C.; Abe, T.; Ogumi, Z.; Kikuchi, K. Charge-Transfer Reaction at the Lithium Phosphorus Oxynitride Glass Electrolyte/Lithium Manganese Oxide Thin-Film Interface and Its Stability on Cycling. *J. Electrochem. Soc.* **2006**, *153*, A821. [CrossRef]
156. Hong, J.; Wang, C.; Dudney, N.J.; Lance, M.J. Characterization and Performance of $LiFePO_4$ Thin-Film Cathodes Prepared with Radio-Frequency Magnetron-Sputter Deposition. *J. Electrochem. Soc.* **2007**, *154*, A805. [CrossRef]
157. Shobana, M.K. Metal oxide coated cathode materials for Li ion batteries—A review. *J. Alloys Compd.* **2019**, *802*, 477–487. [CrossRef]
158. Julien, C.M.; Mauger, A. Review of 5-V electrodes for Li-ion batteries: Status and trends. *Ionics* **2013**, *19*, 951–988. [CrossRef]
159. Yang, X.; Yang, T.; Liang, S.; Wu, X.; Zhang, H. Modification of $LiNi_{0.5}Mn_{1.5}O_4$ high potential cathode from the inner lattice to the outer surface with Cr^{3+}-doping and Li+-conductor coating. *J. Mater. Chem. A* **2014**, *2*, 10359–10364. [CrossRef]
160. Birkl, C.R.; Roberts, M.R.; McTurk, E.; Bruce, P.G.; Howey, D.A. Degradation diagnostics for lithium ion cells. *J. Power Sources* **2017**, *341*, 373–386. [CrossRef]
161. Kim, J.; Kim, H.; Kang, K. Surface-Modified Spinel $LiNi_{0.5}Mn_{1.5}O_4$ for Li-Ion Batteries. *J. Korean Ceram. Soc* **2018**, *55*, 21–35. [CrossRef]
162. Wang, Y.; Peng, Q.; Yang, G.; Yang, Z.; Zhang, L.; Long, H.; Huang, Y.; Lu, P. High-stability 5V spinel $LiNi_{0.5}Mn_{1.5}O_4$ sputtered thin film electrodes by modifying with aluminium oxide. *Electrochim. Acta* **2014**, *136*, 450–456. [CrossRef]
163. Chen, Y.; Zhang, Y.; Chen, B.; Wang, Z.; Lu, C. An approach to application for $LiNi_{0.6}Co_{0.2}Mn_{0.2}O_2$ cathode material at high cutoff voltage by TiO_2 coating. *J. Power Sources* **2014**, *256*, 20–27. [CrossRef]
164. Sun, Y.K.; Lee, Y.S.; Yoshio, M.; Amine, K. Synthesis and Electrochemical Properties of ZnO-Coated $LiNi_{0.5}Mn_{1.5}O_4$ Spinel as 5 V Cathode Material for Lithium Secondary Batteries. *Electrochem. Solid-State Lett.* **2002**, *5*, A99. [CrossRef]
165. Wu, Q.; Zhang, X.; Sun, S.; Wan, N.; Pan, D.; Bai, Y.; Zhu, H.; Hu, Y.-S.; Dai, S. Improved electrochemical performance of spinel $LiMn_{1.5}Ni_{0.5}O_4$ through MgF_2 nano-coating. *Nanoscale* **2015**, *7*, 15609–15617. [CrossRef]

166. Park, B.C.; Kim, H.B.; Myung, S.T.; Amine, K.; Belharouak, I.; Lee, S.M.; Sun, Y.K. Improvement of structural and electrochemical properties of AlF_3-coated $Li[Ni_{1/3}Co_{1/3}Mn_{1/3}]O_2$ cathode materials on high voltage region. *J. Power Sources* **2008**, *178*, 826–831. [CrossRef]
167. Lu, C.; Wu, H.; Zhang, Y.; Liu, H.; Chen, B.; Wu, N.; Wang, S. Cerium fluoride coated layered oxide $Li_{1.2}Mn_{0.54}Ni_{0.13}Co_{0.13}O_2$ as cathode materials with improved electrochemical performance for lithium ion batteries. *J. Power Sources* **2014**, *267*, 682–691. [CrossRef]
168. Konishi, H.; Suzuki, K.; Taminato, S.; Kim, K.; Zheng, Y.; Kim, S.; Lim, J.; Hirayama, M.; Son, J.-Y.; Cui, Y.; et al. Effect of surface Li_3PO_4 coating on $LiNi_{0.5}Mn_{1.5}O_4$ epitaxial thin film electrodes synthesized by pulsed laser deposition. *J. Power Sources* **2014**, *269*, 293–298. [CrossRef]
169. Jang, W.H.; Kim, M.C.; Lee, S.N.; Ahn, J.Y.; Aravindan, V.; Lee, Y.S. Enhanced elevated temperature performance of $LiFePO_4$ modified spinel $LiNi_{0.5}Mn_{1.5}O_4$ cathode. *J. Alloys Compd.* **2014**, *612*, 51–55. [CrossRef]
170. Deng, Y.; Mou, J.; Wu, H.; Jiang, N.; Zheng, Q.; Lam, K.H.; Xu, C.; Lin, D. A superior Li_2SiO_3-Composited $LiNi_{0.5}Mn_{1.5}O_4$ Cathode for High-Voltage and High-Performance Lithium-ion Batteries. *Electrochim. Acta* **2017**, *235*, 19–31. [CrossRef]
171. Lv, S.; Li, M.; Luo, X.; Cheng, J.; Li, Z. High-voltage $LiNi_{0.5}Mn_{1.5}O_4$ thin film cathodes stabilized by LiPON solid electrolyte coating to enhance cyclic stability and rate capability. *J. Alloys Compd.* **2020**, *815*, 151636. [CrossRef]
172. Yang, T.; Zhang, N.; Lang, Y.; Sun, K. Enhanced rate performance of carbon-coated $LiNi_{0.5}Mn_{1.5}O_4$ cathode material for lithium ion batteries. *Electrochim. Acta* **2011**, *56*, 4058–4064. [CrossRef]
173. Fang, X.; Ge, M.; Rong, J.; Zhou, C. Graphene-oxide-coated $LiNi_{0.5}Mn_{1.5}O_4$ as high voltage cathode for lithium ion batteries with high energy density and long cycle life. *J. Mater. Chem. A* **2013**, *1*, 4083–4088. [CrossRef]
174. Yi, T.-F.; Xie, Y.; Ye, M.-F.; Jiang, L.-J.; Zhu, R.-S.; Zhu, Y.-R. Recent developments in the doping of $LiNi_{0.5}Mn_{1.5}O_4$ cathode material for 5 V lithium-ion batteries. *Ionics* **2011**, *17*, 383–389. [CrossRef]
175. Luo, Y.; Lu, T.; Zhang, Y.; Yan, L.; Mao, S.S.; Xie, J. Surface-segregated, high-voltage spinel lithium-ion battery cathode material $LiNi_{0.5}Mn_{1.5}O_4$ cathodes by aluminium doping with improved high-rate cyclability. *J. Alloys Compd.* **2017**, *703*, 289–297. [CrossRef]
176. Aklalouch, M.; Amarilla, J.M.; Rojas, R.M.; Saadoune, I.; Rojo, J.M. Chromium doping as a new approach to improve the cycling performance at high temperature of 5V LiNi0.5Mn1.5O4-based positive electrode. *J. Power Sources* **2008**, *185*, 501–511. [CrossRef]
177. Liu, J.; Manthiram, A. Understanding the Improvement in the Electrochemical Properties of Surface Modified 5 V $LiMn_{1.42}Ni_{0.42}Co_{0.16}O_4$ Spinel Cathodes in Lithium-ion Cells. *Chem. Mater.* **2009**, *21*, 1695–1707. [CrossRef]
178. Wang, H.; Xia, H.; Lai, M.O.; Lu, L. Enhancements of rate capability and cyclic performance of spinel $LiNi_{0.5}Mn_{1.5}O_4$ by trace Ru-doping. *Electrochem. Commun.* **2009**, *11*, 1539–1542. [CrossRef]
179. Xu, X.X.; Yang, J.; Wang, Y.Q.; NuLi, Y.N.; Wang, J.L. $LiNi_{0.5}Mn_{1.5}O_{3.975}F_{0.05}$ as novel 5V cathode material. *J. Power Sources* **2007**, *174*, 1113–1116. [CrossRef]
180. Amine, K.; Yasuda, H.; Yamachi, M. Olivine $LiCoPO_4$ as 4.8 V Electrode Material for Lithium Batteries. *Electrochem. Solid-State Lett.* **2000**, *3*, 178. [CrossRef]
181. Zhang, M.; Garcia-Araez, N.; Hector, A.L. Understanding and development of olivine $LiCoPO_4$ cathode materials for lithium-ion batteries. *J. Mater. Chem. A* **2018**, *6*, 14483–14517. [CrossRef]
182. Ruzgas, T.; Larpant, N.; Shafaat, A.; Sotres, J. Cover Feature: Wireless, Battery-Less Biosensors Based on Direct Electron Transfer Reactions. *ChemElectroChem* **2019**, *6*, 5165. [CrossRef]
183. Wu, B.; Xu, H.; Mu, D.; Shi, L.; Jiang, B.; Gai, L.; Wang, L.; Liu, Q.; Ben, L.; Wu, F. Controlled solvothermal synthesis and electrochemical performance of $LiCoPO_4$ submicron single crystals as a cathode material for lithium ion batteries. *J. Power Sources* **2016**, *304*, 181–188. [CrossRef]
184. Laszczynski, N.; Birrozzi, A.; Maranski, K.; Copley, M.; Schuster, M.E.; Passerini, S. Effect of coatings on the green electrode processing and cycling behaviour of $LiCoPO_4$. *J. Mater. Chem. A* **2016**, *4*, 17121–17128. [CrossRef]
185. Konishi, S.; Murayama, D.; Itadani, A.; Uematsu, K.; Toda, K.; Sato, M.; Arimitsu, N.; Aoki, T.; Yamaguchi, T. Improvement in Electrochemical Performance of $LiCoPO_4$ Using Furnace Blacks with High Surface Areas as a Carbon-based Composite Material. *Electrochemistry* **2017**, *85*, 643–646. [CrossRef]
186. Örnek, A. An impressive approach to solving the ongoing stability problems of $LiCoPO_4$ cathode: Nickel oxide surface modification with excellent core–shell principle. *J. Power Sources* **2017**, *356*, 1–11. [CrossRef]
187. Wang, Y.; Qiu, J.; Yu, Z.; Ming, H.; Li, M.; Zhang, S.; Yang, Y. AlF_3-modified $LiCoPO_4$ for an advanced cathode towards high energy lithium-ion battery. *Ceram. Int.* **2018**, *44*, 1312–1320. [CrossRef]
188. Lee, W.; Muhammad, S.; Sergey, C.; Lee, H.; Yoon, J.; Kang, Y.-M.; Yoon, W.-S. Advances in the Cathode Materials for Lithium Rechargeable Batteries. *Angew. Chem. Int. Ed.* **2020**, *59*, 2578–2605. [CrossRef]
189. Molenda, J. Electronic limitations of lithium diffusibility. From layered and spinel toward novel olivine type cathode materials. *Solid State Ion.* **2005**, *176*, 1687–1694. [CrossRef]
190. Yu, F.D.; Que, L.F.; Wang, Z.B.; Zhang, Y.; Xue, Y.; Liu, B.S.; Gu, D.M. Layered-spinel capped nanotube assembled 3D Li-rich hierarchitectures for high performance Li-ion battery cathodes. *J. Mater. Chem. A* **2016**, *4*, 18416–18425. [CrossRef]
191. Wang, S.; Li, S.; Sun, Y.; Feng, X.; Chen, C. Three-dimensional porous V_2O_5 cathode with ultra high rate capability. *Energy Environ. Sci.* **2011**, *4*, 2854–2857. [CrossRef]

192. Pearse, A.; Schmitt, T.; Sahadeo, E.; Stewart, D.M.; Kozen, A.; Gerasopoulos, K.; Talin, A.A.; Lee, S.B.; Rubloff, G.W.; Gregorczyk, K.E. Three-Dimensional Solid-State Lithium-Ion Batteries Fabricated by Conformal Vapor-Phase Chemistry. *ACS Nano* **2018**, *12*, 4286–4294. [CrossRef] [PubMed]
193. Xia, H.; Wan, Y.; Assenmacher, W.; Mader, W.; Yuan, G.; Lu, L. Facile synthesis of chain-like $LiCoO_2$ nanowire arrays as three-dimensional cathode for microbatteries. *NPG Asia Mater.* **2014**, *6*, e126. [CrossRef]
194. Maximov, M.; Nazarov, D.; Rumyantsev, A.; Koshtyal, Y.; Ezhov, I.; Mitrofanov, I.; Kim, A.; Medvedev, O.; Popovich, A. Atomic Layer Deposition of Lithium–Nickel–Silicon Oxide Cathode Material for Thin-Film Lithium-Ion Batteries. *Energies* **2020**, *13*, 2345. [CrossRef]
195. Wang, G.X.; Lindsay, M.J.; Ionescu, M.; Bradhurst, D.H.; Dou, S.X.; Liu, H.K. Physical and electrochemical characterization of $LiNi_{0.8}Co_{0.2}O_2$ thin-film electrodes deposited by laser ablation. *J. Power Sources* **2001**, *97–98*, 298–302. [CrossRef]
196. Qi, Z.; Tang, J.; Huang, J.; Zemlyanov, D.; Pol, V.G.; Wang, H. Li_2MnO_3 Thin Films with Tilted Domain Structure as Cathode for Li-Ion Batteries. *ACS Appl. Energy Mater.* **2019**, *2*, 3461–3468. [CrossRef]
197. Ramana, C.V.; Zaghib, K.; Julien, C.M. Pulsed-laser deposited $LiNi_{0.8}Co_{0.15}Al_{0.05}O_2$ thin films for application in microbatteries. *Appl. Phys. Lett.* **2007**, *90*, 021916. [CrossRef]
198. Deng, J.; Xi, L.; Wang, L.; Wang, Z.; Chung, C.Y.; Han, X.; Zhou, H. Electrochemical performance of $LiNi_{1/3}Co_{1/3}Mn_{1/3}O_2$ thin film electrodes prepared by pulsed laser deposition. *J. Power Sources* **2012**, *217*, 491–497. [CrossRef]
199. Jacob, C.; Lynch, T.; Chen, A.; Jian, J.; Wang, H. Highly textured $Li(Ni_{0.5}Mn_{0.3}Co_{0.2})O_2$ thin films on stainless steel as cathode for lithium-ion battery. *J. Power Sources* **2013**, *241*, 410–414. [CrossRef]
200. Phillip, N.D.; Westover, A.S.; Daniel, C.; Veith, G.M. Structural Degradation of High Voltage Lithium Nickel Manganese Cobalt Oxide (NMC) Cathodes in Solid-State Batteries and Implications for Next Generation Energy Storage. *ACS Appl. Energy Mater.* **2020**, *3*, 1768–1774. [CrossRef]
201. Yan, B.; Liu, J.; Song, B.; Xiao, P.; Lu, L. Li-rich Thin Film Cathode Prepared by Pulsed Laser Deposition. *Sci. Rep.* **2013**, *3*, 3332. [CrossRef]
202. Fehse, M.; Trócoli, R.; Ventosa, E.; Hernández, E.; Sepúlveda, A.; Morata, A.; Tarancón, A. Ultrafast Dischargeable $LiMn_2O_4$ Thin-Film Electrodes with Pseudocapacitive Properties for Microbatteries. *ACS Appl. Mater. Interfaces* **2017**, *9*, 5295–5301. [CrossRef]
203. Lim, J.; Lee, S.; Suzuki, K.; Kim, K.; Kim, S.; Taminato, S.; Hirayama, M.; Oshima, Y.; Takayanagi, K.; Kanno, R. Synthesis, structure and electrochemical properties of novel Li–Co–Mn–O epitaxial thin-film electrode using layer-by-layer deposition process. *J. Power Sources* **2015**, *279*, 502–509. [CrossRef]
204. Kuwata, N.; Kudo, S.; Matsuda, Y.; Kawamura, J. Fabrication of thin-film lithium batteries with 5-V-class $LiCoMnO_4$ cathodes. *Solid State Ion.* **2014**, *262*, 165–169. [CrossRef]
205. Wang, Y.; Yang, G.; Peng, Q.; Lu, P.X. Excellent Electrochemical Performance and Thermal Stability of $LiNi_{0.5}Mn_{1.5}O_4$ Thin-Film Cathode Prepared by Pulsed Laser Deposition. *Adv. Mater. Res.* **2014**, *853*, 83–89. [CrossRef]
206. Fujimoto, D.; Kuwata, N.; Matsuda, Y.; Kawamura, J.; Kang, F. Fabrication of solid-state thin-film batteries using $LiMnPO_4$ thin films deposited by pulsed laser deposition. *Thin Solid Films* **2015**, *579*, 81–88. [CrossRef]
207. Mosa, J.; Aparicio, M.; Durán, A.; Laberty-Robert, C.; Sanchez, C. Nanocrystalline mesoporous LiFePO4 thin-films as cathodes for Li-ion microbatteries. *J. Mater. Chem. A* **2014**, *2*, 3038–3046. [CrossRef]
208. Zuo, W.; Luo, M.; Liu, X.; Wu, J.; Liu, H.; Li, J.; Winter, M.; Fu, R.; Yang, W.; Yang, Y. Li-rich cathodes for rechargeable Li-based batteries: Reaction mechanisms and advanced characterization techniques. *Energy Environ. Sci.* **2020**, *13*, 4450–4497. [CrossRef]
209. Rana, J.; Stan, M.; Kloepsch, R.; Li, J.; Schumacher, G.; Welter, E.; Zizak, I.; Banhart, J.; Winter, M. Structural Changes in Li2MnO3 Cathode Material for Li-Ion Batteries. *Adv. Energy Mater.* **2014**, *4*, 1300998. [CrossRef]
210. Li, N.; Hwang, S.; Sun, M.; Fu, Y.; Battaglia, V.S.; Su, D.; Tong, W. Unraveling the Voltage Decay Phenomenon in Li-Rich Layered Oxide Cathode of No Oxygen Activity. *Adv. Energy Mater.* **2019**, *9*, 1902258. [CrossRef]
211. Sathiya, M.; Abakumov, A.M.; Foix, D.; Rousse, G.; Ramesha, K.; Saubanère, M.; Doublet, M.L.; Vezin, H.; Laisa, C.P.; Prakash, A.S.; et al. Origin of voltage decay in high-capacity layered oxide electrodes. *Nat. Mater.* **2015**, *14*, 230–238. [CrossRef]
212. Park, C.W.; Kim, S.H.; Nahm, K.S.; Chung, H.T.; Lee, Y.S.; Lee, J.H.; Boo, S.; Kim, J. Structural and electrochemical study of $Li[Cr_xLi_{(1-x)/3}Mn_{2(1-x)/3}]O_2$ ($0 \leq x \leq 0.328$) cathode materials. *J. Alloys Compd.* **2008**, *449*, 343–348. [CrossRef]
213. Chen, R.; Ren, S.; Knapp, M.; Wang, D.; Witter, R.; Fichtner, M.; Hahn, H. Disordered Lithium-Rich Oxyfluoride as a Stable Host for Enhanced Li^+ Intercalation Storage. *Adv. Energy Mater.* **2015**, *5*, 1401814. [CrossRef]
214. Zhao, S.; Guo, Z.; Yan, K.; Wan, S.; He, F.; Sun, B.; Wang, G. Towards high-energy-density lithium-ion batteries: Strategies for developing high-capacity lithium-rich cathode materials. *Energy Stor. Mater.* **2021**, *34*, 716–734. [CrossRef]
215. Jin, X.; Xu, Q.; Liu, H.; Yuan, X.; Xia, Y. Excellent rate capability of Mg doped $Li[Li_{0.2}Ni_{0.13}Co_{0.13}Mn_{0.54}]O_2$ cathode material for lithium-ion battery. *Electrochim. Acta* **2014**, *136*, 19–26. [CrossRef]
216. Qing, R.-P.; Shi, J.-L.; Xiao, D.-D.; Zhang, X.-D.; Yin, Y.-X.; Zhai, Y.-B.; Gu, L.; Guo, Y.-G. Enhancing the Kinetics of Li-Rich Cathode Materials through the Pinning Effects of Gradient Surface Na^+ Doping. *Adv. Energy Mater.* **2016**, *6*, 1501914. [CrossRef]
217. Zhao, J.; Wang, Z.; Guo, H.; Li, X.; He, Z.; Li, T. Synthesis and electrochemical characterization of Zn-doped Li-rich layered $Li[Li_{0.2}Mn_{0.54}Ni_{0.13}Co_{0.13}]O_2$ cathode material. *Ceram. Int.* **2015**, *41*, 11396–11401. [CrossRef]
218. He, Z.; Wang, Z.; Chen, H.; Huang, Z.; Li, X.; Guo, H.; Wang, R. Electrochemical performance of zirconium doped lithium rich layered $Li_{1.2}Mn_{0.54}Ni_{0.13}Co_{0.13}O_2$ oxide with porous hollow structure. *J. Power Sources* **2015**, *299*, 334–341. [CrossRef]

219. Laisa, C.P.; Ramesha, R.N.; Ramesha, K. Enhanced electrochemical performance of lithium rich layered cathode materials by Ca^{2+} substitution. *Electrochim. Acta* **2017**, *256*, 10–18. [CrossRef]
220. Yu, R.; Wang, G.; Liu, M.; Zhang, X.; Wang, X.; Shu, H.; Yang, X.; Huang, W. Mitigating voltage and capacity fading of lithium-rich layered cathodes by lanthanum doping. *J. Power Sources* **2016**, *335*, 65–75. [CrossRef]
221. Pan, L.; Xia, Y.; Qiu, B.; Zhao, H.; Guo, H.; Jia, K.; Gu, Q.; Liu, Z. Structure and electrochemistry of B doped $Li(Li_{0.2}Ni_{0.13}Co_{0.13}Mn_{0.54})_{1-x}B_xO_2$ as cathode materials for lithium-ion batteries. *J. Power Sources* **2016**, *327*, 273–280. [CrossRef]
222. Kapylou, A.; Song, J.H.; Missiul, A.; Ham, D.J.; Kim, D.H.; Moon, S.; Park, J.H. Improved Thermal Stability of Lithium-Rich Layered Oxide by Fluorine Doping. *ChemPhysChem* **2018**, *19*, 116–122. [CrossRef]
223. Li, B.; Yan, H.; Ma, J.; Yu, P.; Xia, D.; Huang, W.; Chu, W.; Wu, Z. Manipulating the Electronic Structure of Li-Rich Manganese-Based Oxide Using Polyanions: Towards Better Electrochemical Performance. *Adv. Funct. Mater.* **2014**, *24*, 5112–5118. [CrossRef]
224. Zhao, S.; Sun, B.; Yan, K.; Zhang, J.; Wang, C.; Wang, G. Aegis of Lithium-Rich Cathode Materials via Heterostructured LiAlF4 Coating for High-Performance Lithium-Ion Batteries. *ACS Appl. Mater. Interfaces* **2018**, *10*, 33260–33268. [CrossRef] [PubMed]
225. Zhang, X.; Xie, X.; Yu, R.; Zhou, J.; Huang, Y.; Cao, S.; Wang, Y.; Tang, K.; Wu, C.; Wang, X. Improvement of the Cycling Stability of Li-Rich Layered Mn-Based Oxide Cathodes Modified by Nanoscale LaPO4 Coating. *ACS Appl. Energy Mater.* **2019**, *2*, 3532–3541. [CrossRef]
226. Shi, S.J.; Tu, J.P.; Mai, Y.J.; Zhang, Y.Q.; Gu, C.D.; Wang, X.L. Effect of carbon coating on electrochemical performance of $Li_{1.048}Mn_{0.381}Ni_{0.286}Co_{0.286}O2$ cathode material for lithium-ion batteries. *Electrochim. Acta* **2012**, *63*, 112–117. [CrossRef]
227. Arai, H.; Okada, S.; Sakurai, Y.; Yamaki, J.-i. Reversibility of LiNiO2 cathode. *Solid State Ion.* **1997**, *95*, 275–282. [CrossRef]
228. Zhang, Y.; Li, H.; Liu, J.; Zhang, J.; Cheng, F.; Chen, J. LiNi0.90Co0.07Mg0.03O2 cathode materials with Mg-concentration gradient for rechargeable lithium-ion batteries. *J. Mater. Chem. A* **2019**, *7*, 20958–20964. [CrossRef]
229. Wang, X.; Ding, Y.-L.; Deng, Y.-P.; Chen, Z. Ni-Rich/Co-Poor Layered Cathode for Automotive Li-Ion Batteries: Promises and Challenges. *Adv. Energy Mater.* **2020**, *10*, 1903864. [CrossRef]
230. Zheng, J.; Ye, Y.; Liu, T.; Xiao, Y.; Wang, C.; Wang, F.; Pan, F. Ni/Li Disordering in Layered Transition Metal Oxide: Electrochemical Impact, Origin, and Control. *Acc. Chem. Res.* **2019**, *52*, 2201–2209. [CrossRef]
231. Zhang, S.; Ma, J.; Hu, Z.; Cui, G.; Chen, L. Identifying and Addressing Critical Challenges of High-Voltage Layered Ternary Oxide Cathode Materials. *Chem. Mater.* **2019**, *31*, 6033–6065. [CrossRef]
232. Lu, Y.; Zhang, Y.; Zhang, Q.; Cheng, F.; Chen, J. Recent advances in Ni-rich layered oxide particle materials for lithium-ion batteries. *Particuology* **2020**, *53*, 1–11. [CrossRef]
233. Noh, H.-J.; Youn, S.; Yoon, C.S.; Sun, Y.-K. Comparison of the structural and electrochemical properties of layered $Li[Ni_xCo_yMn_z]O_2$ (x = 1/3, 0.5, 0.6, 0.7, 0.8 and 0.85) cathode material for lithium-ion batteries. *J. Power Sources* **2013**, *233*, 121–130. [CrossRef]
234. Li, W.; Erickson, E.M.; Manthiram, A. High-nickel layered oxide cathodes for lithium-based automotive batteries. *Nat. Energy* **2020**, *5*, 26–34. [CrossRef]
235. Yan, W.; Yang, S.; Huang, Y.; Yang, Y.; Guohui, Y. A review on doping/coating of nickel-rich cathode materials for lithium-ion batteries. *J. Alloys Compd.* **2020**, *819*, 153048. [CrossRef]
236. Wang, H.; Wang, Q.; Cao, X.; He, Y.; Wu, K.; Yang, J.; Zhou, H.; Liu, W.; Sun, X. Thiol-Branched Solid Polymer Electrolyte Featuring High Strength, Toughness, and Lithium Ionic Conductivity for Lithium-Metal Batteries. *Adv. Mater.* **2020**, *32*, 2001259. [CrossRef]
237. Sun, C.; Liu, J.; Gong, Y.; Wilkinson, D.P.; Zhang, J. Recent advances in all-solid-state rechargeable lithium batteries. *Nano Energy* **2017**, *33*, 363–386. [CrossRef]
238. Inseok, S.; Steve, W.M. New Developments in Solid Electrolytes for Thin-Film Lithium Batteries. In *Lithium Ion Batteries*; Ilias, B., Ed.; IntechOpen: Rijeka, Croatia, 2012; Chapter 5. [CrossRef]
239. Bachman, J.C.; Muy, S.; Grimaud, A.; Chang, H.-H.; Pour, N.; Lux, S.F.; Paschos, O.; Maglia, F.; Lupart, S.; Lamp, P.; et al. Inorganic Solid-State Electrolytes for Lithium Batteries: Mechanisms and Properties Governing Ion Conduction. *Chem. Rev.* **2016**, *116*, 140–162. [CrossRef]
240. Wang, C.; Fu, K.; Kammampata, S.P.; McOwen, D.W.; Samson, A.J.; Zhang, L.; Hitz, G.T.; Nolan, A.M.; Wachsman, E.D.; Mo, Y.; et al. Garnet-Type Solid-State Electrolytes: Materials, Interfaces, and Batteries. *Chem. Rev.* **2020**, *120*, 4257–4300. [CrossRef]
241. Wang, Y.; Lü, X.; Zheng, C.; Liu, X.; Chen, Z.; Yang, W.; Lin, J.; Huang, F. Chemistry Design Towards a Stable Sulfide-Based Superionic Conductor $Li_4Cu_8Ge_3S_{12}$. *Angew. Chem. Int. Ed.* **2019**, *58*, 7673–7677. [CrossRef]
242. Takahashi, T.; Iwahara, H. Ionic conduction in perovskite-type oxide solid solution and its application to the solid electrolyte fuel cell. *Energy Convers.* **1971**, *11*, 105–111. [CrossRef]
243. Boukamp, B.A.; Huggins, R.A. Fast ionic conductivity in lithium nitride. *Mater. Res. Bull.* **1978**, *13*, 23–32. [CrossRef]
244. Stramare, S.; Thangadurai, V.; Weppner, W. Lithium Lanthanum Titanates: A Review. *Chem. Mater.* **2003**, *15*, 3974–3990. [CrossRef]
245. Morales, M.; Laffez, P.; Chateigner, D.; Vickridge, I. Characterisation of lanthanum lithium titanate thin films deposited by radio frequency sputtering on [100]-oriented MgO substrates. *Thin Solid Films* **2002**, *418*, 119–128. [CrossRef]
246. Ohta, H.; Mizoguchi, T.; Aoki, N.; Yamamoto, T.; Sabarudin, A.; Umemura, T. Lithium-ion conducting La2/3−xLi_3xTiO_3 solid electrolyte thin films with stepped and terraced surfaces. *Appl. Phys. Lett.* **2012**, *100*, 173107. [CrossRef]

247. Furusawa, S.-i.; Tabuchi, H.; Sugiyama, T.; Tao, S.; Irvine, J.T.S. Ionic conductivity of amorphous lithium lanthanum titanate thin film. *Solid State Ion.* **2005**, *176*, 553–558. [CrossRef]
248. Ahn, J.-K.; Yoon, S.-G. Characteristics of perovskite $(Li_{0.5}La_{0.5})TiO_3$ solid electrolyte thin films grown by pulsed laser deposition for rechargeable lithium microbattery. *Electrochim. Acta* **2004**, *50*, 371–374. [CrossRef]
249. West, W.C.; Hood, Z.D.; Adhikari, S.P.; Liang, C.; Lachgar, A.; Motoyama, M.; Iriyama, Y. Reduction of charge-transfer resistance at the solid electrolyte—Electrode interface by pulsed laser deposition of films from a crystalline Li_2PO_2N source. *J. Power Sources* **2016**, *312*, 116–122. [CrossRef]
250. Wang, B.; Zhao, Y.; Banis, M.N.; Sun, Q.; Adair, K.R.; Li, R.; Sham, T.-K.; Sun, X. Atomic Layer Deposition of Lithium Niobium Oxides as Potential Solid-State Electrolytes for Lithium-Ion Batteries. *ACS Appl. Mater. Interfaces* **2018**, *10*, 1654–1661. [CrossRef]
251. Ohnishi, T.; Takada, K. Synthesis and orientation control of Li-ion conducting epitaxial $Li_{0.33}La_{0.56}TiO_3$ solid electrolyte thin films by pulsed laser deposition. *Solid State Ion.* **2012**, *228*, 80–82. [CrossRef]
252. Wei, J.; Ogawa, D.; Fukumura, T.; Hirose, Y.; Hasegawa, T. Epitaxial Strain-Controlled Ionic Conductivity in Li-Ion Solid Electrolyte $Li_{0.33}La_{0.56}TiO_3$ Thin Films. *Cryst. Growth Des.* **2015**, *15*, 2187–2191. [CrossRef]
253. Kim, S.; Hirayama, M.; Cho, W.; Kim, K.; Kobayashi, T.; Kaneko, R.; Suzuki, K.; Kanno, R. Low temperature synthesis and ionic conductivity of the epitaxial $Li_{0.17}La_{0.61}TiO_3$ film electrolyte. *CrystEngComm* **2014**, *16*, 1044–1049. [CrossRef]
254. Lü, X.; Wu, G.; Howard, J.W.; Chen, A.; Zhao, Y.; Daemen, L.L.; Jia, Q. Li-rich anti-perovskite Li_3OCl films with enhanced ionic conductivity. *Chem. Comm.* **2014**, *50*, 11520–11522. [CrossRef] [PubMed]
255. Mousavi, T.; Chen, X.; Doerrer, C.; Jagger, B.; Speller, S.C.; Grovenor, C.R.M. Fabrication of $Li_{1+x}Al_xGe_{2-x}(PO_4)_3$ thin films by sputtering for solid electrolytes. *Solid State Ion.* **2020**, *354*, 115397. [CrossRef]
256. Sun, Z.; Liu, L.; Yang, B.; Li, Q.; Wu, B.; Zhao, J.; Ma, L.; Liu, Y.; An, H. Preparation and ion conduction of $Li_{1.5}Al_{0.5}Ge_{1.5}(PO_4)_3$ solid electrolyte films using radio frequency sputtering. *Solid State Ion.* **2020**, *346*, 115224. [CrossRef]
257. Ling, Q.; Yu, Z.; Xu, H.; Zhu, G.; Zhang, X.; Zhao, Y.; Yu, A. Preparation and electrical properties of amorphous Li-Al-Ti-P-O thin film electrolyte. *Mater. Lett.* **2016**, *169*, 42–45. [CrossRef]
258. Nakagawa, A.; Kuwata, N.; Matsuda, Y.; Kawamura, J. Characterization of Stable Solid Electrolyte Lithium Silicate for Thin Film Lithium Battery. *J. Phys. Soc. Japan.* **2010**, *79*, 98–101. [CrossRef]
259. Ohta, N.; Takada, K.; Osada, M.; Zhang, L.; Sasaki, T.; Watanabe, M. Solid electrolyte, thio-LISICON, thin film prepared by pulsed laser deposition. *J. Power Sources* **2005**, *146*, 707–710. [CrossRef]
260. Loho, C.; Djenadic, R.; Bruns, M.; Clemens, O.; Hahn, H. Garnet-Type $Li_7La_3Zr_2O_{12}$ Solid Electrolyte Thin Films Grown by CO_2-Laser Assisted CVD for All-Solid-State Batteries. *J. Electrochem. Soc.* **2017**, *164*, A6131. [CrossRef]
261. Kazyak, E.; Chen, K.-H.; Wood, K.N.; Davis, A.L.; Thompson, T.; Bielinski, A.R.; Sanchez, A.J.; Wang, X.; Wang, C.; Sakamoto, J.; et al. Atomic Layer Deposition of the Solid Electrolyte Garnet $Li_7La_3Zr_2O_{12}$. *Chem. Mater.* **2017**, *29*, 3785–3792. [CrossRef]
262. Reinacher, J.; Berendts, S.; Janek, J. Preparation and electrical properties of garnet-type $Li_6BaLa_2Ta_2O_{12}$ lithium solid electrolyte thin films prepared by pulsed laser deposition. *Solid State Ion.* **2014**, *258*, 1–7. [CrossRef]
263. Kuwata, N.; Kawamura, J.; Toribami, K.; Hattori, T.; Sata, N. Thin-film lithium-ion battery with amorphous solid electrolyte fabricated by pulsed laser deposition. *Electrochem. Commun.* **2004**, *6*, 417–421. [CrossRef]
264. Xie, J.; Sendek, A.D.; Cubuk, E.D.; Zhang, X.; Lu, Z.; Gong, Y.; Wu, T.; Shi, F.; Liu, W.; Reed, E.J.; et al. Atomic Layer Deposition of Stable $LiAlF_4$ Lithium Ion Conductive Interfacial Layer for Stable Cathode Cycling. *ACS Nano* **2017**, *11*, 7019–7027. [CrossRef] [PubMed]
265. Cao, Y.; Meng, X.; Elam, J.W. Atomic Layer Deposition of Li_xAl_yS Solid-State Electrolytes for Stabilizing Lithium-Metal Anodes. *ChemElectroChem* **2016**, *3*, 858–863. [CrossRef]
266. Sakuda, A.; Hayashi, A.; Hama, S.; Tatsumisago, M. Preparation of Highly Lithium-Ion Conductive $80Li_2S_{20}P_{2S5}$ Thin-Film Electrolytes Using Pulsed Laser Deposition. *J. Am. Ceram. Soc.* **2010**, *93*, 765–768. [CrossRef]
267. Quan, Z.; Hirayama, M.; Sato, D.; Zheng, Y.; Yano, T.-a.; Hara, K.; Suzuki, K.; Hara, M.; Kanno, R. Effect of excess Li_2S on electrochemical properties of amorphous Li_3PS_4 films synthesized by pulsed laser deposition. *J. Am. Ceram. Soc.* **2017**, *100*, 746–753. [CrossRef]
268. Chen, S.; Wen, K.; Fan, J.; Bando, Y.; Golberg, D. Progress and future prospects of high-voltage and high-safety electrolytes in advanced lithium batteries: From liquid to solid electrolytes. *J. Mater. Chem. A* **2018**, *6*, 11631–11663. [CrossRef]
269. Goodenough, J.B.; Hong, H.Y.P.; Kafalas, J.A. Fast Na^+-ion transport in skeleton structures. *Mater. Res. Bull.* **1976**, *11*, 203–220. [CrossRef]
270. Mariappan, C.R.; Yada, C.; Rosciano, F.; Roling, B. Correlation between micro-structural properties and ionic conductivity of $Li_{1.5}Al_{0.5}Ge_{1.5}(PO_4)_3$ ceramics. *J. Power Sources* **2011**, *196*, 6456–6464. [CrossRef]
271. Thangadurai, V.; Weppner, W. Recent progress in solid oxide and lithium ion conducting electrolytes research. *Ionics* **2006**, *12*, 81–92. [CrossRef]
272. Wu, F.; Liu, Y.; Chen, R.; Chen, S.; Wang, G. Preparation and performance of novel Li–Ti–Si–P–O–N thin-film electrolyte for thin-film lithium batteries. *J. Power Sources* **2009**, *189*, 467–470. [CrossRef]
273. Kim, H.-S.; Choi, K.S.; Kim, E.J.; Kang, K.; Kim, J.H.; Kim, J.; Yoon, C.S. Characterization of Sputter-Deposited $LiZr_2(PO_4)_3$ Thin Film Solid Electrolyte. *J. Electrochem. Soc.* **2015**, *162*, A2080. [CrossRef]

274. Hartmann, P.; Leichtweiss, T.; Busche, M.R.; Schneider, M.; Reich, M.; Sann, J.; Adelhelm, P.; Janek, J. Degradation of NASICON-Type Materials in Contact with Lithium Metal: Formation of Mixed Conducting Interphases (MCI) on Solid Electrolytes. *J. Phys. Chem. C* **2013**, *117*, 21064–21074. [CrossRef]
275. Li, Y.; Zhou, W.; Chen, X.; Lü, X.; Cui, Z.; Xin, S.; Xue, L.; Jia, Q.; Goodenough, J.B. Mastering the interface for advanced all-solid-state lithium rechargeable batteries. *PNAS* **2016**, *113*, 13313–13317. [CrossRef] [PubMed]
276. Bruce, P.G.; West, A.R. The A-C Conductivity of Polycrystalline LISICON, Li_{2+2x} Zn_{1-x} GeO_4, and a Model for Intergranular Constriction Resistances. *J. Electrochem. Soc.* **1983**, *130*, 662–669. [CrossRef]
277. Robertson, A.D.; West, A.R.; Ritchie, A.G. Review of crystalline lithium-ion conductors suitable for high temperature battery applications. *Solid State Ion.* **1997**, *104*, 1–11. [CrossRef]
278. Kanno, R.; Hata, T.; Kawamoto, Y.; Irie, M. Synthesis of a new lithium ionic conductor, thio-LISICON–lithium germanium sulfide system. *Solid State Ion.* **2000**, *130*, 97–104. [CrossRef]
279. Murayama, M.; Kanno, R.; Irie, M.; Ito, S.; Hata, T.; Sonoyama, N.; Kawamoto, Y. Synthesis of New Lithium Ionic Conductor Thio-LISICON—Lithium Silicon Sulfides System. *J. Solid State Chem.* **2002**, *168*, 140–148. [CrossRef]
280. Thangadurai, V.; Kaack, H.; Weppner, W.J.F. Novel Fast Lithium Ion Conduction in Garnet-Type $Li_5La_3M_2O_{12}$ (M = Nb, Ta). *J. Am. Ceram. Soc.* **2003**, *86*, 437–440. [CrossRef]
281. Murugan, R.; Thangadurai, V.; Weppner, W. Fast Lithium Ion Conduction in Garnet-Type $Li_7La_3Zr_2O_{12}$. *Angew. Chem.* **2007**, *46*, 7778–7781. [CrossRef]
282. Meesala, Y.; Liao, Y.-K.; Jena, A.; Yang, N.-H.; Pang, W.K.; Hu, S.-F.; Chang, H.; Liu, C.-E.; Liao, S.-C.; Chen, J.-M.; et al. An efficient multi-doping strategy to enhance Li-ion conductivity in the garnet-type solid electrolyte $Li_7La_3Zr_2O_{12}$. *J. Mater. Chem. A* **2019**, *7*, 8589–8601. [CrossRef]
283. Rawlence, M.; Garbayo, I.; Buecheler, S.; Rupp, J.L.M. On the chemical stability of post-lithiated garnet Al-stabilized $Li_7La_3Zr_2O_{12}$ solid state electrolyte thin films. *Nanoscale* **2016**, *8*, 14746–14753. [CrossRef] [PubMed]
284. Saccoccio, M.; Yu, J.; Lu, Z.; Kwok, S.C.T.; Wang, J.; Yeung, K.K.; Yuen, M.M.F.; Ciucci, F. Low temperature pulsed laser deposition of garnet Li6.4La3Zr1.4Ta0.6O12 films as all solid-state lithium battery electrolytes. *J. Power Sources* **2017**, *365*, 43–52. [CrossRef]
285. Kalita, D.J.; Lee, S.H.; Lee, K.S.; Ko, D.H.; Yoon, Y.S. Ionic conductivity properties of amorphous Li–La–Zr–O solid electrolyte for thin film batteries. *Solid State Ion.* **2012**, *229*, 14–19. [CrossRef]
286. Lobe, S.; Dellen, C.; Windmüller, A.; Tsai, C.L.; Vondahlen, F.; Uhlenbruck, S.; Guillon, O. Challenges regarding thin film deposition of garnet electrolytes for all-solid-state lithium batteries with high energy density. *Ionics* **2018**, *24*, 2199–2208. [CrossRef]
287. Kamaya, N.; Homma, K.; Yamakawa, Y.; Hirayama, M.; Kanno, R.; Yonemura, M.; Kamiyama, T.; Kato, Y.; Hama, S.; Kawamoto, K.; et al. A lithium superionic conductor. *Nature Mater.* **2011**, *10*, 682–686. [CrossRef] [PubMed]
288. Zhang, Q.; Cao, D.; Ma, Y.; Natan, A.; Aurora, P.; Zhu, H. Solid-State Batteries: Sulfide-Based Solid-State Electrolytes: Synthesis, Stability, and Potential for All-Solid-State Batteries. *Adv. Mater.* **2019**, *31*, 1970311. [CrossRef]
289. Lepley, N.D.; Holzwarth, N.A.W.; Du, Y.A. Structures, Li^+ mobilities, and interfacial properties of solid electrolytes Li_3PS_4 and Li_3PO_4 from first principles. *Phys. Rev. B* **2013**, *88*, 104103. [CrossRef]
290. Bates, J.B.; Dudney, N.J.; Neudecker, B.; Ueda, A.; Evans, C.D. Thin-film lithium and lithium-ion batteries. *Solid State Ion.* **2000**, *135*, 33–45. [CrossRef]
291. Dudney, N.J.; Neudecker, B.J. Solid state thin-film lithium battery systems. *Curr. Opin. Solid State Mater. Sci.* **1999**, *4*, 479–482. [CrossRef]
292. Neudecker, B.J.; Dudney, N.J.; Bates, J.B. "Lithium-Free" Thin-Film Battery with In Situ Plated Li Anode. *J. Electrochem. Soc.* **2000**, *147*, 517–523. [CrossRef]
293. Jung, K.-N.; Shin, H.-S.; Park, M.-S.; Lee, J.-W. Solid-State Lithium Batteries: Bipolar Design, Fabrication, and Electrochemistry. *ChemElectroChem* **2019**, *6*, 3842–3859. [CrossRef]
294. Liu, W.; Song, M.-S.; Kong, B.; Cui, Y. Flexible and Stretchable Energy Storage: Recent Advances and Future Perspectives. *Adv. Mater.* **2017**, *29*, 1603436. [CrossRef]
295. Schnell, J.; Günther, T.; Knoche, T.; Vieider, C.; Köhler, L.; Just, A.; Keller, M.; Passerini, S.; Reinhart, G. All-solid-state lithium-ion and lithium metal batteries—Paving the way to large-scale production. *J. Power Sources* **2018**, *382*, 160–175. [CrossRef]
296. Garche, J. On the historical development of the lead/acid battery, especially in Europe. *J. Power Sources* **1990**, *31*, 401–406. [CrossRef]
297. Bullock, K.R. Progress and Challenges in Bipolar Lead-Acid Battery Development. *J. Electrochem. Soc.* **1995**, *142*, 1726. [CrossRef]
298. Shen, D.H.; Halpert, G. Design concepts of high power bipolar rechargeable lithium battery. *J. Power Sources* **1993**, *43*, 327–338. [CrossRef]
299. Janek, J.; Zeier, W.G. A solid future for battery development. *Nat. Energy* **2016**, *1*, 16141. [CrossRef]
300. Gambe, Y.; Sun, Y.; Honma, I. Development of Bipolar All-solid-state Lithium Battery Based on Quasi-solid-state Electrolyte Containing Tetraglyme-LiTFSA Equimolar Complex. *Sci. Rep.* **2015**, *5*, 8869. [CrossRef]
301. Yoshima, K.; Harada, Y.; Takami, N. Thin hybrid electrolyte based on garnet-type lithium-ion conductor $Li_7La_3Zr_2O_{12}$ for 12 V-class bipolar batteries. *J. Power Sources* **2016**, *302*, 283–290. [CrossRef]
302. Tian, Y.; An, Y.; Wei, C.; Jiang, H.; Xiong, S.; Feng, J.; Qian, Y. Recently advances and perspectives of anode-free rechargeable batteries. *Nano Energy* **2020**, *78*, 105344. [CrossRef]

303. Weber, R.; Genovese, M.; Louli, A.J.; Hames, S.; Martin, C.; Hill, I.G.; Dahn, J.R. Long cycle life and dendrite-free lithium morphology in anode-free lithium pouch cells enabled by a dual-salt liquid electrolyte. *Nat. Energy* **2019**, *4*, 683–689. [CrossRef]
304. Zhang, J.-G. Anode-less. *Nat. Energy* **2019**, *4*, 637–638. [CrossRef]
305. Qian, J.; Adams, B.D.; Zheng, J.; Xu, W.; Henderson, W.A.; Wang, J.; Bowden, M.E.; Xu, S.; Hu, J.; Zhang, J.-G. Anode-Free Rechargeable Lithium Metal Batteries. *Adv. Funct. Mater.* **2016**, *26*, 7094–7102. [CrossRef]
306. Woo, J.-J.; Maroni, V.A.; Liu, G.; Vaughey, J.T.; Gosztola, D.J.; Amine, K.; Zhang, Z. Symmetrical Impedance Study on Inactivation Induced Degradation of Lithium Electrodes for Batteries Beyond Lithium-Ion. *J. Electrochem. Soc.* **2014**, *161*, A827. [CrossRef]
307. Chen, J.; Li, Q.; Pollard, T.P.; Fan, X.; Borodin, O.; Wang, C. Electrolyte design for Li metal-free Li batteries. *Mater. Today* **2020**, *39*, 118–126. [CrossRef]
308. Assegie, A.A.; Chung, C.-C.; Tsai, M.-C.; Su, W.-N.; Chen, C.-W.; Hwang, B.-J. Multilayer-graphene-stabilized lithium deposition for anode-Free lithium-metal batteries. *Nanoscale* **2019**, *11*, 2710–2720. [CrossRef]
309. Kim, S.; Jung, C.; Kim, H.; Thomas-Alyea, K.E.; Yoon, G.; Kim, B.; Badding, M.E.; Song, Z.; Chang, J.; Kim, J.; et al. The Role of Interlayer Chemistry in Li-Metal Growth through a Garnet-Type Solid Electrolyte. *Adv. Energy Mater.* **2020**, *10*, 1903993. [CrossRef]
310. Chen, C.; Eichel, R.A.; Notten, P.H.L. Metal-organic chemical vapor deposition enabling all-solid-state Li-ion microbatteries: A short review. *J. Electroceram.* **2017**, *38*, 230–247. [CrossRef]
311. Horowitz, Y.; Strauss, E.; Peled, E.; Golodnitsky, D. How to Pack a Punch-Why 3D Batteries are Essential. *Isr. J. Chem.* **2021**, *61*, 38–50. [CrossRef]
312. Shaijumon, M.M.; Perre, E.; Daffos, B.; Taberna, P.-L.; Tarascon, J.-M.; Simon, P. Nanoarchitectured 3D Cathodes for Li-Ion Microbatteries. *Adv. Mater.* **2010**, *22*, 4978–4981. [CrossRef]
313. Mattelaer, F.; Geryl, K.; Rampelberg, G.; Dendooven, J.; Detavernier, C. Amorphous and Crystalline Vanadium Oxides as High-Energy and High-Power Cathodes for Three-Dimensional Thin-Film Lithium Ion Batteries. *ACS Appl. Mater. Interfaces* **2017**, *9*, 13121–13131. [CrossRef] [PubMed]
314. Labyedh, N.; Mattelaer, F.; Detavernier, C.; Vereecken, P.M. 3D $LiMn_2O_4$ thin-film electrodes for high rate all solid-state lithium and Li-ion microbatteries. *J. Mater. Chem. A* **2019**, *7*, 18996–19007. [CrossRef]
315. Shui, J.L.; Jiang, G.S.; Xie, S.; Chen, C.H. Thin films of lithium manganese oxide spinel as cathode materials for secondary lithium batteries. *Electrochim. Acta* **2004**, *49*, 2209–2213. [CrossRef]
316. Kim, S.-J.; Moon, S.-H.; Kim, M.-C.; So, J.-Y.; Han, S.-B.; Kwak, D.-H.; Bae, W.-G.; Park, K.-W. Micro-patterned 3D Si electrodes fabricated using an imprinting process for high-performance lithium-ion batteries. *J. Appl. Electrochem.* **2018**, *48*, 1057–1068. [CrossRef]
317. Létiche, M.; Eustache, E.; Freixas, J.; Demortière, A.; De Andrade, V.; Morgenroth, L.; Tilmant, P.; Vaurette, F.; Troadec, D.; Roussel, P.; et al. Atomic Layer Deposition of Functional Layers for on Chip 3D Li-Ion All Solid State Microbattery. *Adv. Energy Mater.* **2017**, *7*, 1601402. [CrossRef]
318. Moitzheim, S.; Balder, J.E.; Poodt, P.; Unnikrishnan, S.; De Gendt, S.; Vereecken, P.M. Chlorine Doping of Amorphous TiO_2 for Increased Capacity and Faster Li+-Ion Storage. *Chem. Mater.* **2017**, *29*, 10007–10018. [CrossRef]
319. Li, Y.; Zhao, Y.; Huang, G.; Xu, B.; Wang, B.; Pan, R.; Men, C.; Mei, Y. ZnO Nanomembrane/Expanded Graphite Composite Synthesized by Atomic Layer Deposition as Binder-Free Anode for Lithium Ion Batteries. *ACS Appl. Mater. Interfaces* **2017**, *9*, 38522–38529. [CrossRef]
320. Put, B.; Vereecken, P.M.; Meersschaut, J.; Sepúlveda, A.; Stesmans, A. Electrical Characterization of Ultrathin RF-Sputtered LiPON Layers for Nanoscale Batteries. *ACS Appl. Mater. Interfaces* **2016**, *8*, 7060–7069. [CrossRef]
321. Nisula, M.; Shindo, Y.; Koga, H.; Karppinen, M. Atomic Layer Deposition of Lithium Phosphorus Oxynitride. *Chem. Mater.* **2015**, *27*, 6987–6993. [CrossRef]
322. Nasreldin, M.; de Mulatier, S.; Delattre, R.; Ramuz, M.; Djenizian, T. Flexible and Stretchable Microbatteries for Wearable Technologies. *Adv. Mater. Technol.* **2020**, *5*, 2000412. [CrossRef]
323. He, Y.; Matthews, B.; Wang, J.; Song, L.; Wang, X.; Wu, G. Innovation and challenges in materials design for flexible rechargeable batteries: From 1D to 3D. *J. Mater. Chem. A* **2018**, *6*, 735–753. [CrossRef]
324. Yao, B.; Zhang, J.; Kou, T.; Song, Y.; Liu, T.; Li, Y. Paper-Based Electrodes for Flexible Energy Storage Devices. *Adv. Sci.* **2017**, *4*, 1700107. [CrossRef] [PubMed]
325. Xu, S.; Zhang, Y.; Cho, J.; Lee, J.; Huang, X.; Jia, L.; Fan, J.A.; Su, Y.; Su, J.; Zhang, H.; et al. Stretchable batteries with self-similar serpentine interconnects and integrated wireless recharging systems. *Nat Commun.* **2013**, *4*, 1543. [CrossRef] [PubMed]
326. Chen, Z.; Ren, W.; Gao, L.; Liu, B.; Pei, S.; Cheng, H.-M. Three-dimensional flexible and conductive interconnected graphene networks grown by chemical vapour deposition. *Nature Mater.* **2011**, *10*, 424–428. [CrossRef]
327. Liu, W.; Chen, J.; Chen, Z.; Liu, K.; Zhou, G.; Sun, Y.; Song, M.-S.; Bao, Z.; Cui, Y. Stretchable Lithium-Ion Batteries Enabled by Device-Scaled Wavy Structure and Elastic-Sticky Separator. *Adv. Energy Mater.* **2017**, *7*, 1701076. [CrossRef]
328. Hu, L.; Wu, H.; La Mantia, F.; Yang, Y.; Cui, Y. Thin, Flexible Secondary Li-Ion Paper Batteries. *ACS Nano* **2010**, *4*, 5843–5848. [CrossRef]
329. Wang, C.; Li, D.; Too, C.O.; Wallace, G.G. Electrochemical Properties of Graphene Paper Electrodes Used in Lithium Batteries. *Chem. Mater.* **2009**, *21*, 2604–2606. [CrossRef]

330. Zhao, X.; Hayner, C.M.; Kung, M.C.; Kung, H.H. In-Plane Vacancy-Enabled High-Power Si–Graphene Composite Electrode for Lithium-Ion Batteries. *Adv. Energy Mater.* **2011**, *1*, 1079–1084. [CrossRef]
331. Rana, K.; Kim, S.D.; Ahn, J.-H. Additive-free thick graphene film as an anode material for flexible lithium-ion batteries. *Nanoscale* **2015**, *7*, 7065–7071. [CrossRef]
332. Cheng, Y.; Chen, Z.; Zhu, M.; Lu, Y. Polyacrylic Acid Assisted Assembly of Oxide Particles and Carbon Nanotubes for High-Performance Flexible Battery Anodes. *Adv. Energy Mater.* **2015**, *5*, 1401207. [CrossRef]
333. Liu, Y.-T.; Zhu, X.-D.; Duan, Z.-Q.; Xie, X.-M. Flexible and robust MoS_2–graphene hybrid paper cross-linked by a polymer ligand: A high-performance anode material for thin film lithium-ion batteries. *Chem. Commun.* **2013**, *49*, 10305–10307. [CrossRef] [PubMed]